University of Calgary

PRISM Repository **https://prism.ucalgary.ca**

The Vault Open Theses and Dissertations

2014-12-03

Weak GPS Signal Acquisition Using Antenna Diversity

Mozaffari, Mohammad

Mozaffari, M. (2014). Weak GPS Signal Acquisition Using Antenna Diversity (Master's thesis, University of Calgary, Calgary, Canada). Retrieved from https://prism.ucalgary.ca. doi:10.11575/PRISM/28677 http://hdl.handle.net/11023/1945

Downloaded from PRISM Repository, University of Calgary

UNIVERSITY OF CALGARY

Weak GPS Signal Acquisition Using Antenna Diversity

by

Mohammad Mozaffari

A THESIS

SUBMITTED TO THE FACULTY OF GRADUATE STUDIES

IN PARTIAL FULFILMENT OF THE REQUIREMENTS FOR THE

DEGREE OF MASTER OF SCIENCE

DEPARTMENT OF GEOMATICS ENGINEERING

CALGARY, ALBERTA

November 2014

© Mohammad Mozaffari 2014

Abstract

GNSS Acquisition in fading and attenuated environments is challenging. In these situations, additional processing gain is required. A common method is to extend the coherent integration time. However, in weak signal situations, using only long coherent integration is limited by navigation data bit transitions and receiver oscillator instability. Using non-coherent and differentially coherent integration mitigates the bit transition problem but has lower processing gain as compared to coherent integration. Coherent, non-coherent and differentially coherent combining methods are not effective in dense multipath fading situations where the carrier-to-noise ratio (C/N_0) varies significantly. Spatial antenna diversity provides additional processing gain to overcome multipath fading since multiple antennas detect signal components from independent fading channels. This thesis evaluates equal gain combining of two independent antennas in a standalone acquisition process. Traditionally acquisition has been evaluated at the cell level, which considers only a single cell, but in this thesis acquisition is assessed at the system level, where the complete acquisition process including the entire search space is examined. Receiver Operating Characteristic (ROC) curves in both cell and system levels are presented and compared both theoretically and using real data. Overall detection probability, probability of false alarm and acquisition time are investigated in terms of the mean and variance values. Optimal values for the integration time as well as combination of coherent and non-coherent integration that minimizes the mean acquisition time are

obtained. The theoretical analysis is compared with Monte Carlo simulations and real GPS data results. Compared to a single antenna, smoother signal-to-noise ratio (*SNR*) values which show the fading mitigation were observed by applying diversity combining. Experimental results demonstrate the improvement of detection probability, enhanced immunity against false alarms, and significant reduction of the mean and variance of acquisition time in dense multipath environments.

Preface

This work has also been proposed in a peer reviewed conference paper and submitted to a journal.

1. Mozaffari, M., A. Broumandan, K. O'Keefe and G. Lachapelle (2014), "Weak GPS Signal Acquisition Using Antenna Diversity," Proceedings of UPINLBS

2. Mozaffari, M., A. Broumandan, K. O'Keefe and G. Lachapelle (2014), "Weak GNSS Signal Acquisition Using Antenna Diversity," submitted to NAVIGATION, Journal of The Institute of Navigation

Acknowledgements

I would like to express my sincere gratitude to my supervisor and co-supervisor, Professors Kyle O'Keefe and Gérard Lachapelle, for all their excellent guidance, encouragement and continuous support during my study. I really appreciate their kind consideration and will always be grateful.

Special thanks to Dr. Ali Broumandan, Senior Research Associate in the PLAN Group, for his great advice, friendship and warm support. I also would like to thank my other wonderful friends in the PLAN Group, in particular Ahmad Shafaati, Drs Saeed Daneshmand, Negin Sokhandan and Ali Jafarnia for their kindness and for being immensely helpful.

Additional gratitude is offered to my friends AmiR, Siavash, Navid, Maryam, Nahid, Ranjeeth, Nahal and Mahshid.

Finally, I am greatly thankful to my family for their sustained encouragement, support and unconditional love.

Dedication

To my beloved parents and my sister

Table of Contents

List of Tables

List of Figures and Illustrations

List of Acronyms

AFD	Average Fade Duration
ADC	Analog-to-Digital Converter
BOC	Binary Offset Carrier
BPSK	Binary Phase Shift Keying
C/A	Coarse/Acquisition
C/N_0	Carrier-to-Noise Ratio
CAF	Cross Ambiguity Function
CAF	Cross Ambiguity Function
CDMA	Code Division Multiple Access
DC	Differentially Coherent
DCOH	Differentially Coherent Combining
EGC	Equal Gain Combining
FFT	Fast Fourier Transform
GNSS	Global Navigation Satellite System
GPS	Global Positioning System
IF	Intermediate Frequency
LCR	Level Crossing Rate
LHCP	Left Hand Circular Polarized
LOS	Line of Sight
MAT	Mean Acquisition Time
MRC	Maximal Ratio Combining
NCOH	Non-Coherent Combining
PDF	Probability Density function
PRN	Pseudo-Random Noise
PSD	Power Spectral Density
PSNR	Post Processing SNR
RHCP	Right Hand Circular Polarized
ROC	Receiver Operating Characteristics
RMS	Root Mean Square

SC	Selection Combining

List of Symbols

A	Signal amplitude
$c(.)$	Ranging code
$d(.)$	Navigation data
F_s	Sampling frequency
f_d	Doppler frequency
H_0	Hypothesis that noise is present
H_1	Hypothesis that the desired signal is present
P_{FA}^{a}	Overall false alarm probability in absence of signal
P_{FA}^{p}	Overall false alarm probability in presence of signal
P_d	Detection probability
P_D	Overall detection probability
P_{fa}	False alarm probability
P_{MD}	Probability of missed detection
Q_K	Marcum Q-function
$R(.)$	Autocorrelation function
$\bar{T}_A$	Mean acquisition time
T_{coh}	Coherent integration time
T_{int}	Integration time
T_p	Penalty time
T_s	Total time required for evaluating the entire CAF
β	Detection threshold
τ	Code phase
σ_N^2	Noise variance

σ_S^2	Signal variance
$\sigma_{T_A}^2$	Variance of acquisition time
χ_K^2	Chi-square distribution with K degrees of freedom

Chapter One: INTRODUCTION

Global Navigation Satellite Systems (GNSS) are widely used in the military and civilian community for navigation, location, and timing. Acquisition and tracking of received signals are two main operation stages performed by receivers. Acquisition is the first operation stage of a GNSS receiver where the signal is detected and a coarse estimate of code phase and carrier Doppler frequency shift is obtained. Once these parameters are found, tracking can begin. However, GNSS signal acquisition and tracking are very difficult when the signal is weak. More specifically, especially in indoor environments, GNSS receivers have to deal with very weak signals due to attenuation and multipath fading. In order to overcome the fading and attenuation difficulties, beside increasing the integration time which uses more samples of the signal for the acquisition purposes and is limited by user dynamics and clock effects, the use of multiple antennas and the benefit of antenna diversity could help significantly in the signal detection process. This research assesses the entire acquisition process to find the overall detection probability, probability of false alarm and mean acquisition time using spatial antenna diversity in weak and faded signal situations.

1.1 Background

This section provides the background and previous research that has been performed in the area of GNSS signal acquisition and antenna diversity.

1.1.1 Acquisition

Signal acquisition, as a two-dimensional search process, is the first operation stage performed by GNSS receivers. In the presence of the signal it can provide coarse estimates of the code delay and Doppler frequency of the GNSS signal (Borio 2008). However, in weak signal situations with high multipath fading and severe attenuation, acquisition becomes a challenging problem. In the acquisition process, the search space consists of an array of cells which represents a range of possible C/A code phases and carrier Doppler frequency shifts. The incoming signal is correlated with local replicas of the pseudorandom noise code generated over a range of Doppler frequencies and correlator output values are assigned to the corresponding cells. The signal is detected and its parameters, code phase (τ) and Doppler frequency (f_d), are estimated if the amplitude of the correlator output in the correct cell (which indicates the best estimate of code and Doppler) passes a detection threshold (O'Driscoll 2007, Borio 2008). Geiger et al (2010) presented a novel detection criterion assuming the Doppler estimate is available. In this method correlation values for all code bins are computed in a parallel way and the GNSS signal presence criterion is based on the comparison of the ratio between the largest and the second largest correlation peak against a threshold. The main advantage of this method is that the threshold is independent of the noise floor so that a fixed threshold can be used in the analyses.

Clearly, as long as the correct cell is not found, the search process continues. Therefore, due to the large number of required operations in the correlator, the

process of acquisition is time consuming and it may require a long time to search the candidate cells. There are some methods based on the fast Fourier transform (FFT) that expedite the acquisition process (Akopian 2005, Sagiraju et al 2008).

In the severe conditions such as indoor environments where the GNSS signal is attenuated by 20 to 30 dB, a high processing gain is required to acquire the signal. One approach is to increase the coherent integration time which enhances the receiver sensitivity (Shanmugam et al 2007). However, navigation bit transition limits the integration time to 10 ms in the acquisition stage. This problem can be mitigated by using other combining techniques such as non-coherent combining (NCOH) and differentially coherent combining (DCC) (Borio 2008). These methods are explained in the next chapter. Wu et al a (2009) showed that DCC can improve acquisition sensitivity by 1.9 dB compared to NCOH and results in faster acquisition.

The acquisition process is evaluated in two levels: cell level and system level (Borio 2008). Cell level evaluates only cell while the system level considers the entire search space and examines the impact of all the cells on the acquisition performance. Typically, the performance of an acquisition system is evaluated in terms of detection probability (P_d), probability of false alarm (P_{fa}) and mean acquisition time. A powerful means for comparing the performance of different algorithms in acquisition process is the receiver operating characteristic (ROC) curve that illustrates P_d versus P_{fa}. Figure 1-1 shows an example of ROC curves for two systems with different performance. Although P_d and P_{fa} defined in the

cell and system domains are related, they are not the same. That is, it is possible to have two acquisition systems with the same cell level performance but different system level performance (Borio 2008). While the cell level acquisition was the foremost focus of previous work, it does not completely reflect the overall acquisition performance. The most important evaluation metric of the acquisition process is the time required to correctly detect the signal. The different approaches to compute mean acquisition time (MAT) are presented by Kassabian et al (2012), O'Driscoll (2007), and Holmes & Chen (1977). Most specifically, the importance of MAT shows up in the weak signal situation.

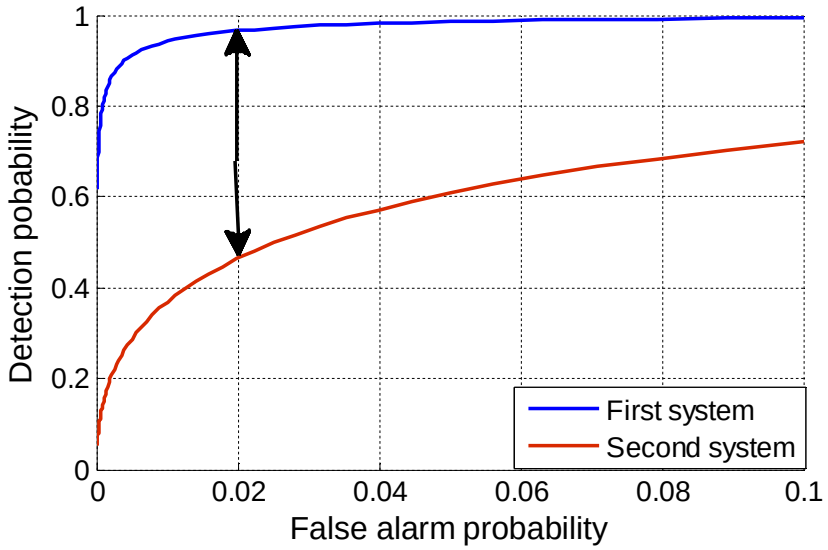

Figure 1-1: ROC curve example

1.1.2 Antenna Diversity

In wireless communications, diversity is a technique used to receive multiple copies of the signal that experience different communication channels. There are different schemes of diversity such as time, frequency, polarization and

space/antenna diversity. Using a synthetic antenna array in which arbitrary spatial motion is considered provides space/time diversity (Broumandan et al 2009).

In antenna diversity two or more antennas are used in both transmitter and/or receiver sides to improve the quality and reliability of a wireless link. Often, especially in urban and indoor environments, there is no clear lines-of-sight (LOS) between transmitter and receiver and the transmitted signal is reflected along multiple paths before finally being received and fading occurs. Antenna diversity is extensively utilized in wireless communication (Vaughan & Andersen 1987, Dietrich et al 2001). Likewise, especially in indoor environments, GNSS receivers suffer from weak signals due to attenuation and multipath fading. In order to overcome the fading and attenuation difficulties, antenna diversity could significantly help by providing additional processing gain. The performance of diversity methods is characterized by diversity gain (Goldsmith 2005) indicating the increase in the average signal to noise ratio (*SNR*) due to the diversity technique. The two most common diversity methods used in GNSS applications are spatial and polarization diversity. In the polarization diversity, two antennas with right hand circular polarization (RHCP) and left hand circular polarization (LHCP) using different signal combination methods such as equal gain combining (EGC) and estimator correlator (EC) are utilized to enhance the GNSS signal detection performance in indoor environments (Zaheri et al 2009). Furthermore, spatial antenna diversity in which two antennas are separated by at least half of a wavelength can be used to receive approximately independent

signals. Sadrieh (2011) has utilized two antennas in order to achieve spatial diversity and the signals were combined based on equal gain combining and selection combining (SC) methods. A good comparison between detection performance of polarization and spatial diversity for indoor GNSS applications is reported by Zaheri et al (2010). It has been shown that considering a specific detection target point, the average diversity gains for circular polarization and spatial diversity are 4.3 dB and 3.2 dB, respectively. Sadrieh (2012) considered another signal combination method, namely weighted diversity combining, and analyzed its signal detection and parameter estimation performance for the spatial antenna diversity system.

1.1.3 Antenna Diversity in the acquisition

Having multiple antennas mounted on a GNSS receiver improves the signal acquisition performance in terms of detection probability and mean acquisition time. Broumandan et al (2011) investigated the detection performance of GNSS signals utilizing a moving antenna which can provide spatial diversity gain. In wireless communication there are a few contributions on the code acquisition of a direct-sequence spread-spectrum signal with antenna diversity. For instance, Rick & Milstein (1997) presented parallel code acquisition using antenna diversity for both frequency-nonselective and frequency-selective fading channels for the case of cellular communications systems. Serial search based code acquisition using multiple transmit/multiple receive antennas has been analyzed by Won & Hanzo (2008). Puska & Iinatti (2009) utilized a beam

forming technique to combine the signals and then passed it through the acquisition strategies including maximum selection and serial search based code acquisition. A new code acquisition method based on fuzzy adaptive detectors that combine antenna diversity techniques and a hybrid search strategy has been studied by Aissaoui & Hammoudi (2009). Shin & Lee (2002) considered code acquisition in the frequency selective fading channel using multiple antennas divided into several groups and highlighted a trade-off between the combining gain and search time.

1.2 Limitations of Previous Work

In the background section some previous research on the acquisition and antenna diversity was presented. In terms of acquisition, there are some significant contributions which have improved weak signal acquisition performance (O'Driscoll 2008, Shanmugam et al 2007, Fallahin et al 2012) by increasing the integration time. However, they only considered the cell level acquisition performance. A few contributions investigated the decision domain acquisition and evaluated the acquisition performance by considering all the cells in the search space (Borio 2008) but none utilized the antenna diversity technique. There are some contributions on the antenna polarization diversity and spatial diversity utilizing multiple antennas to improve the signal detection performance (Zaheri et al 2009, Sadrieh 2011). In these two papers, only one cell detection was analysed with the assumption that the acquisition process was complete and therefore the correct cell was known. In other words, they

have not evaluated the entire search space using antenna diversity. In wireless communication, Rick et al (1997) and Lee et al (2002) investigated code acquisition with multiple antennas. However, they did not have any concern about the weakness of the signal which is one of the main issues in GNSS signals. In these papers the search space was one dimensional in code delay only.

1.3 Objectives and Contribution of this Thesis

The cell level evaluation does not represent the signal acquisition performance. In order to make a reliable decision about the signal presence, all the candidate cells in the uncertainty region should be considered. This leads to overall performance evaluation in terms of detection and false alarm probabilities. This research proposes a spatial antenna diversity scheme using two antennas in multipath fading situations. Based on an equal gain combining method, the received signals at the two antennas are combined at the correlator output level. In addition to cell and system level ROC curves, acquisition time is thoroughly investigated. Acquisition time as a random variable is characterized by mean and variance values. Mean acquisition time does not provide any information about the acquisition time variation that can be caused by *SNR* variations due to noise and fading effects. In a multipath fading channel due to the significant change in the signal strength, variation of the acquisition time in different time intervals is noticeable. In fact, C/N_0 drops due to the fading and consequently longer time is required to acquire the signal while if fading does not occur, the acquisition

process can be performed faster. Hence, the variance of the acquisition becomes a principal metric that should be taken into account. This research provides lower bound estimation for the variance of acquisition time in a Rayleigh fading channel using fading statistics.

In order to have a minimum mean acquisition time, optimal combination methods of coherent and non-coherent integrations considering different C/N_0 values are analyzed. This is based on the fact that increasing the integration time on one hand enhances the detection probability which results faster acquisition; on the other hand, since more samples are processed and a larger search space should be evaluated when increasing the coherent integration time, acquisition time increases.

In summary, the main goal of this research is to assess the entire acquisition search space and find the overall detection probability, that of false alarm and acquisition time using antenna diversity in weak and faded signal situations.

In order to evaluate the diversity performance, the results obtained after the diversity combining are compared with the single antenna results in terms of the ROC curves and acquisition time. Furthermore, the acquisition methods are applied to real GPS data (IF samples) collected in different indoor environments. The theoretical results are verified using Monte Carlo simulations and associated results are compared with the real data results.

1.4 Thesis outline

Chapter 2 discusses GNSS signal acquisition and starts with the GPS L1 signal structure. Afterwards, the serial and parallel (in code or Doppler) acquisition process is described. Different signal combining methods such coherent, non-coherent and differentially coherent integrations are investigated. Furthermore, the alternating half bits method which mitigates the bit transition problem is assessed and its performance is compared with the non-coherent integration method. After distinguishing between cell and system level acquisition, different search strategies including serial, hybrid and maximum search strategy are evaluated. The ROC curves at the cell and system levels of acquisition are considered as the performance evaluation metrics in this chapter.

Chapter 3 investigates the acquisition time in terms of mean and variance values. Furthermore, impact of detection threshold on the acquisition time is assessed. Assuming cold start acquisition, optimal combinations of the coherent and non-coherent integrations which minimize the mean acquisition are addressed.

Chapter 4 describes the fading channel and the diversity system. The Rayleigh and Rician fading channels along with their parameters are explained. Different spatial diversity combining methods including equal gain combining (EGC), selection combining (SC) and maximal ratio combining are introduced but EGC is adopted for further analyses. The detection probability expression in the Rayleigh

fading channel is provided. After applying EGC and assuming uncorrelated channels in two branches, acquisition metrics are evaluated.

Chapter 5 verifies the theoretical results presented in the previous chapters using Monte Carlo simulations and compares associated results with the real data results. This chapter describes the test setup for the real GPS data collection and the correlator design and the method of combining received signals. The performances of diversity combining in terms of ROC curves, diversity gain, mean and variance of the acquisition time are compared to those of single branches using real GPS data and Monte Carlo simulations.

Chapter 6 presents the conclusions and provides recommendations for future work.

Chapter Two: GNSS Signal Acquisition

Since the main focus of this work is GNSS signal acquisition, this chapter introduces the particular GNSS signal studied, different methods of acquisition, and the relevant acquisition performance evaluation metrics.

2.1 GPS L1 signal structure

The GPS L1 C/A signal is transmitted on the carrier frequency of 1575.42 MHz with a main lobe bandwidth of 2.046 MHz. In order to have better immunity against ionospheric effects, it is transmitted using Right Hand Circular Polarization (RHCP). In circular polarization, electric and magnetic fields have a constant strength but their direction rotates clockwise (right hand) or counterclockwise (left hand) .The nominal received signal power for users on or near the surface of the Earth is about -158.5 dBW. Code division multiple access (CDMA) is used in order to avoid intersystem interference in the multiple access scenarios. The signal is modulated with a pseudorandom code using Binary Phase Shift Keying (BPSK). The pseudorandom code is the gold code which is generated using a linear-feedback shift register. The length of the gold code is 1023 chips with a chipping rate of 1.023 MHz, resulting in a 1 ms code period. Another component of the GPS L1 signal is the navigation message which includes orbital parameters for the satellite and is transmitted with 50 Hz rate. This means each period of the navigation message lasts 20 ms. In summary, the signal L1 C/A transmitted from the satellite can be modeled as follows:

$$s(t) = A \times c(t) d(t) \sin(2\pi f_{L1}) \tag{2-1}$$

where A is the signal amplitude, $c(t)$ is the ranging code, $d(t)$ is the navigation data and f_{L1} is the L1 carrier frequency.

2.1.1 Ranging code

The GPS L1 C/A ranging code, which is based on BPSK modulation, has specific autocorrelation and cross correlation properties that allows multiple access to the communication channel. The autocorrelation function of the ranging code is shown in Figure 2-1.

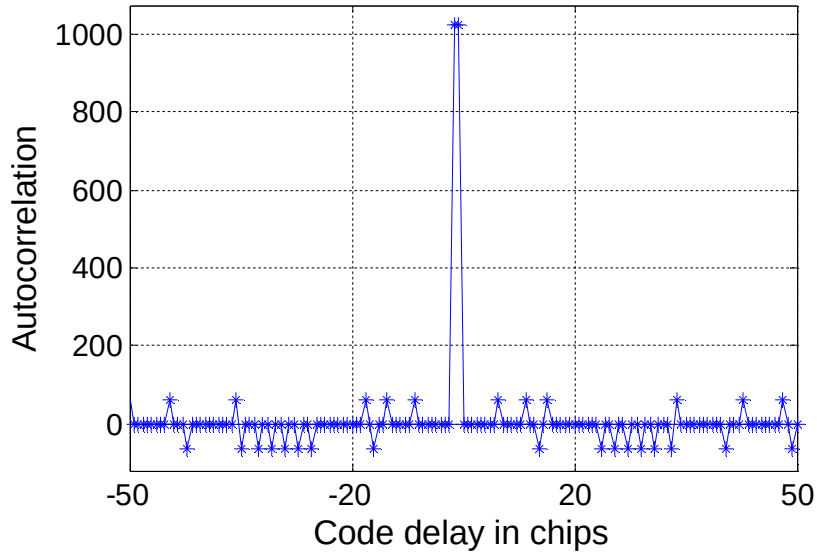

Figure 2-1: Autocorrelation of GPS L1 C/A code for PRN 12

The BPSK subcarrier modulation controls the autocorrelation shape and has the following autocorrelation and power spectral density (PSD):

$$x_{BPSK}(t) = \begin{cases} 1 & 0 \le t \le T_C \\ 0 & \text{else} \end{cases} \tag{2-2}$$

where x_{BPSK} is the BPSK subcarrier and T_C is the code chip duration which is the inverse of the chipping rate. Therefore, $T_C = 1/1.023\ \mu s$.

$$R_{BPSK}(\tau) = \int_{-\infty}^{\infty} x_{BPSK}(t)x_{BPSK}(t-\tau)\ dt = tri(\frac{t}{T_C}) = \begin{cases} 1-|t| & \text{-}T_C \le \text{t} \le T_C \\ 0 & \text{else} \end{cases} \quad (2\text{-}3)$$

$$S_{BPSK}(f) = F[R_{BPSK}(\tau)] = \left[\frac{\sin(\pi f T_C)}{\pi f}\right]^2 = {T_C}^2 \text{sinc}^2(fT_C) \quad (2\text{-}4)$$

where R_{BPSK} and S_{BPSK} are the autocorrelation function and the power spectral density respectively, $F[.]$ is the Fourier transform operation and $\text{sinc(x)} = \frac{\sin(\pi x)}{\pi x}$.

The cross correlation protection of GPS L1 C/A code is defined as

$$\text{Protection} = 20\log(\frac{\max\{\text{code autocorrelation}\}}{\max\{\text{code cross-correlation}\}}) \quad (2\text{-}5)$$

Thus, the gold code cross correlation protection is equal to: $20\log(\frac{1023}{65}) \approx 24$ dB.

The autocorrelation shape and PSD are depicted in Figure 2-2 and 2-3.

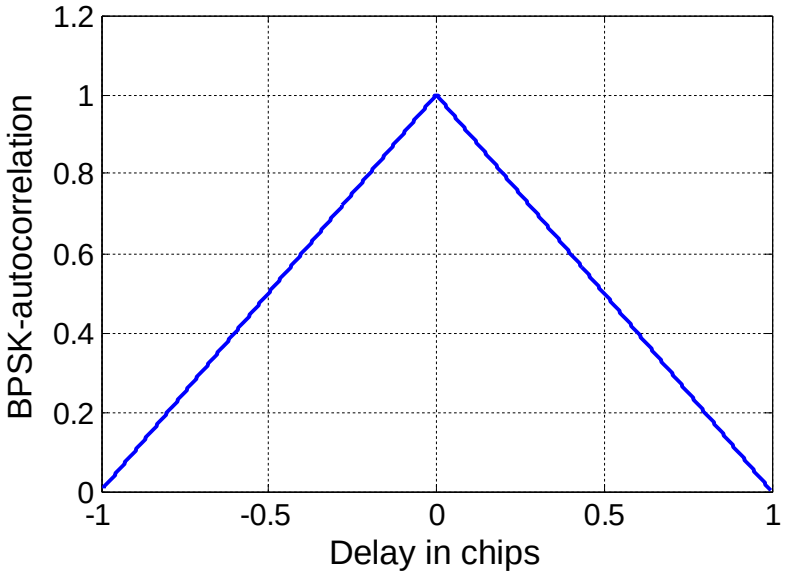

Figure 2-2: BPSK autocorrelation

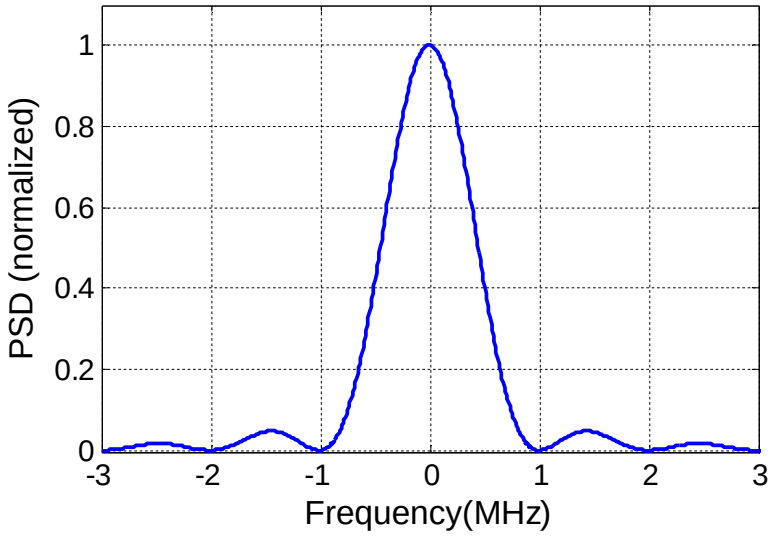

Figure 2-3: Power spectral density for BPSK

2.2 GNSS signal acquisition

Signal acquisition is the first operation stage of a GPS receiver that detects the presence of GNSS signals and provides a coarse estimate of the code delay (τ)

and Doppler frequency (f_d). The incoming signal is correlated with local replicas generated over the code delays and a range of Doppler frequencies and correlator output values are assigned to corresponding cells in a search area. The process is also called despreading. The signal is detected and its parameters (τ, f_d) are estimated if the amplitude of the correlator output in the correct cell passes a detection threshold. The i^{th} correlator output can be expressed as

$$S(\tau_i, f_{d,i}) = \sum_{n=1}^{N} r(n)c(n-\tau_i)\exp\{-j2\pi n f_{d,i}\} \quad (2\text{-}6)$$

where $r(n)$ is the incoming signal, $c(n-\tau_i)$ is local code replica, $f_{d,i}$ is Doppler frequency and $N = (T_{coh} \times F_s)$, is the number of samples which is directly proportional to the coherent integration time (T_{coh}) and the sampling frequency (F_s). The entire set of correlator outputs for different code delays and Doppler frequencies is defined as the Cross Ambiguity Function (CAF) and is expressed as

$$S = \{S(\tau_i, f_{d,i}), \text{ for all i}\} \quad (2\text{-}7)$$

The received signal transmitted from the k^{th} satellite can be modeled as

$$r_k(t) = A \times c(t-\tau)d(t-\tau)\cos(2\pi(f_{L1}+f_d)t+\phi) + n(t) \quad (2\text{-}8)$$

where ϕ is the phase of the received signal and $n(t)$ represents the noise.

Figure 2-4 shows the main parts of the acquisition process. Figure 2-5 and 2-6 illustrate the search space and the correlator outputs. The acquisition process may also have a verification stage that evaluates the candidate correct cell

several times in order to enhance the detection probability and reduce the number of false alarms, but this stage is not considered in this research.

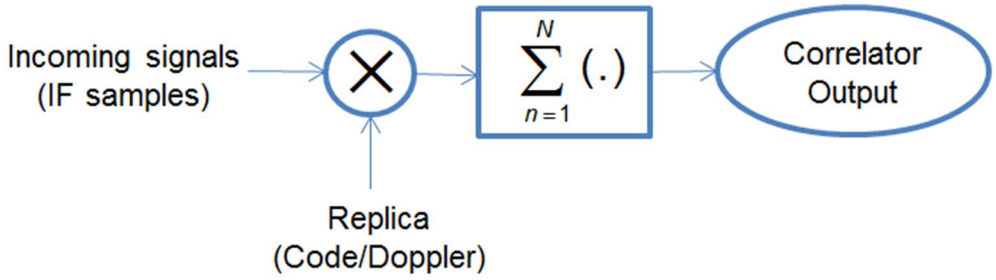

Figure 2-4: Acquisition scheme

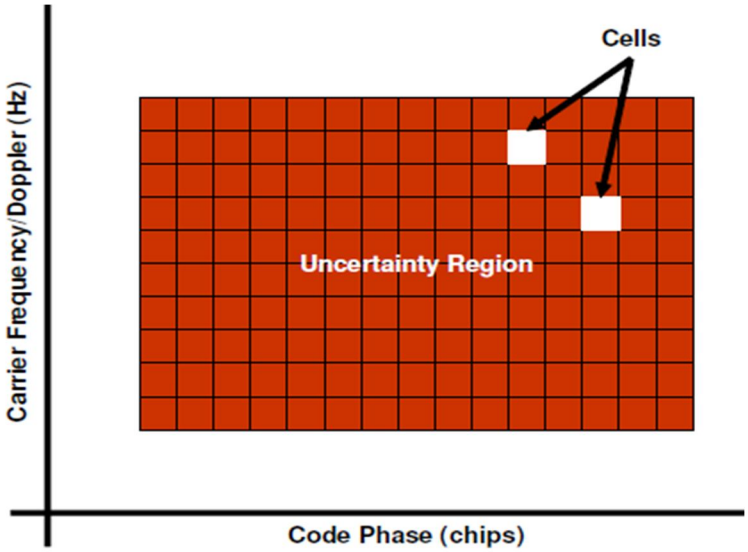

Figure 2-5: Acquisition search space (after O'Driscoll et al 2008)

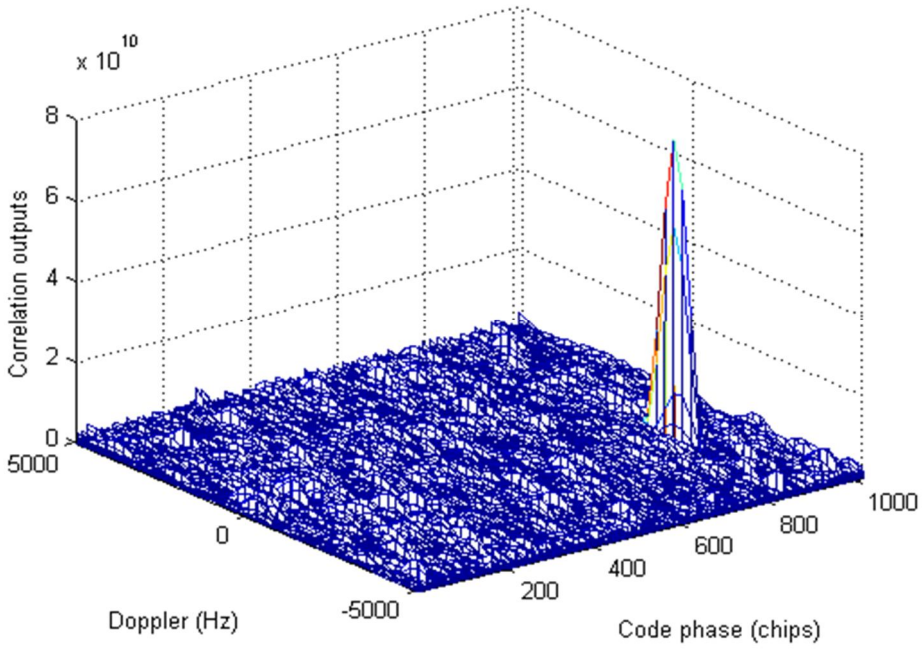

Figure 2-6: Cross ambiguity function (CAF)

2.2.1 Search space

The size of the search space which consists of code and Doppler bins depends on the code and Doppler search resolutions. Any code or frequency mismatch causes a certain amount of power loss compared to the maximum value of CAF. Hence, code and Doppler bin sizes are set in order to guarantee that the maximum power loss due to mismatch does not exceed a specific acceptable loss value. Consider δf and $\delta\tau$ the frequency and code delay error, the power loss due to the frequency (L_f) and code (L_c) mismatches can be expressed as (O'Driscoll 2007)

$$L_f = \left| \frac{\sin(\pi.\delta f.NT_s)}{\pi.\delta f.NT_s} \right|^2 \tag{2-9}$$

$$L_c \approx \left| R(\delta\tau) \right|^2 \tag{2-10}$$

where $R(\delta\tau)$ is the autocorrelation function and its shape depends on the modulation (BPSK in GPS L1).The maximum acceptable errors are generated when the bin sizes during the search process are set to twice the error. Then one has

$$\Delta f_d = 2 \times \delta f \tag{2-11}$$

$$\Delta \tau = 2 \times \delta \tau \tag{2-12}$$

where Δf_d and $\Delta \tau$ are the frequency and code delay bin sizes. It is important to note that the Doppler bin size is inversely proportional to the coherent integration time ($T_{coh} = NT_s$) and by increasing T_{coh}, smaller Doppler bins should be considered.

The number of code and Doppler bins in the search space can be written as

$$N_C = \frac{Code\ Length}{\Delta \tau} \tag{2-13}$$

$$N_D = \left\lceil \frac{Doppler\ Range}{\Delta f_D} \right\rceil \tag{2-14}$$

The code length of the GPS L1 C/A signal is 1023 and based on the satellite velocity, the Doppler values range approximately between -5 KHz to 5 KHz. Finally, the total number of cells in the search space (M) is equal to

$$M = N_D \times N_C \tag{2-15}$$

There are different methods of correlator output generation and CAF evaluation described in the next section.

2.2.2 Time domain acquisition (Serial acquisition)

In this method the acquisition process is performed cell by cell and for each code delay and Doppler values the correlator output is generated serially. The serial acquisition has a simple implementation but it is a slow process as it searches over the search space cell by cell.

2.2.3 Parallel code acquisition

Parallel code acquisition is a fast and efficient acquisition method based on the Fast Fourier Transform (FFT) algorithm. In this method the serial search over the code bins is not required. Instead, by utilizing FFT in code for each specific Doppler bin, the entire row of the search space (which includes different delays but the same Doppler) is evaluated in one attempt. This speeds up the acquisition but is complex in terms of implementation. The details of parallel code acquisition are shown in Figure 2-7.

The correlator outputs for a specific Doppler bin can be written as follows:

$$S_i(\tau, f_{d,i}) = IFFT\{FFT(r[n]\exp\{-j2\pi n f_{d,i}\}) \times FFT\{c[n]\}^*\} \quad (2\text{-}16)$$

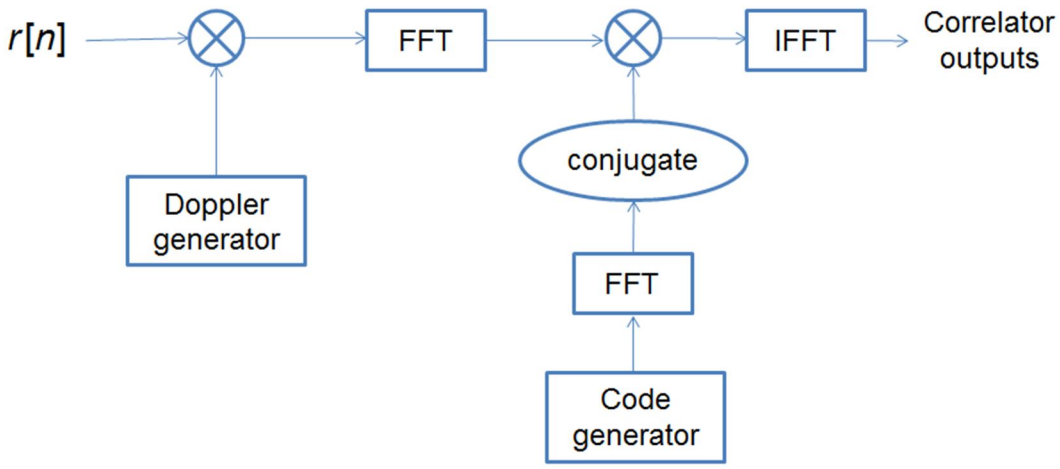

Figure 2-7: Parallel code acquisition

2.2.4 Parallel frequency acquisition

In parallel frequency acquisition for each code bin, the output of FFT is a column of search the space including Doppler frequencies. This method is time demanding due to the wide frequency range and the step-by-step search over the code bins. For the GPS L1 C/A code, considering half chip spacing, a search over 2046 code bins is required. In addition, the Doppler frequency range is typically limited to (-5 KHz to 5 KHz). In order to reduce the search space, pre-filtering {integrates the signal over a certain number of samples and then outputs the one averaged value (integration and dump)} can be applied but it causes slight power degradation (Borio 2008). The parallel frequency acquisition block diagram is shown in Figure 2-8.

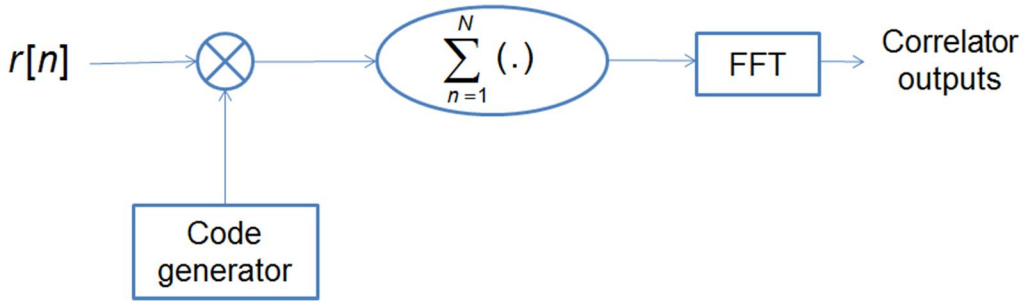

Figure 2-8: Parallel frequency acquisition

2.2.5 Signal combining methods

Different methods of signal combining at the correlator output level can be used to find the final decision variable that should be compared with the detection threshold. Coherent, non-coherent and differentially coherent integrations are the most common methods.

2.2.5.1 Coherent integration

In the coherent integration method, the outputs of the correlators are coherently combined and the result is compared with the detection threshold to determine if the GNSS signal is present. The decision variable is defined as

$$Y = \left|S_i(\tau_i, f_{d,i})\right|^2 = \left|\sum_{n=1}^{N} r(n)c(n-\tau_i)\exp\{-j2\pi n f_{d,i}\}\right|^2 \qquad (2\text{-}17)$$

where N is the number of samples used in coherent integration and $r(n) = Ac(n-\tau)d(n-\tau)\exp\{-j2\pi n f_d + \phi\} + n(n)$.

Obviously, by increasing T_{coh} one can obtain more processing gain. The reason is that during coherent integration, uncorrelated noise is reduced compared to

the signal which remains correlated over the integration. However, T_{coh} is limited due to the navigation bit transition. During acquisition, the location of the navigation bit boundary is unknown and if coherent integration crosses a bit-transition with a sign change, the subsequent outputs will have opposite sign and add destructively. This could happen any time in the coherent integration process (even for T_{coh}=1 ms). Hence, choosing any coherent integration time is vulnerable to power loss due the navigation bit transition.

2.2.5.1.1 Statistical analysis

During detection, two hypotheses are considered, H_0 where only noise is present and H_1 where both signal and noise are present. The decision variable obtained from coherent integration can be written based on in-phase (S_I) and quadrature (S_Q) components as follows:

$$S_i(\tau, f_d) = S_I + jS_Q \tag{2-18}$$

Under the H_0 hypothesis, S_I and S_Q have a Gaussian distribution as

$$\begin{cases} S_I\big|_{H_0} \sim N(0, \sigma_n^2) \\ S_Q\big|_{H_0} \sim N(0, \sigma_n^2) \end{cases} \tag{2-19}$$

where $N(0, \sigma_n^2)$ represents the zero mean Gaussian distribution and σ_n^2 is the noise variance. Under H_1, one has (Borio 2008)

$$\begin{cases} S_I\big|_{H_1} \sim N(A \times \cos\phi_0, \sigma_n^2) \\ S_Q\big|_{H_1} \sim N(A \times \sin\phi_0, \sigma_n^2) \end{cases} \tag{2-20}$$

As a result, $Y = S_I^2 + S_Q^2$ has the following distributions:

$$\begin{cases} Y\big|_{H_0} \sim \chi_2^2(0,\sigma_n^2) \\ Y\big|_{H_1} \sim \chi_2^2(A^2,\sigma_n^2) \end{cases} \tag{2-21}$$

where χ_K^2 is the chi-square distribution with K degrees of freedom and can be written as

$$f(x,K,\sigma^2) = \frac{\left(x/\sigma^2\right)^{(K/2)-1} e^{\frac{-x}{2\sigma^2}}}{\sigma^2 2^{K/2}\Gamma(\frac{K}{2})} \quad , \; x \geq 0 \tag{2-22}$$

where $\Gamma(t) = \int_0^\infty x^{t-1}e^x \, dx$ and $\Gamma(n) = (n-1)!$ for $n \in \mathbb{N}$. According to Kay (1998), the detection and false alarm probabilities are computed as

$$P_{fa} = \int_\beta^\infty f_{Y|H_0}(y) \, dy \tag{2-23}$$

$$P_d = \int_\beta^\infty f_{Y|H_1}(y) \, dy \tag{2-24}$$

where $f_{Y|H_1}(y)$ and $f_{Y|H_0}(y)$ are the probability density functions (PDF) of Y under the H_1 and H_0 conditions and β is the detection threshold. Considering the deterministic signals whose values are completely specified for any given time, for the coherent integration method P_{fa} and P_d become (Kay 1998, Borio 2008)

$$P_{fa}(\beta) = e^{-\frac{\beta}{2\sigma_n^2}} \tag{2-25}$$

$$P_d(\beta) = Q_1(\sqrt{SNR_{coh}}, \sqrt{\frac{\beta}{\sigma_n^2}}) \quad (2\text{-}26)$$

where Q_K is Marcum Q-function (Cantrell 1987), σ_n^2 is the noise variance in the coherent integration process and SNR_{coh} is the coherent signal to noise ratio (*SNR*) value which is related to the carrier to noise ratio (C/N_0) as follows (Borio 2008):

$$SNR_{coh} = 2T_{coh} \times C/N_0 \quad (2\text{-}27)$$

2.2.5.2 Non-coherent integration

In this method, the combiner accumulates the square magnitude of *K* consecutive correlator outputs. By doing this, phase information is lost so longer integration times can be used without any concern about the bit transition. Nevertheless, this method suffers from squaring loss due to an increase in the noise power (noise is not zero mean anymore) but still it improves the *SNR* although the improvement is not as much as that of coherent integration. Unlike the coherent integration method, where the Doppler bin size should be reduced by increasing the coherent integration time, in non-coherent integration the size of the bins does not change by increasing the number of non-coherent integrations for a fixed coherent integration time. Hence, for a specific integration time, the non-coherent integration has a smaller search space compared to coherent integration.

Considering *K* non-coherent integrations and assuming no bit transition during the coherent integration process, one has

$$Y = \sum_{i=1}^{K} \left| S_i(\tau, f_D) \right|^2 \tag{2-28}$$

$$\begin{cases} Y\big|_{H_0} \sim \chi^2_{2K}(0, \sigma_n^2) \\ Y\big|_{H_1} \sim \chi^2_{2K}(KA^2, \sigma_n^2) \end{cases} \tag{2-29}$$

$$P_{fa} = e^{\frac{-\beta}{2\sigma_n^2}} . \sum_{i=0}^{K-1} \frac{1}{i!} \left(\frac{\beta}{2\sigma_n^2} \right)^i \tag{2-30}$$

$$P_d = Q_K\left(\sqrt{K \times SNR_{coh}}, \sqrt{\frac{\beta}{\sigma_n^2}} \right) \tag{2-31}$$

2.2.5.3 Differentially coherent integration

The main difference between the differentially coherent (DC) and the non-coherent integration is that in DC, phase information is not lost and differential phase information remains. Hence, noise terms in the correlator outputs remain uncorrelated and, compared to the signal power, it is reduced over the integration. As a result, DC outperforms non-coherent integration especially in weak signal situations. The final CAF can be written as follows (Borio 2008):

$$Y = \mathrm{Re}\{ \sum_{i=1}^{L} S_{2i-1}(\tau, F_D) . S_{2i}^*(\tau, F_D) \} \tag{2-32}$$

where *2L* is the total number of CAF obtained from coherent integration that are then combined. For the differentially coherent integration, there is a closed form expression for false alarm probability but finding the detection probability is

complicated and it has been reported in an approximation form (Rodriguez 2004, O'Driscoll 2007).

Alternating half bits method

The alternating half bits method was presented by Psiaki et al (2001) in order to eliminate the bit transition problem. This method is very similar to non-coherent combining but it does not accumulate all the squared correlator outputs as is normally done in non-coherent combining. Instead, these are divided into two groups, namely odd and even and the accumulation is applied to each of these groups separately. The group that has a higher value is considered as the final CAF. In the presence of the signal the destructive effect of bit transition is removed. The CAF, which can be used as the decision variable, is written as

$$Y = \underset{Y_{EO}}{\arg}(\max\{\max\{Y_E\},\max\{Y_O\}\}) \tag{2-33}$$

where $Y_{EO} = \{Y_E, Y_O\}$, $Y_O = \sum_{i=1}^{K} \left|S_{2i-1}\right|^2$ and $Y_E = \sum_{i=1}^{K} \left|S_{2i}\right|^2$ and Y could be either Y_O or Y_E.

Note that when data bit assistance is not available, in the acquisition stage T_{coh} is usually limited to at most 10 ms to limit the possibility of coherent integration across a data bit boundary. For instance, consider 20 ms data samples divided into two 10 ms sections; since the maximum number of navigation bit transition during every 20 ms is one, at least one of the 10 ms parts is free of bit transition. As a result, this part (10 ms) is almost immune to the destructive effect of bit

transition and the coherent integration time can be easily increased up to 10 ms in this part of data. Due to the higher processing gain achieved from coherent integration, the corresponding CAF has higher power than the other part and is selected as the decision variable (*Y*).

2.2.5.4 Comparison between non-coherent integration and alternating half bits methods

In this section non-coherent and alternating methods are compared in terms of the detection probability.

The main advantage of using alternating half bits method is that the intervals used in the integration are free of bit transition but obviously half of the observations are lost. However, non-coherent combining uses all the observations but in some of them bit transition may occur which diminish the post processing *SNR*. Simply put, the performance of non-coherent combining depends on the location of bit transition occurrence in the coherent integration process. If bit transition takes place in the middle of an interval, the coherent integration part of non-coherent combining does not provide any processing gain and in fact only noise is added to the result. However, if the bit transition happens at the beginning or end of the interval, coherent integration provides some processing gain. Since in the GPS L1 C/A signal the length of the navigation data is 20 ms, in order to obtain the highest processing gain, the coherent integration time can be set to 10 ms during the unaided acquisition process. In this case, by applying the alternating half bits method at each interval the 10 ms coherent integration without any bit transition provides a considerable processing gain.

Here, the comparison between the non-coherent integration and alternating methods is based on 10 ms coherent integration time.

Assuming that the total number of non-coherent integrations is *2K*, only half of the observations (which is equal to *K* non-coherent integrations) are used in the alternating method. The detection and false alarm probabilities are expressed as follows:

For the alternating method,

$$P_{fa,alt} = e^{\frac{-\beta_{alt}}{2\sigma_n^2}} . \sum_{i=0}^{K} \frac{1}{i!} (\frac{\beta_{alt}}{2\sigma_n^2})^i \tag{2-34}$$

$$P_{d,alt} = Q_K (\sqrt{K \times SNR_{coh}} \ , \ \sqrt{\frac{\beta_{alt}}{\sigma_n^2}}) \tag{2-35}$$

where $P_{fa,alt}$ and $P_{d,alt}$ represent the false alarm and detection probabilities in the alternating method.

For the non-coherent integration method with the possibility of bit transition occurrence during the coherent integration part,

$$P_{fa,non} = e^{\frac{-\beta_{non}}{2\sigma_n^2}} . \sum_{i=0}^{2K} \frac{1}{i!} (\frac{\beta_{non}}{2\sigma_n^2})^i \tag{2-36}$$

$$P_{d,non} = Q_{2K} (\sqrt{K.SNR_{coh} + \sum_{i=1}^{K} SNR_i} \ , \ \sqrt{\frac{\beta_{non}}{\sigma_n^2}}) \tag{2-37}$$

where $\sum_{i=1}^{K} SNR_i$ is the total *SNR* in the intervals which bit transition might occur. Assuming a ratio factor, $\alpha = \frac{\sum_{i=1}^{K} SNR_i}{K.SNR_{coh}}$, the previous equation can be rewritten as

$$P_{d,non} = Q_{2K}(\sqrt{(1+\alpha)K.SNR_{coh}}\ ,\ \sqrt{\frac{\beta_{non}}{\sigma_n^2}}) \tag{2-38}$$

The ROC curve, which plots P_d versus P_{fa} will show which method has a higher detection probability for a give false alarm probability.

Now, one can try to find the minimum value of α ($\alpha_{\min}$) that satisfies the following inequality:

$$P_{d,non} \geq P_{d,alt} \tag{2-39}$$

where $\alpha_{\min}$ indicates the minimum required ratio between the *SNR* obtained in the intervals where bit transitions may occur and the ones that are free of bit transition so that non-coherent integration outperforms the alternating method. This simply means that for $\alpha \geq \alpha_{\min}$, adding all the non-coherent components improves the detection probability more than the alternating method. It is important to note that $\alpha_{\min}$ depends on the C/N_0 value. The minimum ratio factor versus C/N_0 for $T_{coh} = 10$ ms, $K = 3$ and $P_{fa} = 10^{-6}$ is shown in Figure 2-9.

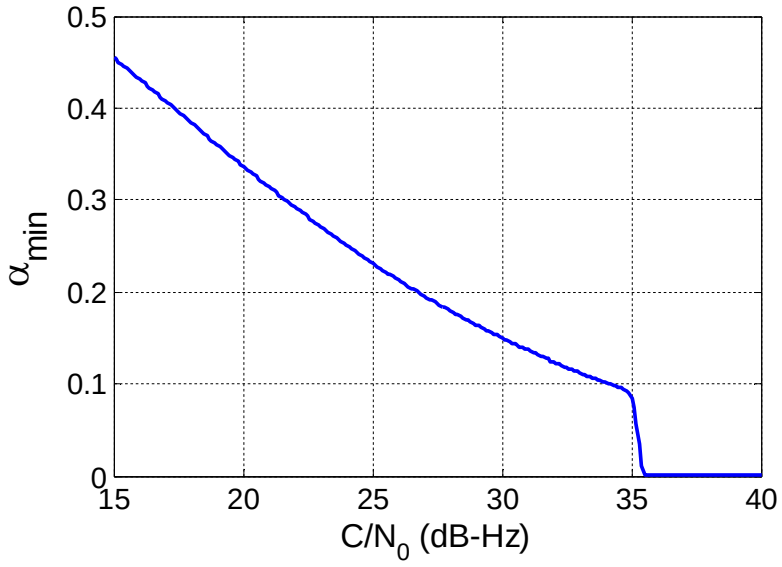

Figure 2-9: Minimum Ratio factor versus C/N_0

The proposed modified method which combination of both non-coherent and alternating method is now described:

Considering that Y_{alt} is defined in Eq. (2-33), $Y_{non} = Y_O + Y_E$ and $1+\alpha = \dfrac{\max\{Y_{non}\}}{\max\{Y_O, Y_E\}}$,

$$Y_c = \begin{cases} Y_{alt} & \alpha < \alpha_{\min} \\ Y_{non} & \alpha \geq \alpha_{\min} \end{cases} \tag{2-40}$$

Clearly, using Y_c improves the detection probability compared to non-coherent and alternating methods separately.

2.2.6 Performance evaluation

This section describes the acquisition performance evaluation metrics with focus on the detection and false alarm probabilities.

2.2.6.1 Cell level and system level acquisition

In cell level acquisition, only the detection performance of a single cell is evaluated and the decision variable is compared with the detection threshold (β). The probability of false alarm (P_{fa}) and detection (P_d) associated with the threshold can be calculated in the cell level but since the acquisition is a process over an uncertainty region including several cells, this level of acquisition does not entirely evaluate the acquisition performance. In the previous section cell level probabilities were computed. System level acquisition considers the entire uncertainty region of the search space and shows the overall performance of acquisition. Similar to the cell level, the overall false alarm probability (P_{FA}), overall detection probability (P_D) and furthermore the probability of missed detection (P_{MD}) are defined in this case. Herein missed detection is defined slightly differently than the traditional definition and means that neither signal nor noise are detected. Although cell and system level acquisition metrics are related, they are not the same. In other words, two acquisition systems may have the

same cell level characteristics but different system level performance (Borio 2008). The three main search strategies used in GNSS acquisition are serial, hybrid and maximum search (Baum 1994, Borio et al 2008). The impact of the search strategies on the acquisition performance appears in the overall detection and false alarm probabilities as well as the mean acquisition time.

The overall false alarm probability can be defined differently with respect to the presence or absence of the signal, indicated as P_{FA}^{p} and P_{FA}^{a} respectively. In the absence of the signal, false alarm occurs if the noise amplitude at any cells of the search space exceeds the detection threshold. In the presence of the signal, in order to have a false alarm, noise amplitude in an incorrect cell not only should pass the detection threshold but also should exceed the amplitude of the signal that is detected in the correct cell (in the maximum search strategy). P_{FA}^{a} only depends on the detection threshold and noise power. Since in general there is no a priori information about the presence of the signal, this definition is the best criterion for the detection threshold setting in the receiver. If the signal is present, the real overall false alarm that the receiver experiences is a function of the detection threshold and P_D, which is related to *SNR*.

2.2.6.1.1 Maximum search

In the maximum search strategy, correlator outputs or similarly the CAF is computed in all cells of the search space and the maximum one that passes the

threshold represents the coarse estimate of code phase and Doppler frequency. One has (Corazza 1996, Borio 2008)

$$P_{FA}^{a} = 1-(1-P_{fa}(\beta))^{M} \tag{2-41}$$

$$P_{MD} = (1-P_{fa}(\beta))^{M-1} \times (1-P_{d}(\beta)) \tag{2-42}$$

$$P_{D}(\beta) = \int_{\beta}^{+\infty} [1-P_{fa}(x)]^{M-1} f(x|H_1)\, dx \tag{2-43}$$

$$P_{FA}^{p} = 1-P_{D}-P_{MD} \tag{2-44}$$

where $M = (N_D \times N_C)$ is the total number of cells in the uncertainty region of the search space, and N_D and N_C are the total number of Doppler and code bins respectively.

It is important to note that the false alarm probability in the absence of the signal and the probability of missed detection are independent of signal power as well as the search strategy. Therefore, P_{FA}^{a} and P_{MD} expressions hold for all the strategies.

2.2.6.1.2 Serial search

This strategy evaluates the CAF cell by cell and once a correlator output passes the threshold the search stops and the estimated code and Doppler are declared. Using this search strategy the overall detection probability is expressed as

$$P_D = \frac{1-[1-P_{fa}]^M}{MP_{fa}} \times P_d \tag{2-45}$$

Although the serial search requires the minimum computational load; as it does not need to search over the entire search space, it is more vulnerable to the false alarms due to not evaluating the entire search space. On the other hand, the maximum search has the best performance in term of correct detection but it is more computationally demanding.

2.2.6.1.3 Hybrid search

In this strategy the CAF is evaluated row by row or column by column and its maximum value in each row or column is compared with the threshold in order to find the appropriate cell. Hybrid search is used in the FFT-based acquisition algorithms. The overall detection probability for parallel code acquisition becomes

$$P_D(\beta) = \frac{1}{N_D} \times \frac{1-[1-P_{fa}]^M}{1-[1-P_{fa}]^{N_C}} \times \int_{\beta}^{+\infty} [1-P_{fa}(x)]^{N_D-1} f(x|H_1)\, dx \tag{2-46}$$

2.2.6.2 ROC curves

The ROC curve that shows the detection probability versus the probability of false alarm can be presented in both the cell and system level acquisition. Cell level ROC deals with the cell level detection and false alarm probabilities while the system level ROC represents the overall probabilities.

Figure 2-10 shows the cell level ROC curves for the coherent, non-coherent and differentially coherent integrations considering 2 ms integration time. It is

assumed that during the coherent integration, bit transition does not occur. The considered parameters are as follows:

T_{int} = 2 ms for all cases

T_{coh} = 1 ms for non-coherent and differentially coherent integrations

K=2 and *L*=1 for non-coherent and differentially coherent cases respectively

C/N_0 = 35 dB-Hz

As it can be seen, for a given P_{fa}, the detection performance of DC is higher than non-coherent integration and is slightly lower than coherent integration. Non-coherent integration has the highest noise power compared to signal, which leads to the lowest detection performance. However, since the coherent integration is limited by the navigation data bit transition, in weak signal situations the non-coherent integration is the most practical method.

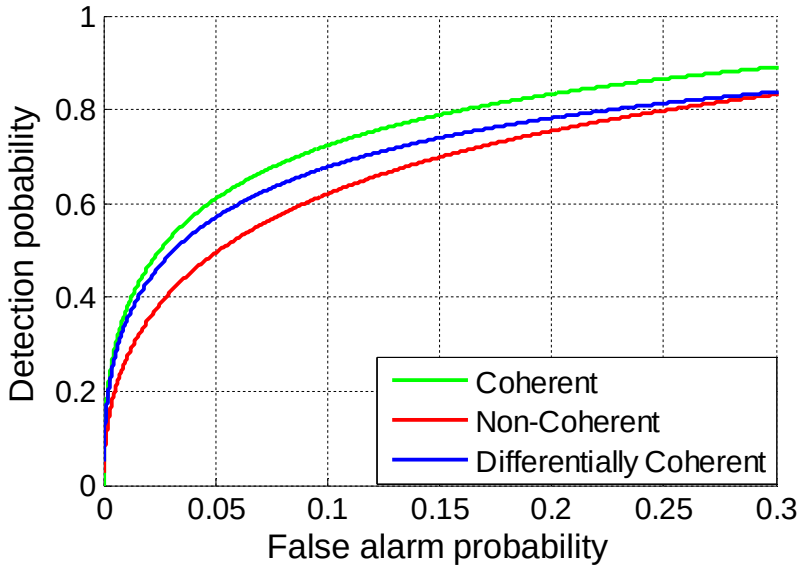

Figure 2-10: Cell level ROC curves- C/N_0=35 dB-Hz

Figure 2-11 highlights the difference between overall false alarm probability in the absence and presence of the signal for different *SNR* values assuming 1 ms coherent integration time. Hence, the total number of cells is the same for all cases. As shown in the figure, overall false alarm probability decreases as the signal becomes stronger.

Figure 2-12 compares the three different search strategies in terms of system level ROC curves. The result is based on 1 ms coherent integration time and C/N_0 = 40 dB-Hz. Note that, in this figure, the overall false alarm probability is computed in the absence of signal. As expected the maximum search strategy has better performance than the other strategies because the entire search space is evaluated and this increases the chance of correct detection. The hybrid search performs slightly better than serial search. However, the cost of evaluating more cells and having fewer false alarms is computational complexity.

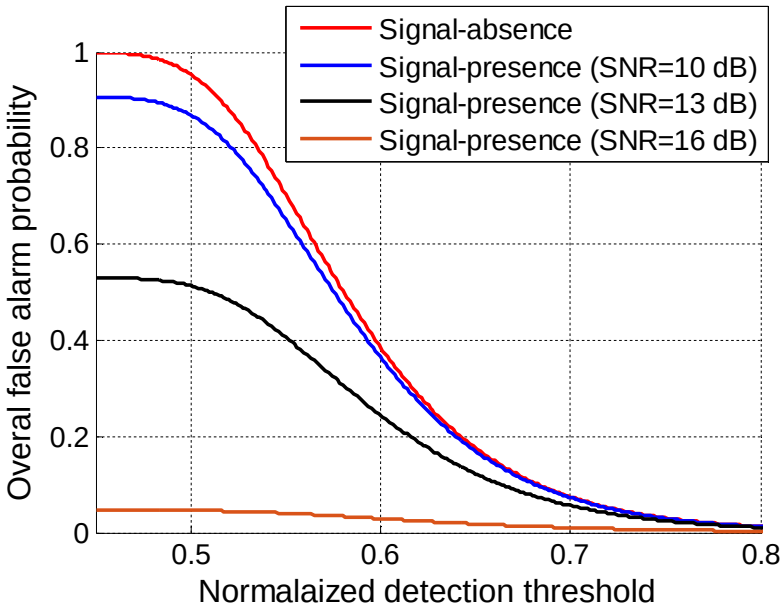

Figure 2-11: Overall false alarm probability vs. normalized threshold

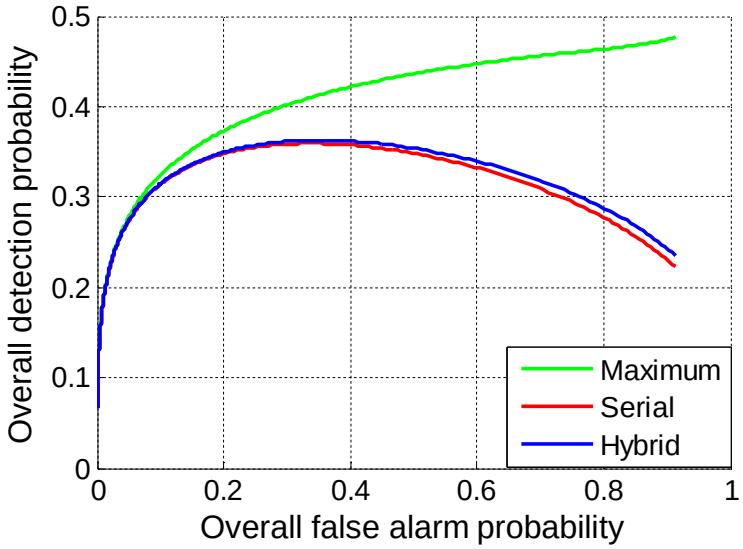

Figure 2-12: System level ROC curves

In order to clarify the difference between cell level and system level ROC plots, the following two scenarios are considered:

A: C/N_0= 40 dB-Hz , T_{coh}=1 ms , which results in SNR=13 dB

B: C/N_0= 30 dB-Hz , T_{coh}=10 ms , which results in SNR=13 dB

According to Figure 2-13, cell level ROC curves are the same for both scenarios. The reason is that the post processing *SNRs* are the same and as a result cell level detection probabilities which only depend on the *SNR*, are the same. Nevertheless, as shown in Figure 2-14, they have different system level ROCs because the overall detection probability depends on both *SNR* and the total number of cells in the search space. In fact, by increasing the coherent integration the search space also increases which leads to a higher false alarm probability or equivalently lower ROC performance. As a result, two acquisition systems may have the same cell level detection probability but different system level detection probability.

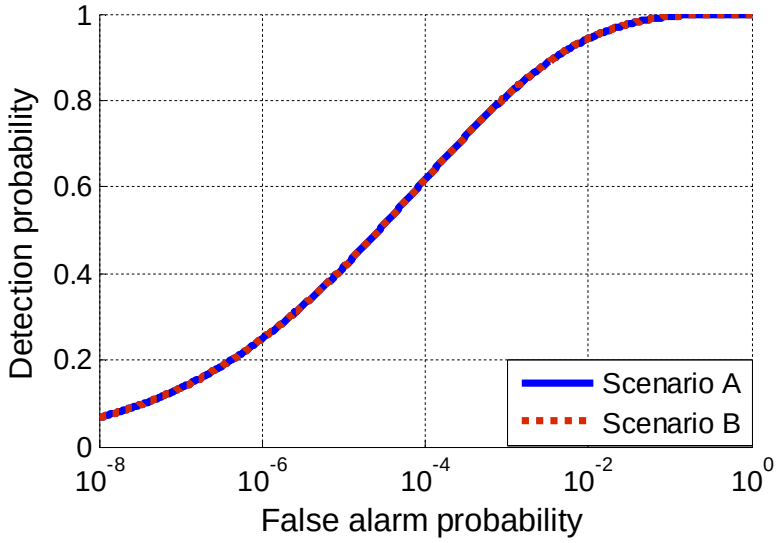

Figure 2-13: Cell level ROC curves for two different scenarios

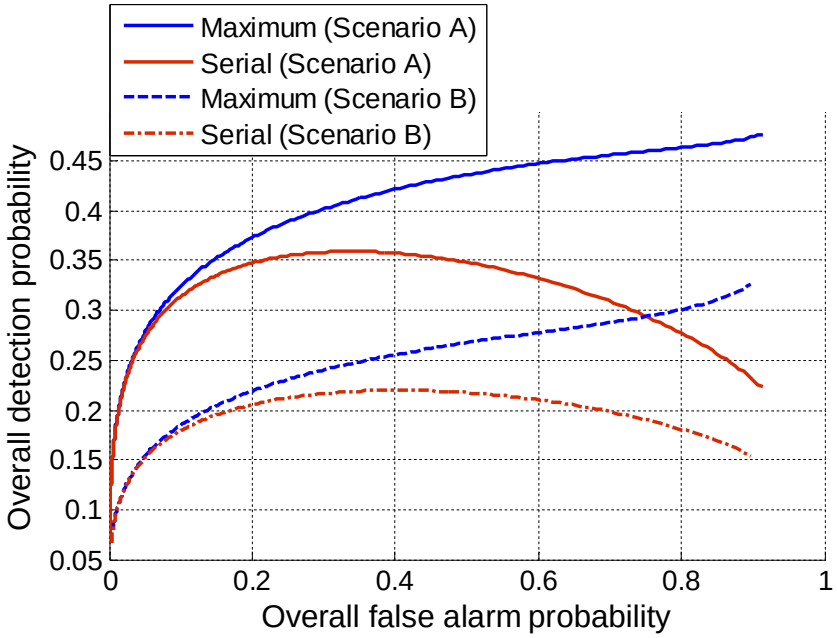

Figure 2-14: System level ROC curves for two different scenarios

Since the overall acquisition performance depends on the number of candidate cells in the uncertainty region, if there is any assistance that reduces the uncertainty region of the search space, the performance is improved in terms of ROC curve and mean acquisition time. As an example, using the following parameters and the maximum search strategy, the system level ROC curves for different assistance factors are depicted in Figure 2-15:

$$\left.\begin{array}{l} M: \text{total number of cells} \\ As: \text{Assistance factor} \end{array}\right\} \rightarrow M_{As} = \frac{M}{As}$$

$T_{coh} = 1\,ms \;\rightarrow M \approx 30000$

$C/N_0 = 40\ dB-Hz$

$10^{-8} \le P_{fa} \le 10^{-2}$

where M_{As} is the size of the uncertainty region after assistance; the assistance factor is related to any aiding information which can reduce the code delay and/or

Doppler range search. In fact, assistance information limits the search process over a smaller search space.

Obviously, as the assistance factor increases and search space gets smaller, the overall false alarm probability for a given overall detection probability decreases. This is the expected result, since assistance data can be considered as a priori information about the signal.

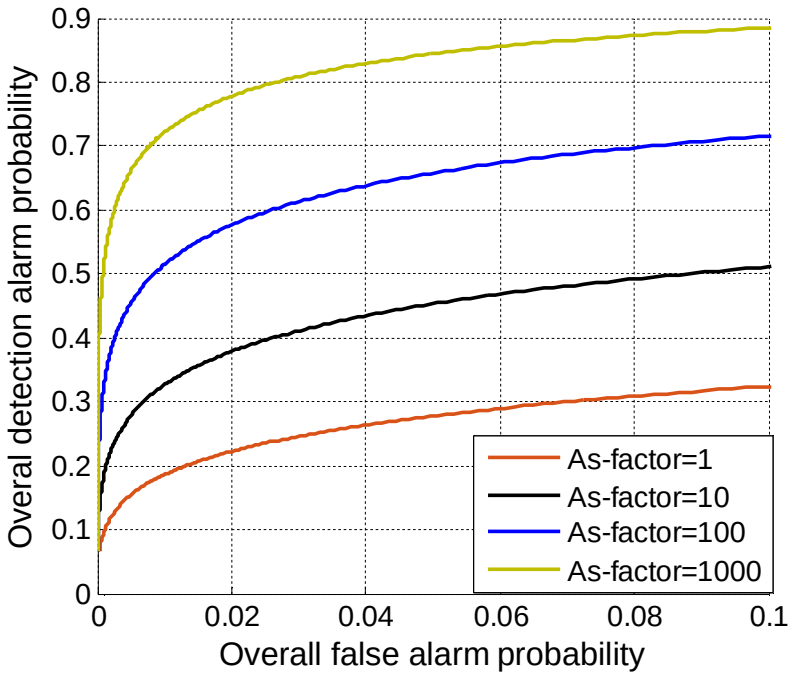

Figure 2-15: System level ROC after assistance

In order to assess the impact of the number of cells in the search space on the overall detection and false alarm probabilities, fixed values are considered for the detection threshold computed based on $P_{fa} = 10^{-4}$ and *SNR,* which is assumed to be 13 dB. As shown in Figure 2-16 the overall detection probability decreases

as the number of cells increases. This is because having more cells in the search space increases the possibility of false alarm and consequently reduces the chance of correct detection as shown in Figure 2-17.

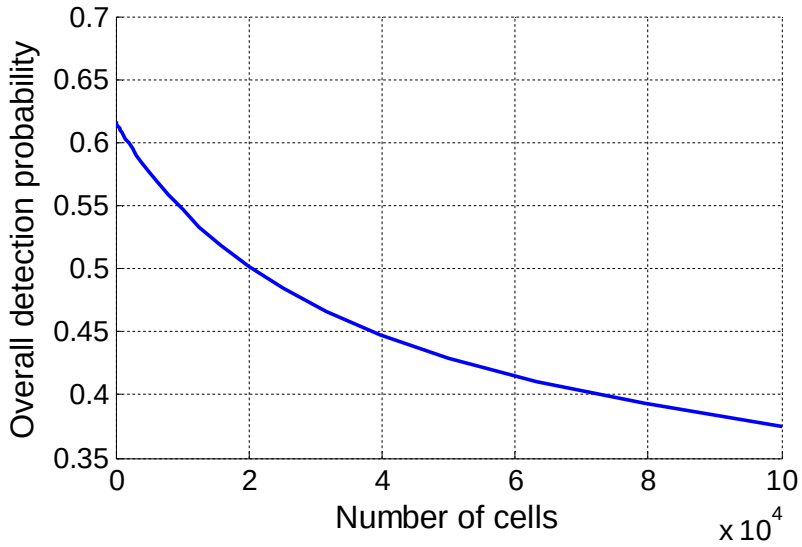

Figure 2-16: Overall detection probability vs. number of cells in the search space

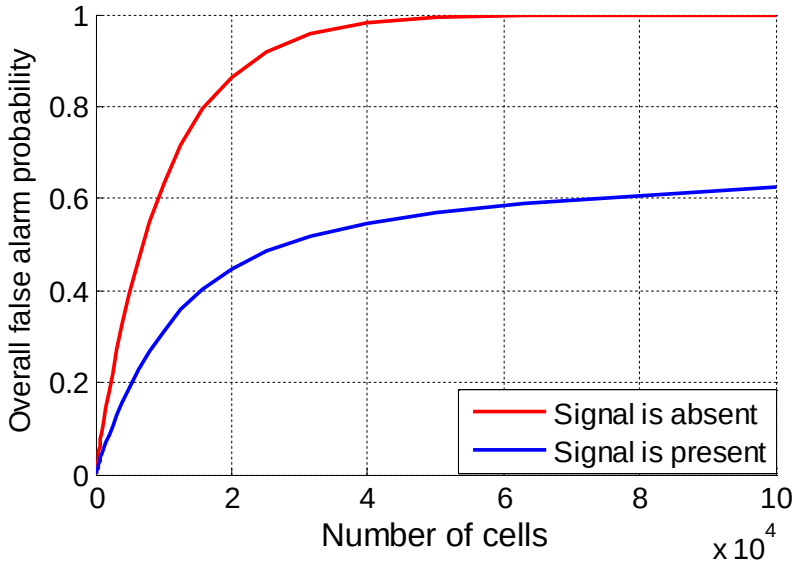

Figure 2-17: Overall false alarm probability vs. number of cells in the search space

In summary, this chapter described the different acquisition methods and discussed different search strategies commonly used in the acquisition process. The difference between the cell level and system level acquisition was highlighted and the impact of search space size on the acquisition performance was investigated.

Chapter Three: Acquisition Time

Acquisition time is an important metric showing the required time to acquire a signal which is a function of the detection probability, the probability of false alarm, the number of cells that need to be evaluated, the search strategy and the number of available correlators. In this section, only the maximum search strategy is considered. Acquisition time as a function of detection and false alarm probabilities is a random variable and it has mean and variance values. In this section the acquisition time statistic in terms of the mean and variance values is investigated.

3.1 Mean acquisition time (MAT)

Kassabian et al (2012) and Holmes (1977) have studied MAT in detail. Typically, MAT computation is based on Markov processes and uses probability generating functions and flow graph diagrams.

For the maximum search strategy and assuming a single-dwell scheme that has no verification mode, MAT can be written as (Kassabian et al 2012)

$$\bar{T}_A = T_s + T_s \frac{P_{MD}}{P_D} + (T_s + T_p)\frac{P_{FA}^p}{P_D} \tag{3-1}$$

where P_{MD} is the probability of missed detection. Using Eq. (2-44), Eq. (3-1) can be rewritten as

$$\bar{T}_A = \frac{T_s}{P_D} + \frac{P_{FA}^p T_p}{P_D} \tag{3-2}$$

where P_D is the overall detection probability and P_{FA}^{p} is the overall false alarm probability in the presence of the signal. T_p is the penalty time resulting from false acquisition and is equal to wasted time in an unsuccessful tracking mode because of wrong acquisition. Practically, T_p is considered as tracking transient time, which is around 500 ms (Kassabian et al 2012). Also, T_s is the total time required for evaluating the whole CAF which depends on the size of the search space, total integration time, coherent integration time, number of non-coherent integrations, number of correlators and the processor speed. In the following a derivation for the MAT calculation is provided.

Figure 3-1 shows the acquisition system including the search mode, false alarm and successful acquisition. In the search mode, using the maximum search strategy, each round requires T_s seconds for execution. If acquisition is not successful, it can be due to either false alarm or missed detection. In both cases the search mode repeats but if the former happens an additional penalty time should also be taken into account. Successful acquisition can be performed at any one of the search rounds.

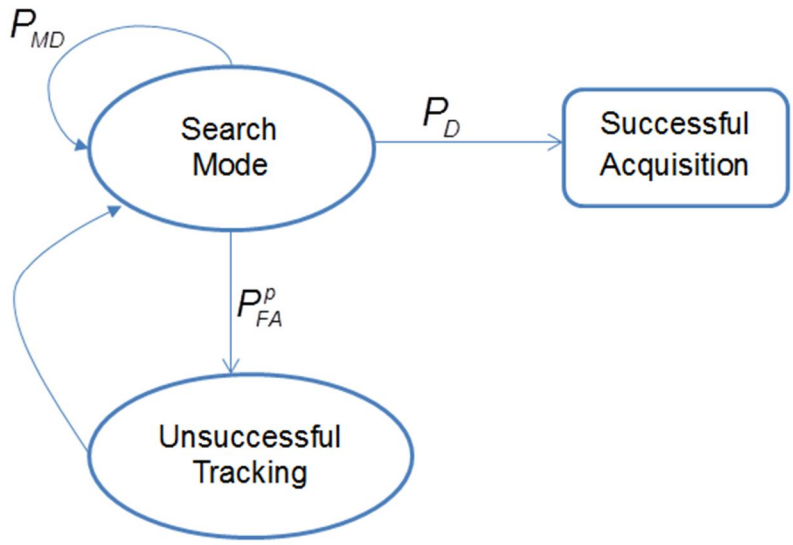

Figure 3-1: Acquisition process

Assume the signal is acquired at the i^{th} trial and the total spent time until the successful acquisition at the i^{th} trial is τ_i . Obviously, if the acquisition is successful at the first trial, the total spent time is T_s. At the second trial, the search space needs to be evaluated two times plus a penalty time due to a false alarm that could happen at the previous trial with the probability of P_p. As a result, $\tau_2 = 2T_s + P_p \times T_p$. Note that a successful acquisition after i trials means unsuccessful acquisition at the $(i-1)$ and other previous attempts and successful acquisition at i^{th} trial. The time spent at each unsuccessful trial is the time required to evaluate the search space (T_s) plus a penalty time (penalty arises with the probability of P_p) while the time spent at the successful trial is T_s. Hence, one has

$$\tau_i = (i-1)[T_s + P_p \times T_p] + T_s \tag{3-3}$$

Note that P_p is the false alarm probability under the condition of failed detection, which occurs with a probability of $(1-P_D)$ that can be written as follows:

$$P_p = Prob\ (false\ alarm \mid unsuccessful\ acquisition) = \frac{P_{FA}^{p}}{1-P_D} \tag{3-4}$$

The probability of reaching the i^{th} trial (P_i) and having the acquisition done is expressed as

$$P_i = Prob\ (unsuccessful\ acquisition\ at\ the\ first\ (i-1)\ attempts) \times Prob\ (successful\ acquisition\ at\ the\ i^{th}\ round) \tag{3-5}$$

hence,

$$P_i = P_D(1-P_D)^{i-1} \tag{3-6}$$

Since successful acquisition may occur after any round from one to infinity, the mean acquisition is computed as (Kassabian et al 2012)

$$\bar{T}_A = \sum_{i=1}^{\infty} P_i \times \tau_i = \sum_{i=1}^{\infty} P_D(1-P_D)^{i-1}\left[(i-1)[T_s + P_p \times T_p] + T_s\right] = \frac{T_s}{P_D} + \frac{P_{FA}^{p} T_p}{P_D} \tag{3-7}$$

3.2 Variance of acquisition time

In order to better characterize the acquisition time, beside the mean value, the acquisition time variance is taken into account. Mean acquisition time does not provide any information about the acquisition time variation that can be caused by the *SNR* variations. A good approximation for the variance of acquisition time

for a deterministic signal that has approximately constant power has been provided by Corazza (1996). The approximate distribution of acquisition time is Gaussian for relatively large MAT values and is a gamma distribution in the more general case that can be written as (Corazza 1996)

$$P(T_A) \cong \frac{T_A^{a-1} e^{-T_A/b}}{b^a \Gamma(a)} \tag{3-8}$$

where $a = \frac{\bar{T}_A^2}{\sigma_{T_A}^2}$, $b = \frac{\sigma_{T_A}^2}{\bar{T}_A}$ and $\Gamma(.)$ is the gamma function.

The variance of acquisition time is expressed as

$$\sigma_{T_A}^2 = \frac{1}{P_D}(T_s^2 + T_p^2 P_{FA}^p + 2T_s T_p P_{FA}^p + T_s C_1 + T_p C_2) + \bar{T}_A - \bar{T}_A^2 \tag{3-9}$$

where $C_1 = 2\bar{T}_A(1-P_D) - 1$ and $C_2 = P_{FA}^p(2\bar{T}_A - 1)$.

As shown in Figure 3-2 and 3-3, the mean and variance of the acquisition time increases as the signal power decreases for the fixed $P_{fa} = 10^{-6}$ and T_{coh}=1 ms values. Note that in this case, the time required for evaluating the entire search space and the penalty time are assumed to be 0.1 s and 0.5 s, respectively. Considering that C/N_0 =35 dB-Hz and T_{coh}=1 ms, Figure 3-4 and 3-5 demonstrate the effect of false alarm probability as the main metric for the detection threshold setting on the acquisition time. Evidently, for low false alarm probability or equivalently higher detection threshold the detection probability also decreases. Consequently, mean acquisition time increases. On the other hand, for a low detection threshold more penalties due to the false alarm occur that results in the higher acquisition time. Hence, depending on the C/N_0 and the integration time

as well as number of coherent and non-coherent integrations, an optimum detection threshold that has the minimum mean acquisition time could exist.

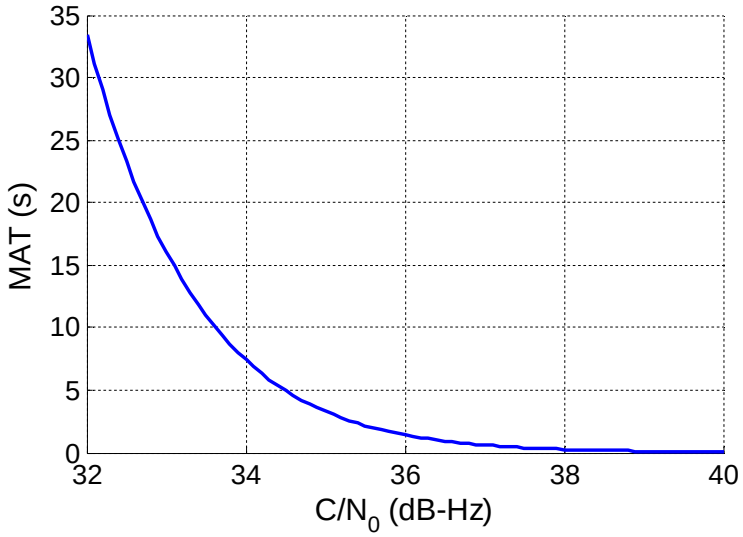

Figure 3-2: Mean acquisition time versus C/N_0 for $P_{fa}=10^{-6}$ and T_{coh}=1 ms

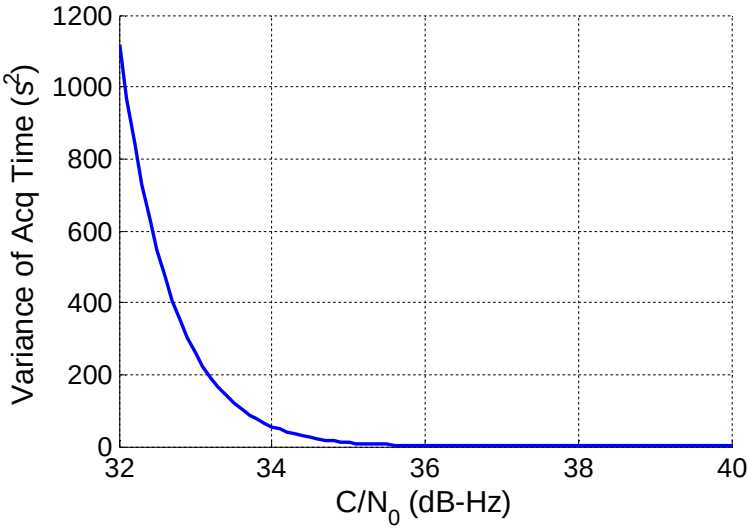

Figure 3-3: Variance of acquisition time versus C/N_0 for $P_{fa}=10^{-6}$ *and* T_{coh}=1 ms

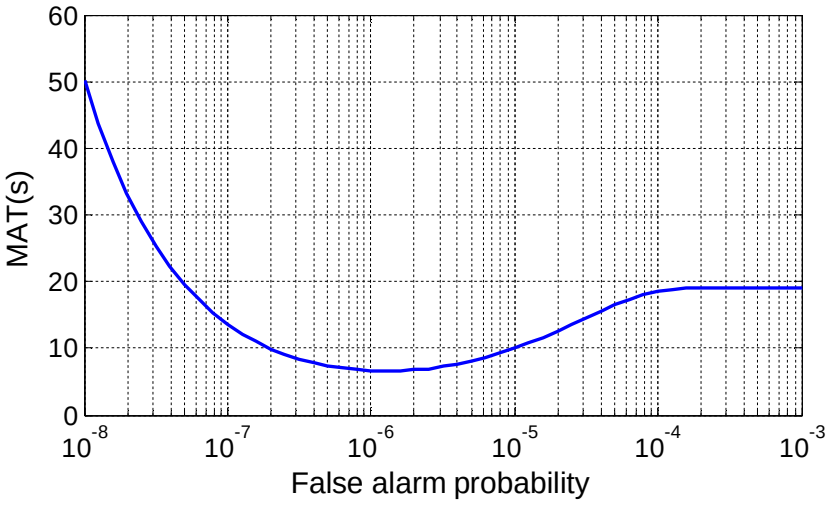

Figure 3-4: Mean acquisition time versus false alarm probability for C/N_0= *35* dB-Hz *and* T_{coh}=1 ms

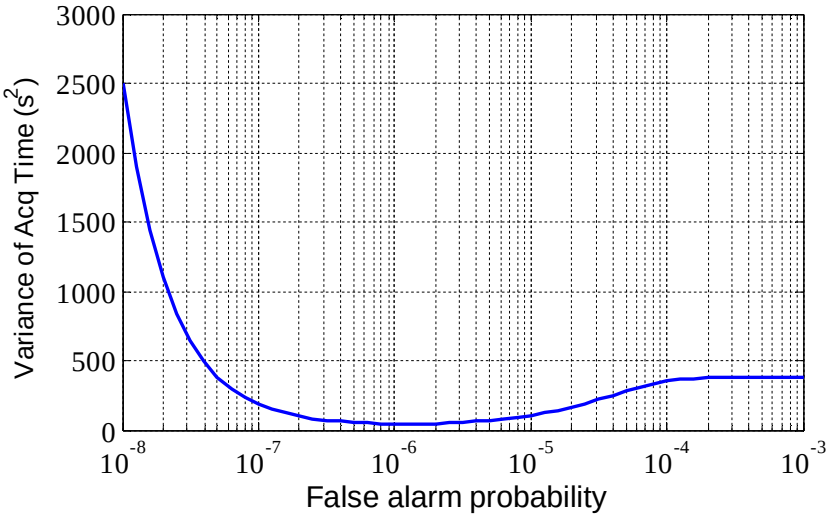

Figure 3-5: Variance of acquisition time versus false alarm probability for C/N_0=*35dB-Hz and* T_{coh}=1 ms

3.3 Impact of number of cells on the acquisition time

The maximum size of the search space is computed based on the coherent integration time. However, if there is any a priori information about code phase/Doppler availability, the uncertainty region decreases and fewer cells need

to be evaluated. The number of cells in the search space impacts acquisition time from two points. First, as discussed earlier, the number of cells affects the performance of overall detection and false alarm and hence affects the acquisition time as a function of detection and false alarm probabilities. Second, the acquisition time is directly proportional to the time required for evaluating the entire uncertainty region (T_s), which depends on the number of cells. Considering the parameters presented in Table 3-1, the normalized (to the maximum value corresponding to the maximum number of cells) values of the acquisition time mean and variance versus number of cells are depicted in Figure 3-6 and 3-7. As it was expected, by increasing the number of cells, the acquisition time mean and variance increase due the higher number of false alarms and longer T_s .

Table 3-1: Parameters used in acquisition time computation

C/N_0	30 dB-Hz
T_{coh}	10 ms
K (number of non-coherent)	1
T_p (penalty time)	0.5 s
P_{fa}	10^{-4}
Search strategy	Maximum likelihood

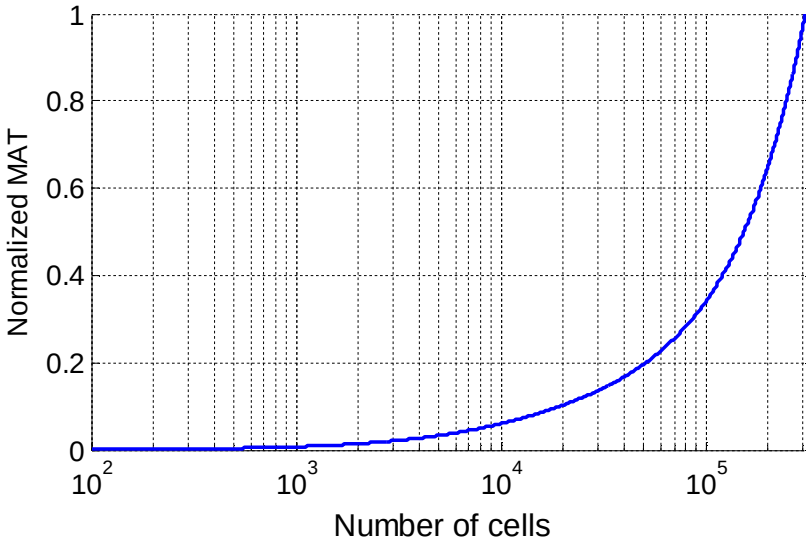

Figure 3-6: Normalized MAT vs. number of cells in the search space

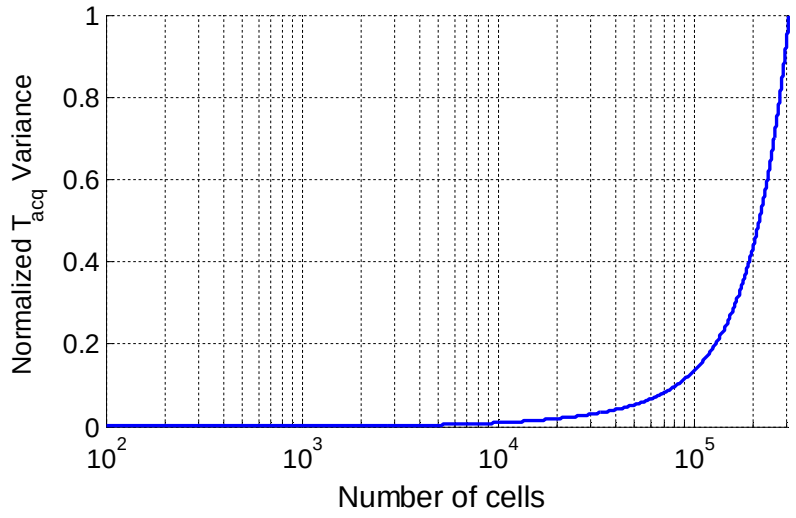

Figure 3-7: Normalized acquisition time variance vs. number of cells in the search space

3.4 Optimal combination of coherent and non-coherent integrations

Increasing the integration time can increase MAT values because more samples are processed and more specifically, by increasing the coherent integration time, the search space gets larger due to reducing the Doppler bins, which results in a

longer acquisition time. However, since detection probability also increases, MAT decreases. Hence, there might be an optimal value for the integration time based on an optimal combination of coherent and non-coherent integrations that minimizes MAT for a given P_{fa}. Of course the optimum combination depends on the C/N_0 value, search strategy, false alarm probability and the availability of assistance data to reduce the search space. Interestingly, increasing the coherent integration time is not always efficient in terms of MAT. To clarify this, assuming C/N_0=*37* dB-Hz, $P_{fa} = 10^{-6}$ and applying only coherent integration, MAT is plotted versus coherent integration time in Figure 3-8. In this case the minimum MAT is obtained for T_{coh}= 3 ms. Note that after considering the entire possible combinations of coherent and non-coherent integrations, the minimum MAT is achieved for T_{coh}=1 ms and 5 non-coherent combining (i.e. K=5).

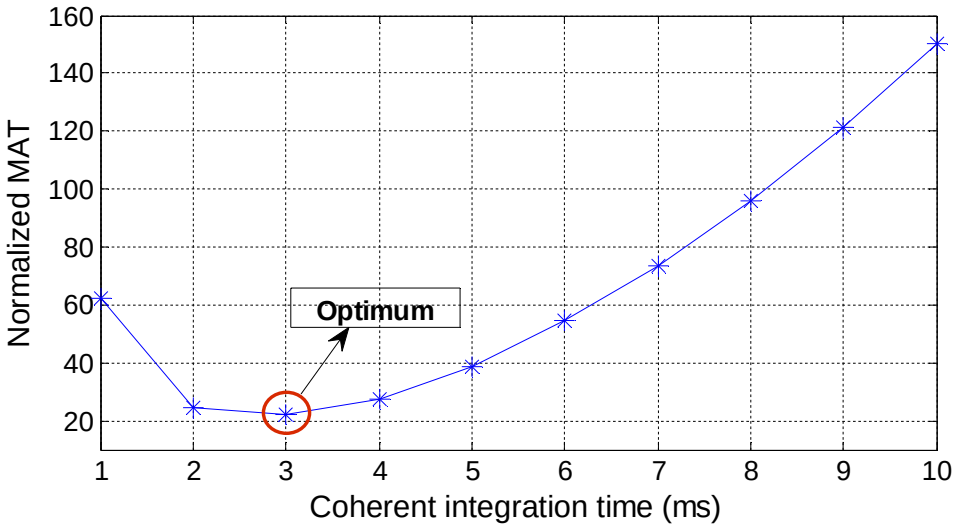

Figure 3-8: MAT versus coherent integration time for C/N_0= *37* dB-Hz *and* $P_{fa}=10^{-6}$

The remainder of this section examines the optimum integration time and the best combination of coherent and non-coherent integrations in order to have the minimum MAT. Depending on the availability of information about the C/N_0 values, two scenarios will be considered. The results are based on parallel code acquisition, the maximum search strategy and $P_{fa} = 10^{-6}$.

3.4.1 Receiver has a priori information about C/N_0 of the signal

For a given C/N_0 value the optimum combination of coherent and non-coherent integrations can be found as follows:

$$\{T_{coh}, K\} = \arg\min\left\{\overline{T}_A(C/N_0, T_{coh}, K)\right\} \tag{3-10}$$

Note that the total integration time is equal to $(T_{coh} \times K)$. Since in general there is no closed form to express P_D and hence for $\overline{T}_A$, it is not possible to solve the above equation analytically. A numerical solution considering all different $\{T_{coh}, K\}$ values and finding the one that results in the minimum MAT can be computed. It should be noted that in practice the integration time is limited by several factors such as user and satellite motions. Here the maximum integration time is set to 100 ms, that is $T_{\text{int}}^{\max} = 100\,\text{ms}$.

Practically, knowing the exact value of C/N_0 is not possible. Instead, it is assumed that the receiver considers C/N_0 to be uniformly distributed over a range of values. In this case the expected value of MATs over the interval of

C/N_0 values is considered in the optimization problem. Hence Eq. (3-10) is rewritten as

$$\{T_{coh}, K\} = \arg\min\left\{E\left[\overline{T}_A(C/N_0, T_{coh}, K)\right]\right\} \tag{3-11}$$

The expectation operator ($E[.]$) is applied to MAT values corresponding to different C/N_0 values. As an example, for $C/N_0 \geq 24$ dB-Hz and assuming the receiver knows the C/N_0 value with a 3 dB accuracy, optimal combinations of coherent and non-coherent integrations for different intervals of C/N_0 values are presented in Table 3-2.

Table 3-2: Optimal combination of coherent and non-coherent integrations for different C/N_0 ranges

C/N_0 (dB-Hz)	T_{int} (ms)	Optimum Combination	$E\{T_A\}$ (s)
$C/N_0 \geq 42$	1 ms	$T_{coh} = 1$ms , $K = 1$	1.6
$39 \leq C/N_0 < 42$	2 ms	$T_{coh} = 1$ms , $K = 2$	3.7
$36 \leq C/N_0 < 39$	4 ms	$T_{coh} = 1$ms , $K = 4$	9
$33 \leq C/N_0 < 36$	11 ms	$T_{coh} = 1$ms , $K = 11$	23.3
$30 \leq C/N_0 < 33$	33 ms	$T_{coh} = 1$ms , $K = 33$	67.1
$27 \leq C/N_0 < 30$	99 ms	$T_{coh} = 1$ms , $K = 99$	215.2
$24 \leq C/N_0 < 27$	100 ms	$T_{coh} = 4$ms , $K = 25$	1240

3.4.2 Receiver has no information about C/N_0 of the signal

In this scenario the C/N_0 value could be anything between 0 and 50 dB-Hz and the receiver does not have any further information. Since it is assumed that the integration time is limited to 100 ms, acquiring extremely weak signals is not possible. In this section acquisition of signals which have C/N_0 values below 24 dB-Hz (as an example of a weak signal that has a low chance to be acquired using 100 ms integration time) is not considered. Therefore, a uniform distribution of C/N_0 values over the range of 24-50 dB-Hz is assumed. The goal is to minimize the overall MAT. Clearly, having only one strategy regarding the integration time and the combining methods (coherent/non-coherent) is not efficient in terms of the acquisition time. If the signal is weak and the receiver uses a strategy based on low integration time, the signal may not be detected or it can be acquired after a very long time. On the other hand, if the signal is strong enough that it can be acquired using low integration time but the receiver chooses long integration time, which is suitable for weak signal situations, the acquisition time is longer than it could be. In order to deal with the general case in which the C/N_0 value is unknown, an adaptive strategy can be utilized. Hence, the receiver operates in different stages, each one with a specific integration time and a combination of coherent and non-coherent integration. Intuitively, the receiver starts with a low integration time and if it fails to acquire the signal, it goes to the next stage which uses a higher integration time and the procedure continues. Note that since the signal may not be present or it could be so weak that it cannot be detected using standard methods of weak signal acquisition, the

acquisition time approaches to infinity. To avoid such a problem, it is assumed that successful acquisition can be performed with the probability of α. With this assumption, the time spent for acquisition becomes limited and the acquisition search process stops after a certain time specified as a function of α.

In this case, besides the combination of coherent and non-coherent integrations, the number of operation stages affects the overall mean acquisition time. Therefore, the optimum number of stages should also be taken into account. Then the optimum combination corresponding to the i^{th} stage can be expressed as

$$\left\{T_{coh},K\right\}_i = \arg\min\left\{E[\bar{T}_A(C/N_0,T_{coh},K)]\right\} \tag{3-12}$$

where $\left\{T_{coh},K\right\}_i$ is the combining method at i^{th} stage.

Note that the number of operation stages affects the overall mean acquisition time. A high number of stages increases the acquisition time due to the extra time spent during stages when signal is not acquired. On the other side, for a low number of stages, the adaptive strategy is not utilized efficiently which leads to the longer acquisition time.

Considering the PDF of acquisition time, the maximum time to be spent at the i^{th} stage (T_m^i) to guarantee successful acquisition with the probability of α is computed as follows:

$$\text{Prob}\{0 \le T_{acq}^i \le T_m^i\} = \alpha \tag{3-13}$$

$$\alpha \cong \frac{\gamma(a, T_m^i / b)}{\Gamma(a)} \rightarrow T_m^i = b \times gammaincinve(\alpha, a) \tag{3-14}$$

where $\gamma(.)$ and *gammaincinve*(.) are the incomplete gamma function and its inverse. The incomplete gamma function can be written as (Arfken & Weber 2005)

$$\gamma(a,x) = \int_0^x t^{a-1} e^{-t}\, dt \tag{3-15}$$

Figure 3-9 shows the overall mean acquisition time versus the number of operation stages where each stage represents a specific coherent/non-coherent combination, assuming a uniform distribution of C/N_0 values over the range of 24-50 dB-Hz and $\alpha = 0.90$. As it can be seen, for the given parameters the optimum number of stages is four. The best strategies and the maximum time during which the receiver should stay at the i^{th} each stage (T_m^i) are given in Table 3-3. Note that the receiver starts from the first stage and if the signal is not acquired at the maximum stay time, it switches to the next stage and continues.

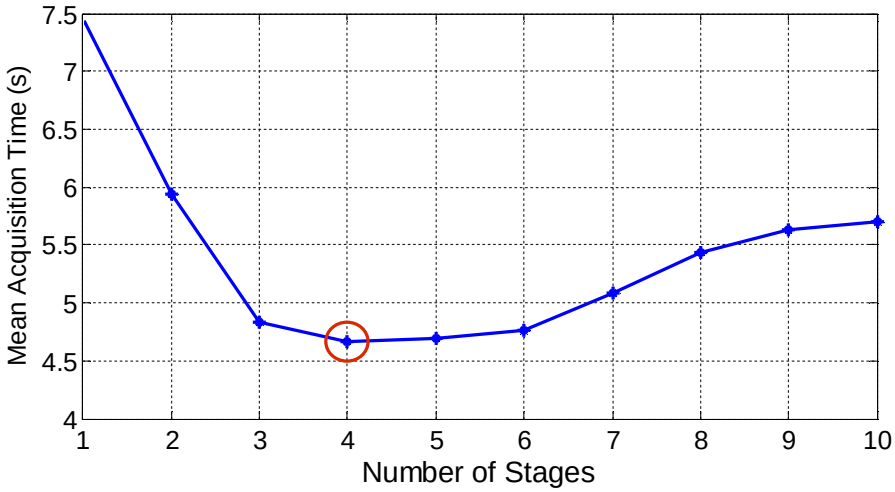

Figure 3-9: Overall mean acquisition time versus number of operation stages

Table 3-3: Optimal strategies at each stage

Stage	T_{int} **(ms)**	T_{coh} **(ms)**	***K***	T_m **(s)**
1	1	1	1	0.035
2	6	1	6	0.216
3	37	1	37	1.17
4	100	4	25	17.22

In summary, this chapter investigated acquisition time and discussed some aspects that minimize mean acquisition time. The results showed that the detection threshold and coherent/non-coherent integrations impact the acquisition time and can be adjust somehow that leads to a minimum mean acquisition time.

Chapter Four: Fading and Antenna Diversity System

This chapter describes multipath fading channel models and diversity combining methods along with the acquisition performance evaluation after the diversity combining.

4.1 Radio propagation and wireless channel

In wireless communications the wave propagation is affected by reflection, diffraction, scattering and penetration as shown in Figure 4-1. These phenomena lead to three main radio propagation models namely path-loss, shadowing and multipath fading (Rappaport 1996, Goldsmith 2005).

- Path-loss: The signal is attenuated due to the distance between the transmitter and receiver. Larger distances result in higher signal attention. The path-loss is categorized as a large scale effect {large scale fading (power degradation)} because the signal power changes over large distances (usually hundreds of meters). The mean power of the received signal can be calculated as

$$P_R = P_T G_T G_R d^{-n} \tag{4-1}$$

where P_R is the received signal power, P_T is the transmitted signal power, G_T and G_R are the transmitter and receiver antennas gain respectively. d is the transmitter-receiver distance and n represents the path-loss

exponent which can be between 2 to 6 depending on the environment. A pathloss exponent of 2 is valid for free space propagation and higher pathloss exponents are considered for more attenuating environments such as buildings and indoor environments. In the case of the GNSS signals, *d* is the distance between the satellite and receiver and assuming free space propagation *n* is equal to 2.

- Shadowing: Shadowing also known as shadow fading is a medium scale fading due to local obstructions such as buildings. This effect causes received signal power fluctuation around the mean value determined by the path-loss. The power fluctuation has a log-normal distribution or equivalently a normal distribution if it is expressed in dB scale.
- Multipath fading: Due to several signal reflections, multiple copies of a signal may arrive at the receiver antenna with different phases. Multipath fading occurs if the phases add destructively. This type of fading is a small scale fading that affects over small distances (order of carrier wavelength which in case of GPS L1 is about 19 cm). Rapid fluctuations that are observed in signal amplitude can be modeled by the Rayleigh or Rician distribution (Blaunstein & Andersen 2002).

Finally, considering the three mentioned propagation models, the received signal power is expressed as

$$P_R = P_T G_T G_R d^{-n} 10^{x/10} A^2 \quad (4\text{-}2)$$

where x is zero-mean Gaussian variable showing the shadowing effect and A is the signal amplitude determined by the Rayleigh or Rician distribution due to the multipath fading effect.

Figure 4-2 shows the received power affected by the path-loss, shadowing and multipath fading versus the transmitter-receiver distance. In the following section, the multipath fading effect will be discussed in more detail.

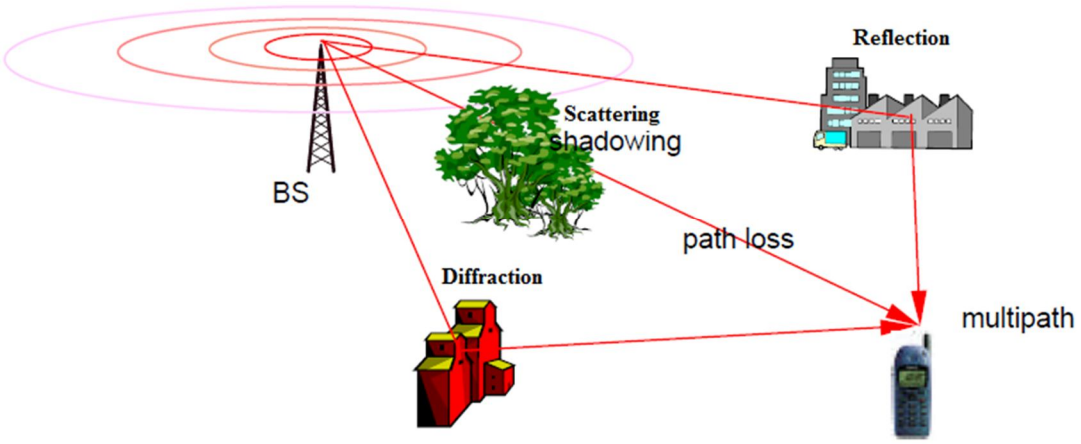

Figure 4-1: Wireless channel propagation (after Mahmood 2012)

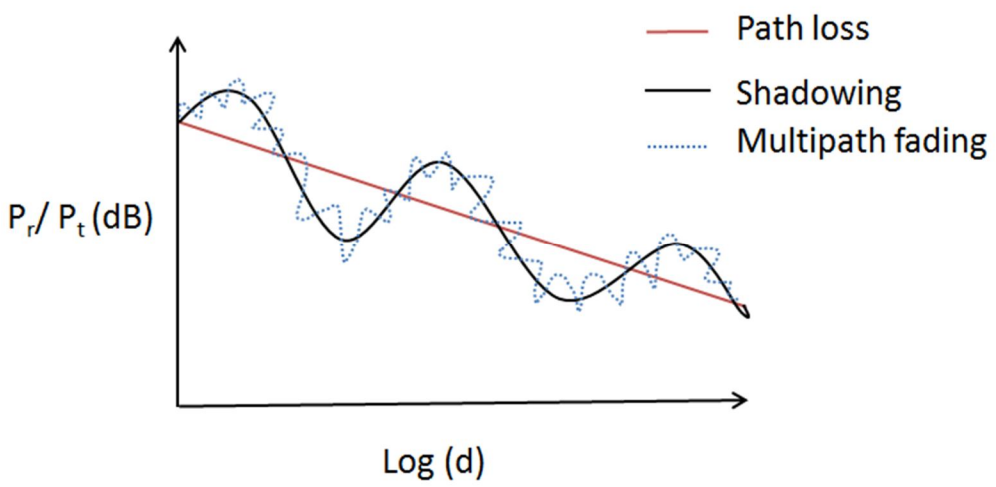

Figure 4-2: Path-loss, shadowing and multipath fading versus distance (after Goldsmith 2005)

4.2 Multipath fading

In a dense multipath environment the received signal is a superposition of several reflected signal components with different phases and amplitudes. Normally, fading occurs due to the destructive effect of multipath phenomenon when the signal reflections arrive from different paths. Figure 4-3 illustrates the multipath phenomenon. As shown in Figure 4-4 signal power degradation due to the multipath fading could be up to 30 dB and different signal strength is observed when the receiver moves by half a carrier wavelength.

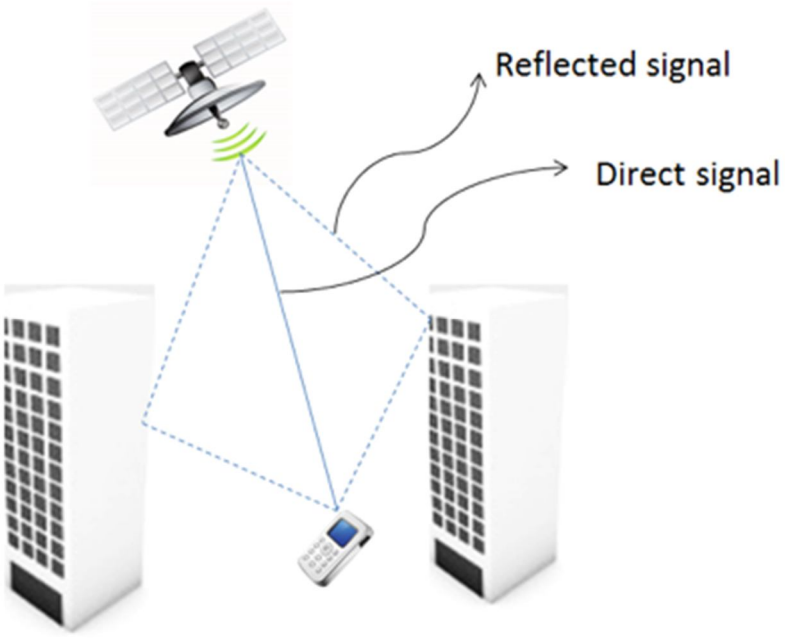

Figure 4-3: Multipath phenomenon

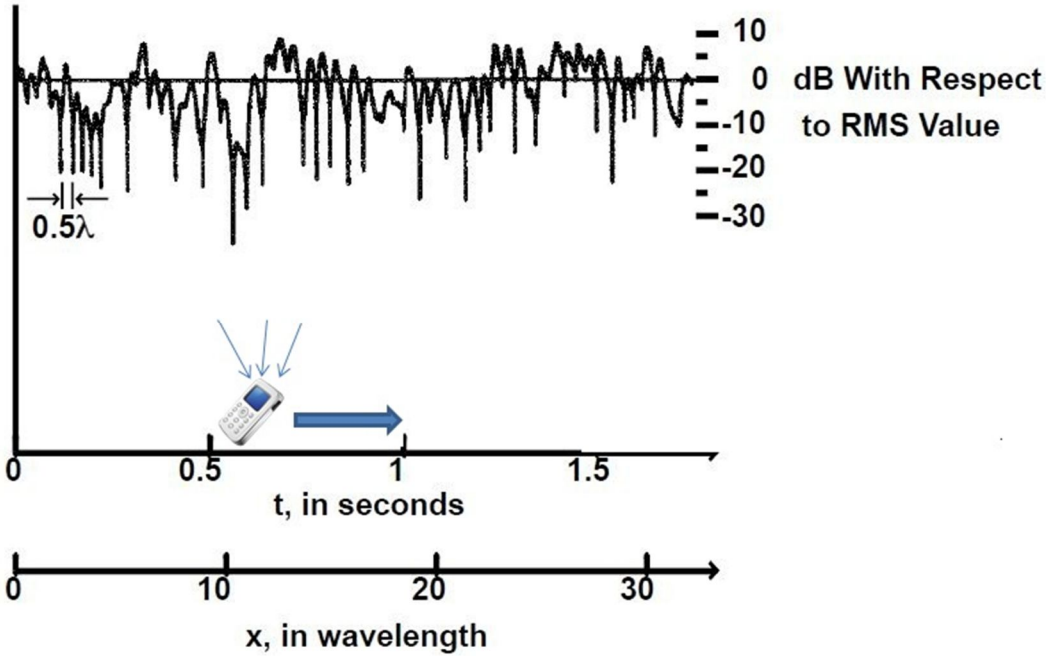

Figure 4- 4: Multipath fading effect (after Goldsmith 2005)

4.2.1 Rician fading

In multipath situations when in addition to the reflected signal components, a dominant component such as a line-of-sight (LOS) signal exists, the multipath channel can be modeled by a Rician distribution. This dominant path can significantly decrease the depth of fading. The amplitude of the received signal is expressed as

$$p_r(x) = \frac{x}{\sigma^2} e^{\frac{-(x^2+s^2)}{2\sigma^2}} I_0\left(\frac{xs}{\sigma^2}\right) \qquad x \geq 0 \tag{4-3}$$

where σ^2 is the variance of in-phase or quadrature components of the signal, s is the power of dominant component and $I_0(.)$ is the zero order Bessel function of the first kind, defined by

$$I_0(y) = \frac{1}{2\pi} \int_0^{2\pi} e^{-y\cos\theta} d\theta \tag{4-4}$$

An important parameter that characterizes the Rician fading is the Rician factor (K) defined as the ratio of power in the dominant path to the total power in the reflected paths, that is

$$K = \frac{\text{power in the dominant path}}{\text{total power in the reflected paths}} \tag{4-5}$$

4.2.2 Rayleigh fading

In the absence of a dominant component, the amplitude of the received signal can be modeled by a Rayleigh distribution. In this case the overall received

signal is only the summation of several scattered signals with different phase and amplitude. Then the amplitude of the signal becomes

$$p_r(x) = \frac{x}{\sigma^2} e^{\frac{-x^2}{2\sigma^2}} \qquad x \geq 0 \tag{4-6}$$

Note that the Rayleigh fading is a special case of Rician fading where the Rician factor approaches zero or equivalently a dominant path is not present. Furthermore if $K \to \infty$, it means that there is no multipath and the channel is a simple Gaussian channel that is only affected by noise. Figure 4-5 depicts the Rician fading for different K values.

The focus of this chapter is on the Rayleigh fading channel and the acquisition performance is evaluated in this situation.

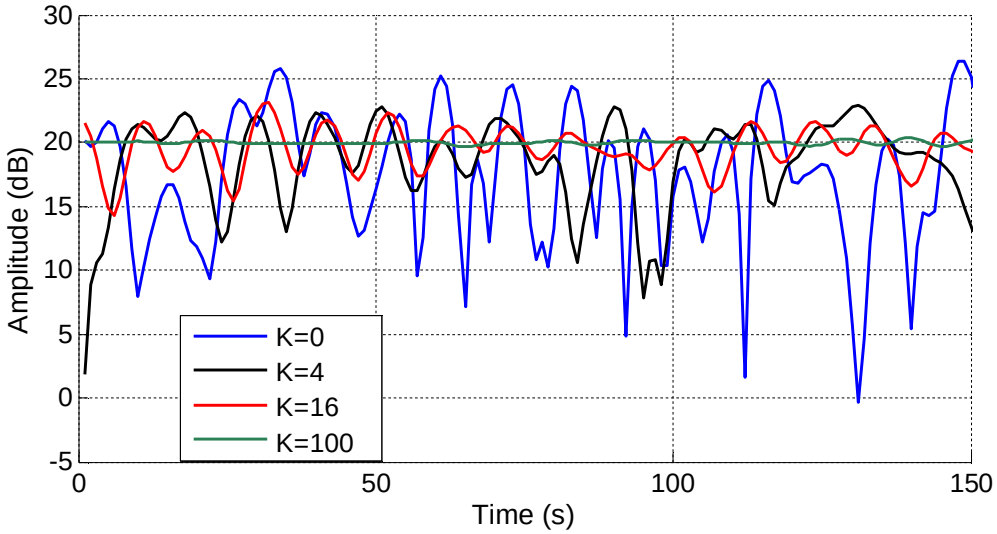

Figure 4-5: Rician fading for different Rician factors

4.2.3 Fading Statistics

The two important parameters which characterize the fading effect are the Level Crossing Rate (LCR) and the Average Fade Duration (AFD), as shown in Figure 4-6. AFD indicates the average time that the signal spends under the detection threshold. LCR shows how frequently the amplitude of the signal drops below a defined threshold in a certain period of time. LCR and AFD for a Rician channel are complicated but they have a simple closed form expression in a Rayleigh fading channel as follows (Blaunstein & Andersen 2002):

$$LCR = \sqrt{2\pi} f_m \rho e^{-\rho^2} \tag{4-7}$$

$$\rho = \frac{\beta}{A_{rms}} = \frac{\beta}{\sqrt{2}\sigma} \tag{4-8}$$

$$f_m = f_c \frac{v}{c} \tag{4-9}$$

where β is the specified detection threshold, A_{rms} is the root mean square (RMS) signal amplitude and σ is the standard deviation of in-phase/quadrature components of the signal. f_m is the maximum Doppler shift mostly due to the user motion, v is the user velocity, f_c is the carrier frequency (1575.42 MHz for GPS L1) and c is the speed of light. Considering the relationship between LCR and AFD as

$$LCR \times AFD = 1 - e^{-\rho^2} \tag{4-10}$$

one can write

$$AFD = \frac{e^{\rho^2} - 1}{\rho f_m \sqrt{2\pi}} \tag{4-11}$$

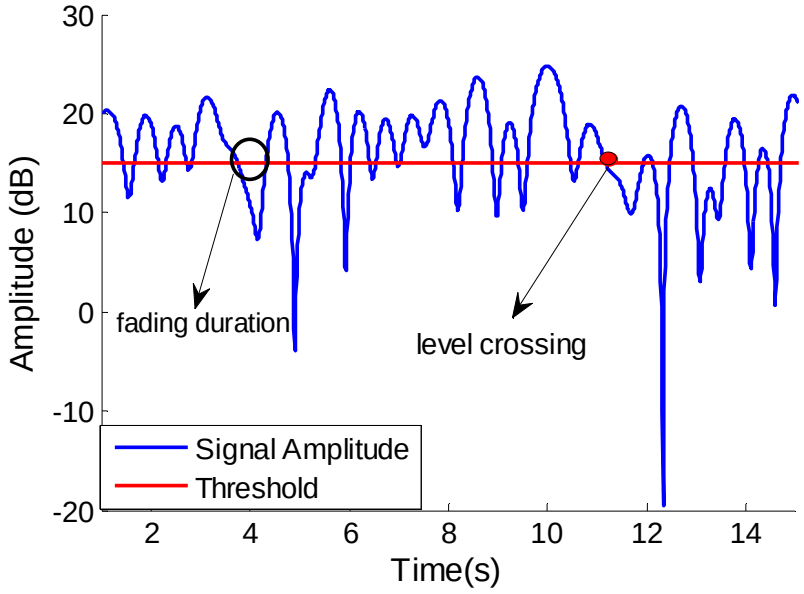

Figure 4-6: Level crossing and fade duration

4.3 Acquisition performance in the Rayleigh fading channel

Acquisition performance for the deterministic signals (which have approximately constant power) in a Gaussian channel was discussed in Chapter 3. Now the acquisition performance in terms of the detection and false alarm probabilities as well as acquisition time is investigated in the Rayleigh fading channel.

4.3.1 Detection performance

In the Rayleigh fading channel, the distribution of in-phase and quadrature components of the signal plus noise (X) is Gaussian with zero mean. As a result, the distribution of the received signal can be considered as a zero mean

complex Gaussian which means the real and imaginary components of the signal follow zero mean Gaussian distributions. Hence, the amplitude of the signal (and also signal plus noise) follows the Rayleigh distribution.

Under the H_0 hypothesis where only noise is present and the H_1 hypothesis that both noise and signal exist, X is distributed according to (Kay 1998)

$$\begin{cases} X|H_0 \sim CN(0,\sigma_N^2) \\ X|H_1 \sim CN(0,\sigma_{SN}^2) \end{cases} \tag{4-12}$$

where CN represents the complex Gaussian distribution, $\sigma_{SN}^2 = \sigma_S^2 + \sigma_N^2$, σ_S^2 and σ_N^2 are the signal and noise variances, respectively.

In weak signal situations due to the limitation on increasing the coherent integration time because of navigation bit transitions, non-coherent integration might be required. After applying K non-coherent integrations to both in-phase and quadrature components of the signal (so in total, sum of the squares of $2K$ normal random variables), the decision variable defined in Eq. (2-28) is written as (Kay 1998)

$$\begin{cases} Y|H_0 \sim \chi_{2K}^2(0,\sigma_N^2) \\ Y|H_1 \sim \chi_{2K}^2(0,\sigma_{SN}^2) \end{cases} \tag{4-13}$$

where χ^2_{2K} is a chi-square distribution with $2K$ degrees of freedom. By definition, using Eq. 2-23 and Eq. 2-24 the false alarm and detection probabilities can be expressed as (Kay 1998)

$$P_{fa} = \exp\{\frac{-\beta}{2\sigma_N^2}\}\sum_{i=0}^{K-1}\frac{1}{i!}\left(\frac{\beta}{2\sigma_N^2}\right)^i \tag{4-14}$$

$$P_d = \exp\{\frac{-\beta}{2\sigma_{SN}^2}\}\sum_{i=0}^{K-1}\frac{1}{i!}\left(\frac{\beta}{2\sigma_{SN}^2}\right)^i \tag{4-15}$$

The overall detection and false alarm probabilities can be obtained using Eq. 2-41, Eq. 2-43 and Eq. 2-44.

4.3.2 Acquisition time

4.3.2.1 Mean acquisition time

As shown in Chapter 3, the mean acquisition time is computed as a function of detection and false alarm probabilities. In the MAT computation there is no assumption involving the channel condition. The important assumption considered is that the receiver has buffers and during each round of acquisition the same data set is processed although after an unsuccessful attempt for the acquisition, a new data set is used for the next round. Hence, the MAT expression in the Rayleigh fading channel is identical to the MAT determined for the deterministic signals. Therefore, assuming the maximum search strategy without any verification mode, one has

$$\bar{T}_A = \frac{T_s}{P_D} + \frac{P_{FA}^p T_p}{P_D} \quad (4\text{-}16)$$

4.3.2.2 Variance of acquisition time

A good approximation for the variance of acquisition time for a deterministic signal that has approximately a constant power has been proposed by Corazza (1996). However, none of the prior studies has analyzed the variance of acquisition time in the multipath fading channel. In a fading channel due to the significant changes in the signal strength, acquisition time variation over time is significant. In fading situations, C/N_0 drops and consequently a longer time is required to acquire the signal. Due to rapid and random changes of C/N_0 values in the fading channel, finding the exact variance of acquisition time is complicated. This section provides a lower bound estimation for the variance of acquisition time in a Rayleigh fading channel using the fading statistics.

In multipath fading situations, the acquisition time can be separated into two groups with respect to the faded and non-faded signals. According to Figure 4-7, a fading situation is defined as a moment when the signal amplitude falls below the detection threshold and in the non-fading situation when the signal is above the threshold. In fact, the acquisition engine meets the signals in two situations, faded situations, where the signal amplitude is below the detection threshold, and non-faded situations, in which the signal amplitude exceeds the threshold. If the receiver tries to acquire the faded signals, it should wait until the fading period ends and then detect the non-faded signal because detection is possible only if the signal amplitude passes the threshold. Otherwise, if the acquisition engine

hits the non-faded signals, it can successfully acquire them with the probability of P_D^{NF}. If the acquisition engine cannot acquire the signal, it processes a new set of samples. In the following state machine the acquisition process in the fading situation is simply depicted. The acquisition engine should deal with the faded and non-faded signals. In the former case the acquisition process should be repeated with a new set of samples while in the latter case signal is acquired with the probability of P_D^{NF} and reacquisition is required with the probability of $1-P_D^{NF}$.

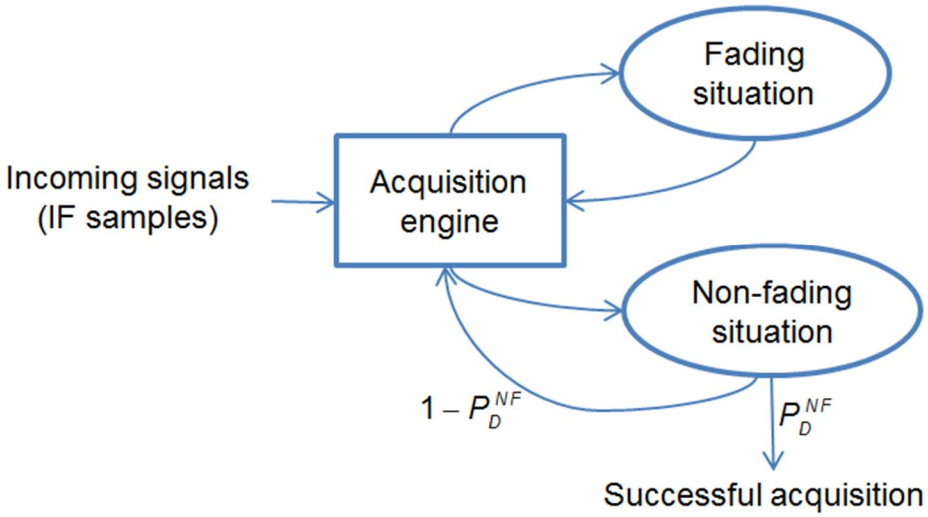

Figure 4-7: Acquisition process in the fading situation

The overall detection probability (P_D^{NF}) when the signal does not fade (signal amplitude is above the threshold) is determined. Simply, the detection threshold can be obtained from P_{fa}. If the signal is above the threshold, it will be certainly detected at the cell level i.e. $P_d = 1$. However, the overall detection probability is not 1 due to the false alarm effect that happens when the noise amplitude is

higher than the detection threshold and signal amplitude. In this case, using Eq. (2-43) the overall detection probability is computed as follows:

$$P_D^{NF} = \int_{\beta}^{\infty} f_{A|x\geq\beta}(x|H_1)\times(1-P_{fa}(x))^{M-1}\,dx = \int_{\beta}^{\infty} \frac{f_A(x|H_1)}{f_A(x\geq\beta)}\times(1-P_{fa}(x))^{M-1}\,dx$$
$$= \frac{1}{P_d(\beta)}\int_{\beta}^{\infty} f_A(x|H_1)\times(1-P_{fa}(x))^{M-1}\,dx \qquad (4\text{-}17)$$

where β is the detection threshold , $f_A(x|H_1)$ is the Rayleigh distribution of signal amplitude (under the H_1 hypothesis) which is presented in Eq. (4-6) and $f_{A|x\geq\beta}$ is the PDF of signal amplitude under the condition of having an amplitude greater than β . It is important to note that in this section $K=1$ is considered for simplicity.

The above P_D^{NF} computation is under the condition of having signal amplitude greater than the detection threshold. Since $P_d = 1$, according to Eq. (2-42), $P_{MD} = 0$ and hence, $P_{FA} = 1 - P_D^{NF}$.

The important assumption here is $T_s < AFD$. This assumption is satisfied when the antennas move with a slow speed so that during several trials for the acquisition, channel characteristics do not change significantly or the processor speed is high enough to evaluate the search space before the channel characteristics change.

If the signal amplitude is above the detection threshold and assuming $P_D^{NF} = 1$, only one attempt is adequate to acquire the signal and the acquisition time is

equal to time the required to evaluate the entire search space (T_s). When the signal amplitude is below the threshold (fading situations), it can be acquired after the fading duration. Therefore, acquisition time in two situations can be written as

$$\begin{cases} T_{acq}^{NF} = T_s & \text{non-fading situation} \\ T_{acq}^{F} = AFD + T_s & \text{fading situation} \end{cases} \tag{4-18}$$

According to the relationship between AFD and fading level crossing rate and considering N trials for the acquisition in the time period of T, the number of fading situations (N_F) and non-fading situations (N_{NF}) are expresses as follows:

$$\begin{cases} T_F = T \times (1 - e^{-\rho^2}) \\ T_{NF} = T - T_F = T \times e^{-\rho^2} \end{cases} \tag{4-19}$$

$$\begin{cases} N_F = \left\lceil \dfrac{T_F}{AFD} \right\rceil \\ N_{NF} = \left\lceil \dfrac{T_{NF}}{T_{acq}^{NF}} \right\rceil \end{cases} \tag{4-20}$$

Since in general P_D^{NF} is not necessarily one and the signal is acquired with a probability of P_D^{NF} (or equivalently in a P_D^{NF} portion of the times a successful acquisition is performed), the acquisition times increase by a factor of $1/P_D^{NF}$. Hence, considering a successful acquisition which can be performed only in the non-fading situations, the mean acquisition time and a lower bound for the acquisition time variance become

$$L_v = (\frac{1}{P_D^{NF}})^2 \times \text{var}\{\underbrace{T_{acq}^{NF},...,T_{acq}^{NF}}_{N_{NF}-N_F},\underbrace{T_{acq}^{F},...,T_{acq}^{F}}_{N_F}\} \quad (4\text{-}21)$$

where $\sigma_{T_A}^2 > L_v$

$$\bar{T}_A = \frac{1}{P_D^{NF}} \times \text{mean}\{\underbrace{T_{acq}^{NF},...,T_{acq}^{NF}}_{N_{NF}-N_F},\underbrace{T_{acq}^{F},...,T_{acq}^{F}}_{N_F}\} \quad (4\text{-}22)$$

In the case of penalty time, MAT increases by $P_{FA} \times T_p$. Note that this is a lower bound for the variance of acquisition time. Since the acquisition time is a function of fade duration, any variation in the fade duration leads to variation in acquisition time. Hence, in computing the variance of the acquisition time, using AFD instead of variable fade duration results in a lower variance estimate than the real value.

4.4 Antenna Diversity

Antenna diversity is defined as using multiple antennas in the receiver which can improve the wireless link quality by enhancing the *SNR* values. The most useful application of antenna diversity is in multipath environments where fading occurs. The two main categories of antenna diversity are described as follows:

- Spatial diversity: This type of diversity is also called spatial diversity and uses two or more spatially separated antennas. This method provides additional processing gain since multiple receiver antennas are able to detect different signal components from different fading channels. If one of

the antennas fails to detect the signal, the other still has a chance to acquire it. In other words, at a given time the *SNR* values can be different at different antennas. As shown in Figure 4-8, the receiver is equipped with two antennas and each one can receive signals with different characteristics (phase and amplitude). In this Figure h_1 and h_2 represent the channel gain, which impacts the signal characteristics in two different paths.

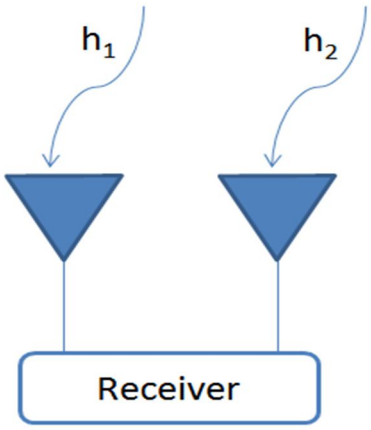

Figure 4-8: Receive antenna diversity

- Polarization diversity: In multipath situations, the signal polarization can change due to the reflections. Usually, most of the antennas are designed for a specific polarization and if they receive the signals with a different polarization, polarization mismatch may occur. Table 4-1 shows the power loss due to polarization mismatch for different received signals and antenna polarizations. Obviously, when the received signal and antenna polarizations are right hand circular polarized (RHCP) and left hand

circular polarized (LHCP), the practical power loss due to the polarization mismatch is significant. This can happen especially in cases of GNSS signals which have RHCP. The reflection of RHCP signals (from metal materials) are LHCP and if the antenna is designed for RHCP signals, it experiences an extreme loss.

Using two antennas with orthogonal polarization such as RHCP and LHCP or a single antenna with the dual polarization property provides polarization diversity and mitigates the fading due to the polarization mismatch. This type of diversity in the field of GNSS has been examined by Zaheri (2011).

Table 4-1: Polarization mismatches loss for different polarizations (from Electronic warfare and radar systems engineering handbook 1997)

Received signal polarization	Receive antenna polarization	Power loss in dB
Vertical	Vertical	0 dB
Vertical	Slant(45^o or 135^o)	3 dB
Vertical	Horizontal	30 dB (practical loss)
Vertical	Circular (left or right)	3 dB
Horizontal	Horizontal	0 dB
Horizontal	Slant(45^o or 135^o)	3 dB
Horizontal	Circular (left or right)	3 dB
RHCP	RHCP	0 dB
RHCP	LHCP	30 dB (practical loss)
Circular (left or right)	Slant(45^o or 135^o)	3 dB

Spatial antenna diversity using two antennas in Rayleigh fading channels is now investigated. In a Rayleigh fading channel, depending on the antenna separation, antenna diversity can provide mostly independent samples that can aid the acquisition process. The reason is that in a multipath fading environment if the antennas are separated by one carrier wavelength (19 cm for GPS L1) the signals received at different antennas experience approximately independent channels and consequently the signal fades differently at each branch. In other words, as shown in Figure 4-9, the signal can fade in one branch while it is not or is less faded in the other one. Hence, at each time, combining the signals at two branches can mitigate the fading effect. Note that the more uncorrelated channels the more efficient the diversity method. In the following, different diversity combining methods are described.

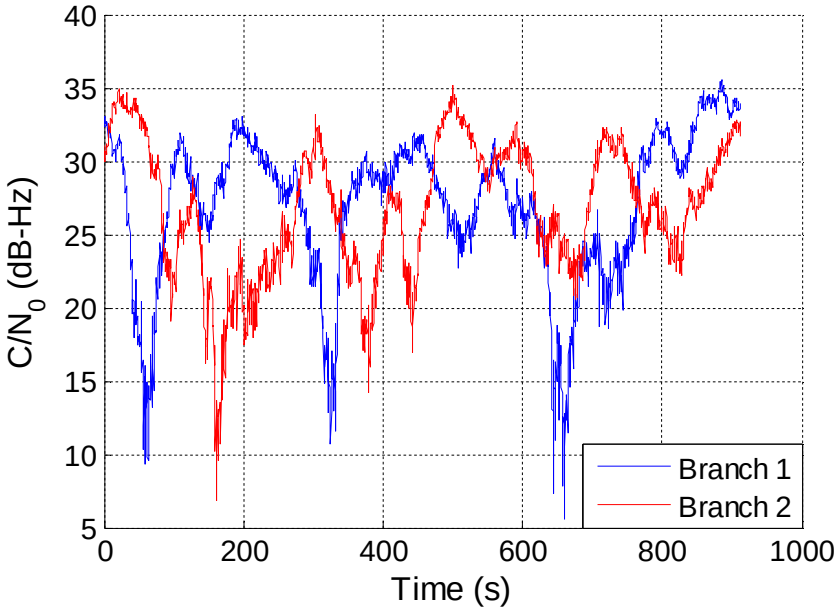

Figure 4-9: Signal power at two different branches in a fading environment

4.4.1 Diversity combining methods

Three well-known combining methods in wireless communications, as they have been discussed by Goldsmith (2005), are equal gain combining (EGC), selection combining (SC) and maximal ratio combining (MRC). The combiner shown in Figure 4-10 chooses one of the mentioned methods.

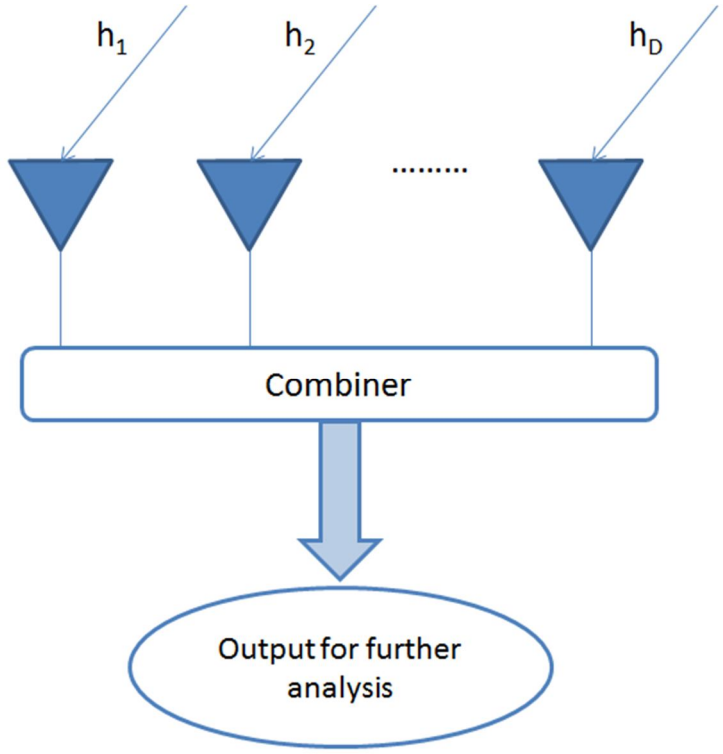

Figure 4-10: Diversity combining

4.4.1.1 Equal gain combining

In EGC, signals from different branches are added together with equal weights. The received signal at the i^{th} branch can be modeled as

$$S_r^i(t) = r_i e^{j\phi_i} S_t(t) \qquad (4\text{-}23)$$

where $S_t(t)$ and $S_r(t)$ are the transmit and receive signals respectively, $r_i e^{j\phi_i}$ is the channel gain effect (h_i) with the amplitude scale of r_i and phase of ϕ_i. If the phase of the received signals can be estimated, diversity combining methods have higher performance. If the phase of arrival is known, the co-phasing process can be utilized. In this process, the phase difference between received signals at different branches can be removed and signals are combined with the same phase. Hence, the destructive effect of combining due to the phase difference between signals is eliminated. After applying the co-phasing, the combined signal becomes

$$S_{com}(t) = \sum_{i=1}^{D} r_i S_t(t) \tag{4-24}$$

where $S_{com}(t)$ is the combined signal and D is the number of antennas (branches)

4.4.1.2 Selection combining

In this method at each time a branch with the strongest signal power or equivalently highest *SNR* is selected. Therefore, the output *SNR* at each time is expressed as

$$SNR_{out} = \max\{SNR_i \ , \ 1 \le i \le D\} \tag{4-25}$$

where SNR_i corresponds to the *SNR* value at the i^{th} branch.

4.4.1.3 Maximal ratio combining (MRC)

MRC combines the signals with respect to the *SNR* values at the branches by adding the signals together with appropriate weights as

$$S_{com}(t) = \sum_{i=1}^{D} w_i S_t(t) \tag{4-26}$$

where w_i are the optimal combining weights and can be computed as follows (Goldsmith 2005):

$$w_i = \frac{h_i^*}{\sigma_{n,i}^2} \tag{4-27}$$

where $\sigma_{n,i}^2$ represents the noise power at the i^{th} branch.

Regarding the comparison of combining methods, there is a tradeoff between performance and complexity. Since MRC uses appropriate weights to combine the signals, it has the best performance in term of the output *SNR*. However, it is the most complicated method in term of implementation. EGC has a relatively lower complexity but its performance is not as good as MRC. Finally assuming the received signals at different branches have equal average power, SC has the lowest performance. Table 4-2 compares the three diversity combining methods (Goldsmith 2005).

Table 4-2: Diversity combining techniques comparison

Combining method	Relative performance	Complexity
Selection	Minimum	Simple
Equal gain	Mediocre	Requires co-phasing
Maximal ratio	Maximum	Requires co-phasing and channel estimator

Note that in the fading channels co-phasing and channel estimation are complicated and require some special techniques. More specifically, in GNSS these methods are not efficiently applicable in the acquisition stage where the signal parameters are unknown. In this research the EGC method, which does not need a priori information about the *SNR*s of the incoming signals, is adopted. As a result, after the despreading process, signals from different branches are added together non-coherently with equal weights. The reason for non-coherent combining of signals at the correlator outputs level is that in Rayleigh fading situations, at the acquisition stage, the phase of the signals is unknown and the GNSS signal is under the noise floor. Therefore, before despreading, non-coherently adding the samples from different branches destroys the phase information and consequently the Doppler and code phase cannot be determined properly. In addition, in these environments the phase difference between the received signals is not known and the coherent combining method is not applicable. In the next section equal gain combining of two branches for the GNSS signal is investigated.

4.5 Equal gain combining applied to GNSS signals

As mentioned previously, EGC is performed at the correlator output level. Considering two branches in a Rayleigh fading environment, the combining process is shown in Figure 4-11.

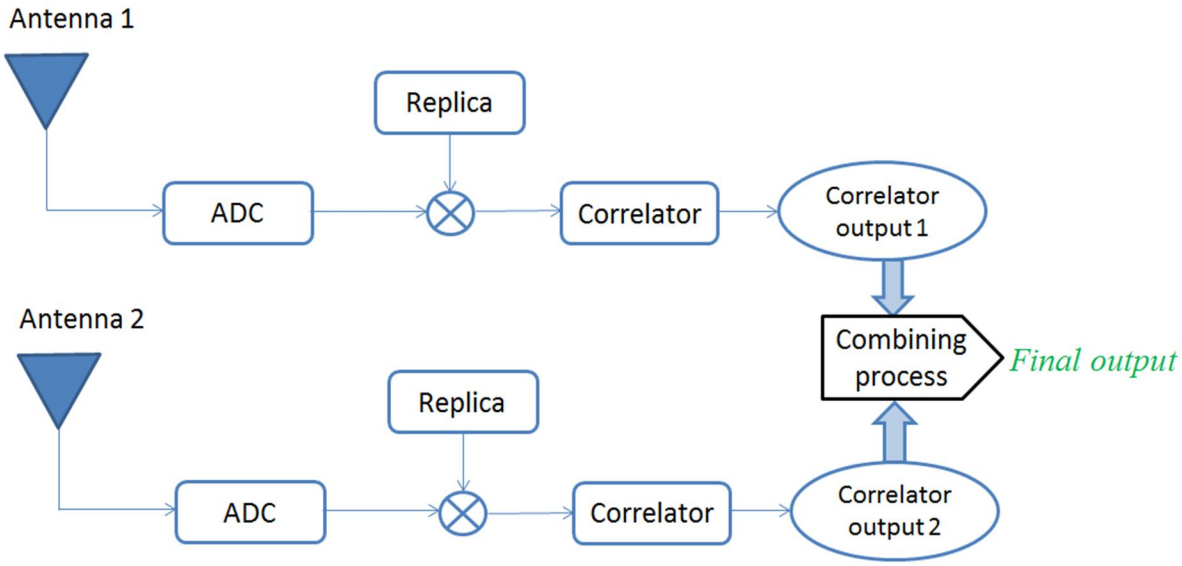

Figure 4-11: Combining the signals of two branches at the correlator output level

The practical consideration in the combining procedure such as the noise calibration should be implemented. Since the noise powers in different branches could be different due to any difference in hardware elements of the receivers including low-noise amplifier (LNA), mixer, amplifiers and an analog-to-digital converter (ADC) (Alink et al 2011), they have to be calibrated before combining.

4.5.1.1 Acquisition performance for uncorrelated signals

Assuming the received signals at two antennas are uncorrelated, the decision variable after EGC and noise calibration becomes

$$Y_{EG} = Y_1 + \frac{\sigma_{N1}^2}{\sigma_{N2}^2} Y_2 \tag{4-28}$$

$$Y_{EG} \big| H_0 \sim \chi_{4K}^2(0, \sigma_N^2) \tag{4-29}$$

where σ_{N1}^2 and σ_{N2}^2 are the noise power in two different branches which can be estimated before or after despreading. Note that the ratio $\frac{\sigma_{N1}^2}{\sigma_{N2}^2}$ in Eq. (4-28) is used in order to calibrate the noise power in different branches. If signals in two branches are statistically identical and have similar average *SNR* values, one obtains

$$Y_{EG} \big| H_1 \sim \chi_{4K}^2(0, \sigma_{SN}^2) \tag{4-30}$$

Using Eq. (2-23) and Eq. (2-24), P_{fa}^{EG} and P_d^{EG} obtained from EGC are given by

$$P_{fa}^{EG} = \exp\{\frac{-\beta}{2\sigma_N^2}\} \sum_{i=0}^{2K-1} \frac{1}{i!} \left(\frac{\beta}{2\sigma_N^2} \right)^i \tag{4-31}$$

$$P_d^{EG} = \exp\{\frac{-\beta}{2\sigma_{SN}^2}\} \sum_{i=0}^{2K-1} \frac{1}{i!} \left(\frac{\beta}{2\sigma_{SN}^2} \right)^i \tag{4-32}$$

The overall detection, missed detection and false alarm probabilities using the maximum search strategy after EGC can be expressed as

$$P_D^{EG}(\beta) = \int_{\beta}^{+\infty} [1 - P_{fa}^{EG}(y)]^{M-1} f_{Y_{EG}|H_1}(y)\, dy \tag{4-33}$$

$$P_{MD}^{EG} = (1 - P_{fa}^{EG}(\beta))^{M-1} \times (1 - P_d^{EG}(\beta)) \tag{4-34}$$

$$P_{FA}^{p,EG} = 1 - P_D^{EG} - P_{MD}^{EG} \tag{4-35}$$

where $f_{Y_{EG}|H_1}$ is presented in Eq. (4-30). Finally, $\bar{T}_A^{EG}$ can be written as

$$\bar{T}_A^{EG} = \frac{T_s}{P_D^{EG}} + \frac{P_{FA}^{p,EG} T_p}{P_D^{EG}} \tag{4-36}$$

A more general case is when *D* diversity branches are available and the received signals can have different average *SNR* values or in fact different σ_S^2 values that could be due to different antenna gain. The decision variable after *K* non-coherent integration in each branch and equal gain combining of *D* branches is written as

$$Y_{EG} = \sum_{k=1}^{D} Y_k \tag{4-37}$$

where $Y_k = \sum_{l=1}^{K} |S_l|^2$, K is the number of non-coherent integration and S_l is a zero mean complex Gaussian random variable which is the correlator output obtained from the coherent integration defined in Eq. (2-6). Under the H_1 condition, Y_{EG} follows a generalized chi-square distribution because it is sum of the squared magnitudes of different zero mean complex Gaussian random variables with different variances (σ_{SN}^2). According to Bjornson et al (2009) and Amari & Misra (1997), the distribution of Y_{EG} under the H_1 hypothesis becomes

$$f_{Y_{EG}|H_1}(y;\sigma_1^2,...,\sigma_M^2) = \prod_{m=1}^{D} \frac{1}{\sigma_m^2} \times \sum_{k=1}^{D} \sum_{l=1}^{K} \frac{\varphi_{k,l}}{(K-1)!} (-y)^{K-1} e^{\frac{-y}{\sigma_k^2}} \qquad y \geq 0 \tag{4-38}$$

where $\varphi_{k,l} = (-1)^{K-1} \sum_{i \in \Omega_k} \prod_{j \neq k} \binom{i_j + K - 1}{i_j} \left(\frac{1}{\sigma_j^2} - \frac{1}{\sigma_k^2}\right)^{-(K+i_j)}$,

$\Omega_k = \{[i_1,...,i_D] \in \mathbb{Z}; \sum_{j=1}^{D} i_j = l-1, i_k = 0, i_j \geq 0, \text{ for all } j\}$ and $\sigma_1^2,...,\sigma_D^2$ correspond to the signal plus noise variance of each in-phase/quadrature components at D different branches.

For the two branch case ($D = 2$), one has

$$f_{Y_{EG}|H_1}(y;\sigma_1^2,\sigma_2^2) = \prod_{m=1}^{2} \frac{1}{\sigma_m^2} \times \sum_{k=1}^{2} \sum_{l=1}^{K} \frac{\varphi_{k,l}}{(K-1)!} (-y)^{K-1} e^{\frac{-y}{\sigma_k^2}} \qquad y \geq 0 \tag{4-39}$$

where $\varphi_{k,l} = (-1)^{K-1} \binom{i_j + K - 1}{i_j} \left(\frac{1}{\sigma_j^2} - \frac{1}{\sigma_k^2}\right)^{-(K+i_j)}$ and

$\{j \text{ and } k \in \{1,2\}, j \neq k, i_j = l-1, 1 \leq l \leq K\}$

Assuming the special case when the signals in two branches are statistically identical, Eq. (4-39) can be simplified to Eq. (4-30) and is written as

$$f_{Y_{EG}|H_1} = \chi^2_{4K}(0,\sigma^2_{SN}) \quad (4\text{-}40)$$

Note that the received signals at different antennas may not be completely independent and hence could be correlated. Furthermore, the diversity performance is affected by the correlation between the signals in different branches. The more uncorrelated two channels are, the higher the performance from the diversity combining. Hence, for uncorrelated fading channels antenna diversity provides the highest improvement in the acquisition performance. The common metric used to evaluate the similarity between two signals is the correlation coefficient which is a function of antennas separation. A comprehensive analysis on the detection performance considering the correlated channels with equal and unequal received signals has been provided by Kay (1998) and Zaheri (2011).

Chapter Five: Simulations and Experimental Results

In this chapter the theoretical results are verified by Monte Carlo simulations and are compared with real measurements of GPS signals made in an indoor multipath fading environment.

5.1 Monte Carlo simulations

A series of simulations was conducted to depict ROC curves and evaluate the acquisition time in terms of mean and variance values. Both deterministic and Rayleigh fading channels were considered in the simulations, but equal gain combining of multiple signals was only performed in the Rayleigh fading channels.

In the simulations a search space including M cells is generated and computed using Eq. (2-15). Incorrect cells include uncorrelated Gaussian noise and the correct cell consists of a signal with a specific power.

In order to depict the ROC curves, detection and false alarm probabilities need to be determined. Detection and false alarm in the cell and system levels are defined as follows:

- False alarm (cell level): If in a cell of the search space that does not contain the desired signal and only has noise, the noise amplitude passes the threshold, false alarm occurs.
- Detection (cell level): The correlator output (decision variable) in the correct cell, which represents the best estimate of code and Doppler, is compared

with the detection threshold. If it exceeds the threshold, correct detection in is obtained.

- Overall false alarm (in the absence of the signal): Considering the entire search space, when the signal is not present, all the cells only contain noise. False alarm happens if the noise amplitude at any cell of the search space passes the detection threshold. In this case a false alarm can be generated in any cells of the search space whereas the cell level false alarm is due to the contribution of a single cell.

- Overall false alarm (in the presence of the signal): In this case, the presence of the signal affects the probability of false alarm. The condition for false alarm occurrence during the maximum search method is that the noise amplitude at any of the cells exceeds both the threshold and the signal amplitude. Therefore, the overall false alarm probability depends on the *SNR* value, noise power and the detection threshold.

- Overall detection: For the maximum likelihood search strategy, signal detection is successfully performed in the correct cell if the signal amplitude is the maximum of CAF and it passes the detection threshold. This means false alarm does not happen among the incorrect cells of the search space. The main difference between overall detection and cell level detection is that the former is affected by the false alarms occurring in the cells containing noise while the latter only deals with the correct cell. In other

words, it is possible to have cell level detection (signal passes the threshold in the correct cell) but due to a false alarm the overall detection failed.

The method to find false alarm and detection probabilities in cell and system acquisition levels, and the acquisition time using simulations and real data are described as follows:

For a specific detection threshold value, the amplitude of the noise in an incorrect cell (H_0 condition) is compared with the threshold. Each time that the noise amplitude exceeds the threshold, one false alarm is generated. By monitoring the incorrect cell for several times, the false alarm probability corresponding to the certain threshold is calculated. The false alarm probability as a function of detection threshold is obtained by successively setting the threshold to different values. Likewise, the detection probability as a function of detection threshold can be obtained by monitoring the correct cell (H_1 condition). Then one has

$$P_{fa} = \frac{\text{number of times noise passes threshold}}{\text{total number of evaluations}} \tag{5-1}$$

$$P_{d} = \frac{\text{number of times signal passes threshold}}{\text{total number of evaluations}} \tag{5-2}$$

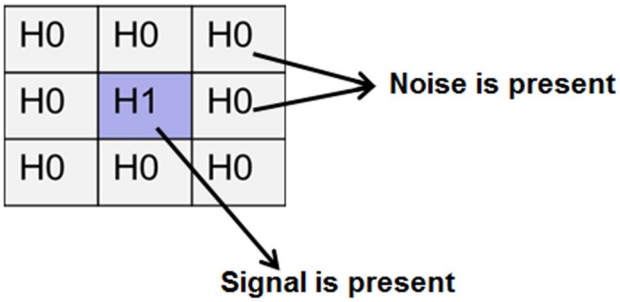

Figure 5-1: H_0 and H_1 conditions

Accordingly, overall detection and false alarm probabilities can be computed by evaluating the entire cells of the search space.

To compute the acquisition time for a successful acquisition, the search space is evaluated several times, each time with a new data set, until the first correct detection is attained. Acquisition time for each successful detection is equal to the number of required attempts for the successful acquisition multiplied by the time needed for evaluating one search space (T_s), plus penalty time due to the false alarms. Considering L successful acquisitions in the simulations, a set of acquisition times including L elements with each one corresponding to a successful acquisition time is generated. Finally, the mean and variance values of the set are computed.

Figure 5-2 and 5-3 show the theoretical and Monte Carlo simulation results for cell and system level ROC curves. Also, the mean and variance of acquisition time for the parameters listed in Table 5-1 are illustrated in Figure 5-4 and 5-5. As can be seen, there is a strong agreement between the theoretical and simulations results.

By setting the detection threshold to higher values or equivalently decreasing the false alarm probability (Note that each detection threshold corresponds a specific false alarm probability), the detection probability also decreases. Due to the reduction of the detection probability, more attempts are required to acquire the signal and hence the acquisition time increases.

Table 5-1: Parameters used in the simulations (deterministic signal)

C/N_0	40 dB-Hz
T_{coh}	1 ms
K (number of non-coherent)	1
T_s	1.5 s
T_p (penalty time)	0.5 s
Search strategy	Maximum likelihood

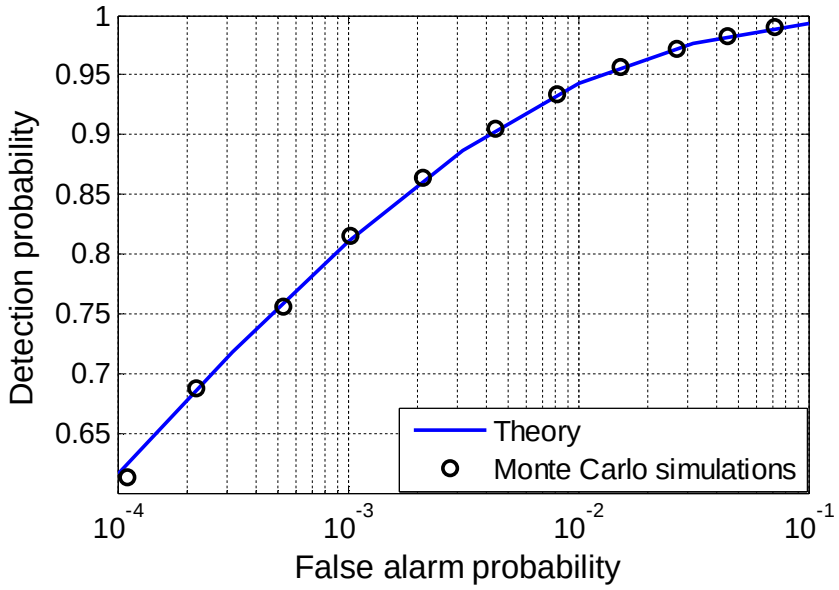

Figure 5-2: Cell level ROC curves

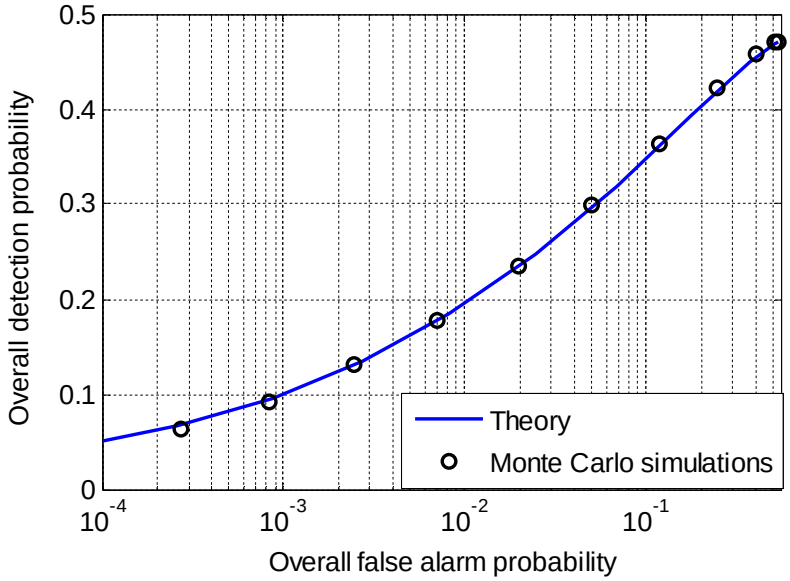

Figure 5-3: System level ROC curves

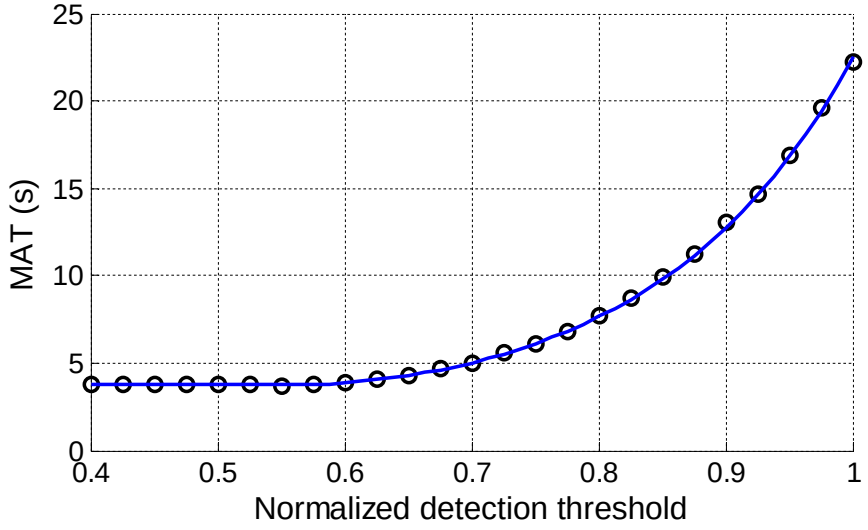

Figure 5-4: Mean acquisition time versus detection threshold

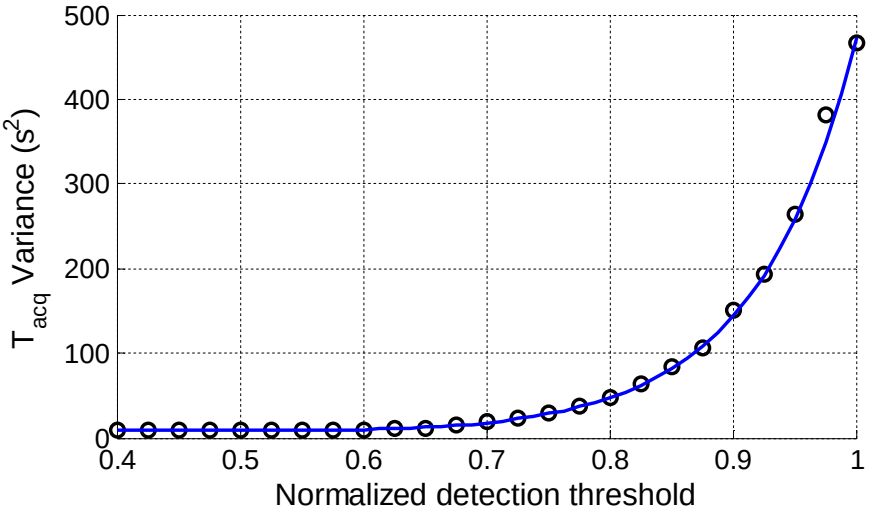

Figure 5-5: Variance of acquisition time versus detection threshold

5.1.1 Equal gain combining in Rayleigh fading channels

To further investigate the theoretical results presented in Chapter 3, a Rayleigh fading channel was simulated in MATLAB® using the MATLAB communication toolbox. Fading channel parameters such as the maximum Doppler shift due to the receiver motion and the average signal power were set in the simulation. Here the maximum Doppler shift of 1 Hz is considered which corresponds to having a moving antenna with a speed of 20 cm/s. The Monte Carlo simulations results are based on 10 ms coherent integration, one non-coherent ($K = 1$) and cold start acquisition (without using any assistance information for the acquisition process). Therefore, considering GPS L1 C/A code length of 1023 chips, Doppler values range between -5 kHz to 5 kHz as a result the search space includes $N_C = 2046$, $N_D = 151$ and $M = 308946$. Furthermore, the same $\sigma_S^2 / \sigma_N^2 = 12$ dB value is chosen for both fading channels resulting in the same average *SNR* values. A

search space with the size of *M* cells, was generated 10^5 times. Incorrect cells include uncorrelated Gaussian noise and the correct cell consists of signal plus noise with a Rayleigh distributed amplitude. The simulated post processing *SNRs* for each branch after combining are shown in Figure 5-6. It should be emphasized that due to the non-coherent combining operation, noise is not zero mean and in contrast to the zero mean Gaussian noise situations there is not any unique definition for *SNR*. Instead, especially in the GNSS context, the deflection coefficient metric which is also called output *SNR* (*SNR* at the detector output) is used (Kay 1998, Borio et al 2008). The deflection coefficient (DC) is expressed as

$$DC = \frac{E\{Y|H_1\} - E\{Y|H_0\}}{\sqrt{\text{var}\{Y|H_0\}}} \tag{5-3}$$

where *Y* is the decision variable that is defined for single branch and EGC provided in the previous chapter. Herein, the post processing *SNR* corresponds to the deflection coefficient.

As shown in Figure 5-6, after the diversity combining using the EGC techniques, the output signal has a smoother *SNR* compared to the single branches and this increases the detection probability. Figure 5-7 illustrates the instantaneous *SNR* improvement achieved by the equal gain combining for a certain part of simulated signals. Having higher and smoother *SNR* values over time enhances the chance of successful acquisition at each attempt to acquire the signal. More than 25 dB *SNR* improvement can be observed when one of the branches

experiences deep fading. However, when the signals at both antennas almost equally fade, diversity combining does not provide a significant gain.

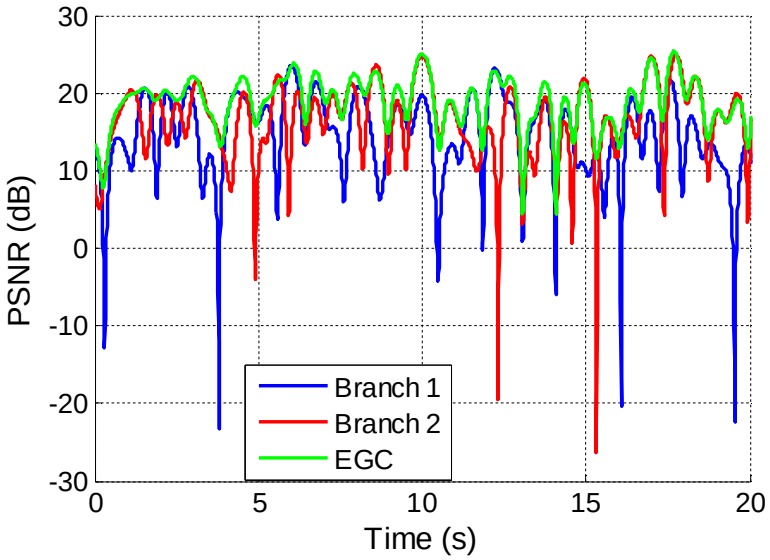

Figure 5-6: Post processing *SNR* for simulated fading channels

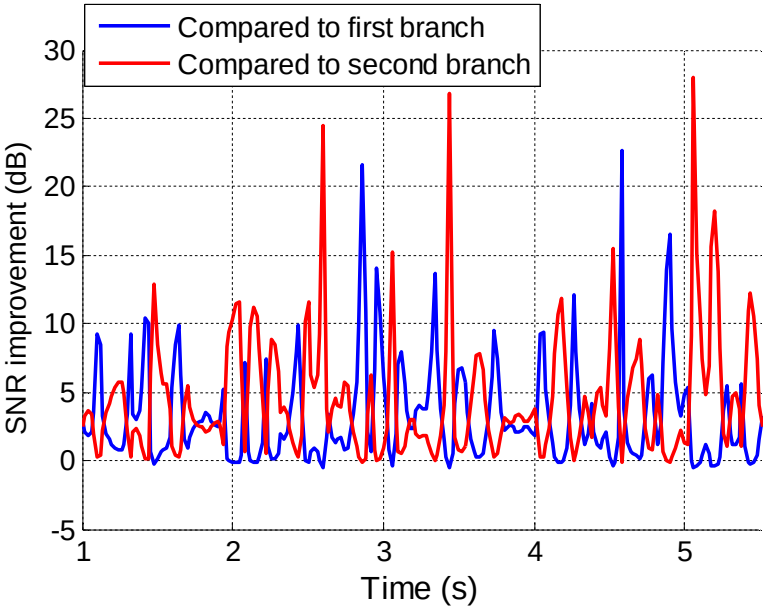

Figure 5-7: *SNR* improvement after equal gain combining versus time – Simulation

Figure 5-8 illustrates the cell level ROC curves for the single branches and EGC resulting from the Monte Carlo simulations. Obviously, single branches (Branch 1 and 2) have similar performance since the average *SNR* value is similar in both branches.

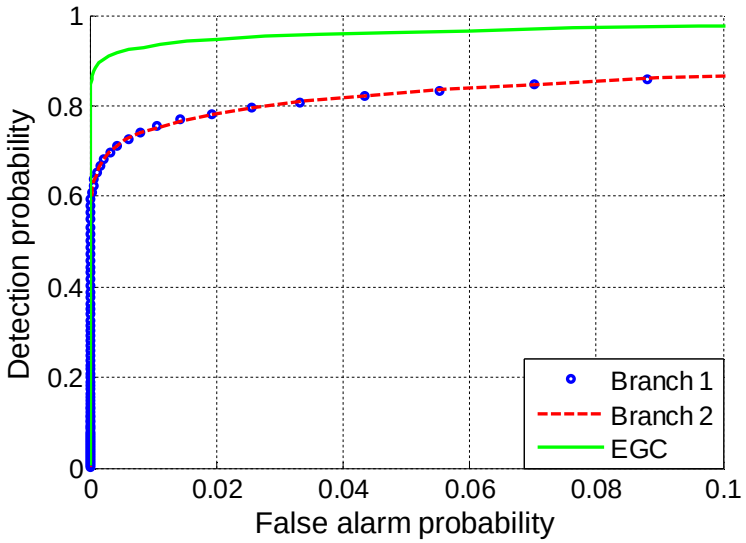

Figure 5-8: Cell level ROC curves- Simulations

Figure 5-9 and 5-10 show the cell level and system ROC curves obtained from theory and Monte Carlo simulations where it is assumed that the two channels are uncorrelated. Obviously, strong agreement exists between theory and Monte Carlo simulations. Significant improvement in cell level detection probability after applying the EGC method is realized. In order to evaluate the diversity performance, the diversity gain metric (G) is used.

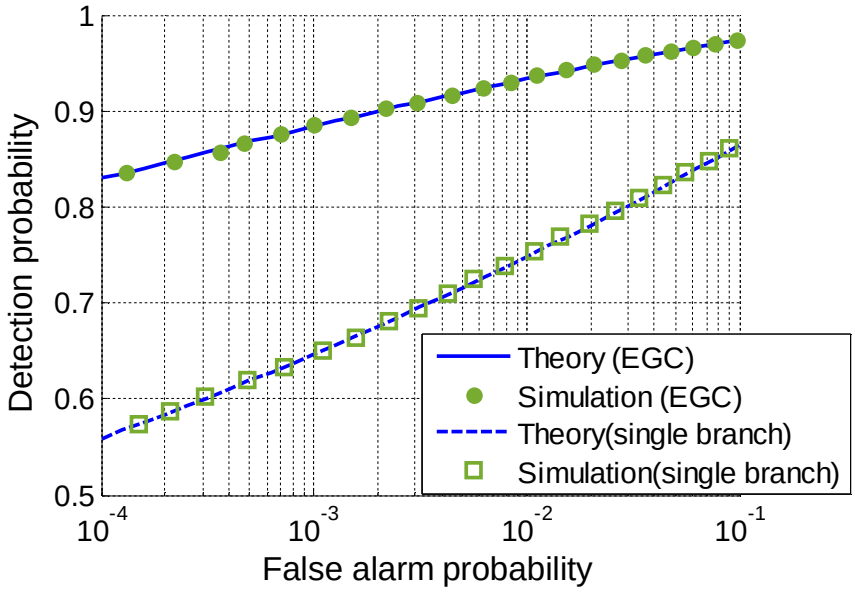

Figure 5-9: Cell level ROC curves –Theory and Simulation

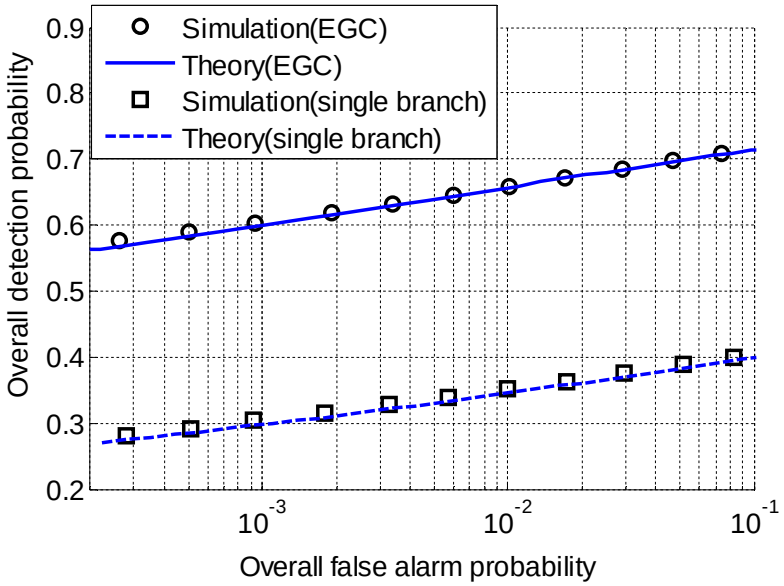

Figure 5-10: System level ROC curves in the signal presence –Theory and Simulation

5.1.1.1 Diversity gain

Broumandan et al (2009) assumed the desired goal is to reach a specific target detection parameters as (P_{fa},P_d). To this end, if the required *SNR* values for single branch and EGC to reach the target point are SNR_S and SNR_{EGC} respectively, the diversity gain is defined as $G = SNR_S / SNR_{EGC}$. In this case, assuming a specific target detection point $(P_{fa} = 10^{-4}, P_d = 0.9)$ in the cell level, $G \approx 5$ dB. In the system level, for a target point of $(P_{FA} = 0.01, P_D = 0.7)$, the overall diversity gain is about 4.5 dB, which is a remarkable gain improvement. The improvement in the cell and system level detection probabilities for given false alarm probabilities is shown in Figure 5-11 and Figure 5-12. The diversity gain is expressed as

$$\begin{cases} T_{cell} : (P_{fa} = 10^{-4}, P_d = 0.9) \\ G_{cell} = \dfrac{SNR_S \to T_{cell}}{SNR_{EGC} \to T_{cell}} \approx 5\ dB \end{cases} \tag{5-4}$$

$$\begin{cases} T_{system} : (P_{FA} = 10^{-2}, P_D = 0.7) \\ G_{system} = \dfrac{SNR_S \to T_{system}}{SNR_{EGC} \to T_{system}} \approx 4.5\ dB \end{cases} \tag{5-5}$$

Without using the diversity technique and having only one antenna, 2.8 times longer coherent integration time is required in order to obtain a 4.5 dB additional gain by increasing the integration time. However, since increasing the coherent integration time in the acquisition stage is limited due to the navigation bit

transition, non-coherent integration should be adopted. Considering the squaring loss resulting from the non-coherent combining method, which reduces processing gain compared to using coherent integration, integration time should be increased by a factor greater than 2.8 to achieve the 4.5 dB gain. Consequently, acquisition time and the computational complexity increases.

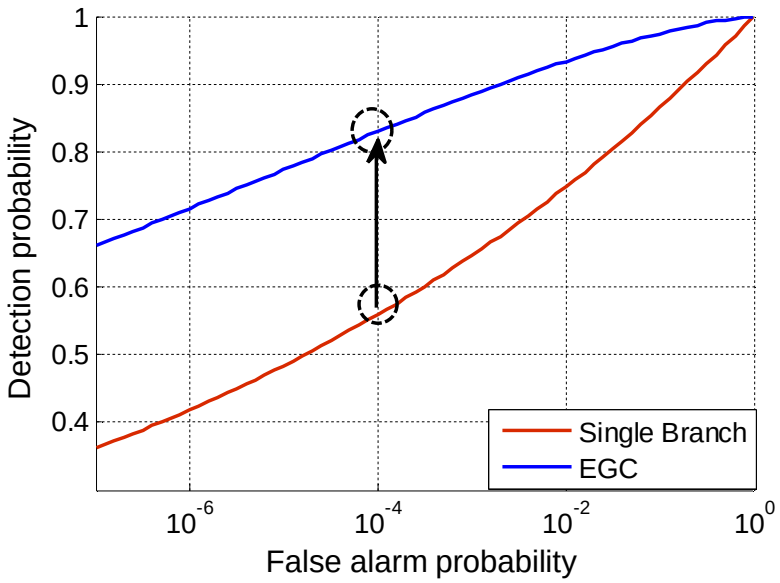

Figure 5-11: Improvement in cell level ROC after EGC

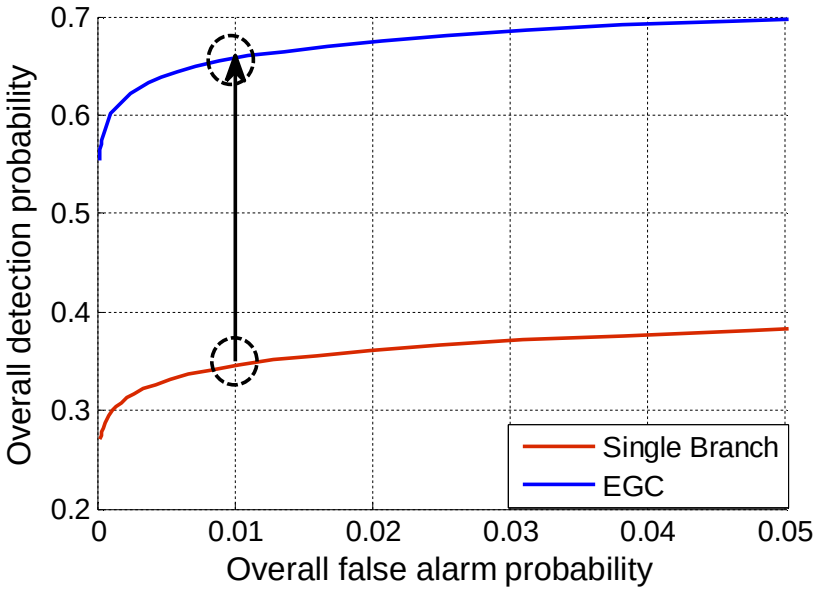

Figure 5-12: Improvement in system level ROC after EGC

5.1.1.2 Acquisition time

The next important evaluation metric is the acquisition time which is defined as the time required for successful acquisition. Especially, in weak signal situations this metric becomes crucial. Acquisition time as a function of detection and false alarm probabilities is a random variable and in addition to the mean value, it has a variance. The mean acquisition time versus P_{fa}, considering $T_p = 0.5$ s and $T_s = 1.5$ s, is shown in Figure 5-13. Note that here each P_{fa} value corresponds to a certain detection threshold and it is computed theoretically. For example, assuming $P_{fa} = 10^{-7}$, the detection threshold is computed theoretically and it is used in the acquisition time simulations. Figure 5-14 illustrates the MAT improvement after the equal gain combining. According to the theory and the

simulation results, more than 43% reduction in MAT considering $P_{fa} = 10^{-6}$ is achieved from the diversity combining. This provides a significant improvement in the acquisition time especially in a severe fading environment where MAT could be of the order of several minutes. As discussed, MAT depends on the false alarm probability or equivalently on the detection threshold. Intuitively, setting the detection threshold to a higher level leads to more immunity against false alarms. Having fewer false alarms reduces the penalty time and as a result reduces the acquisition time. On the other hand, choosing a higher threshold value can decrease the chance of detection and consequently acquisition time increases. This means depending on the detection probability, search strategy and penalty time, it is possible to have an optimal detection threshold for which MAT is minimized. In practice, if there is a priori information about C/N_0 values, considering the integration strategies, integration time and penalty time, a fixed optimum detection threshold can be used. Otherwise, if the C/N_0 value is not known, assuming different values for C/N_0 the detection threshold should be adaptively set.

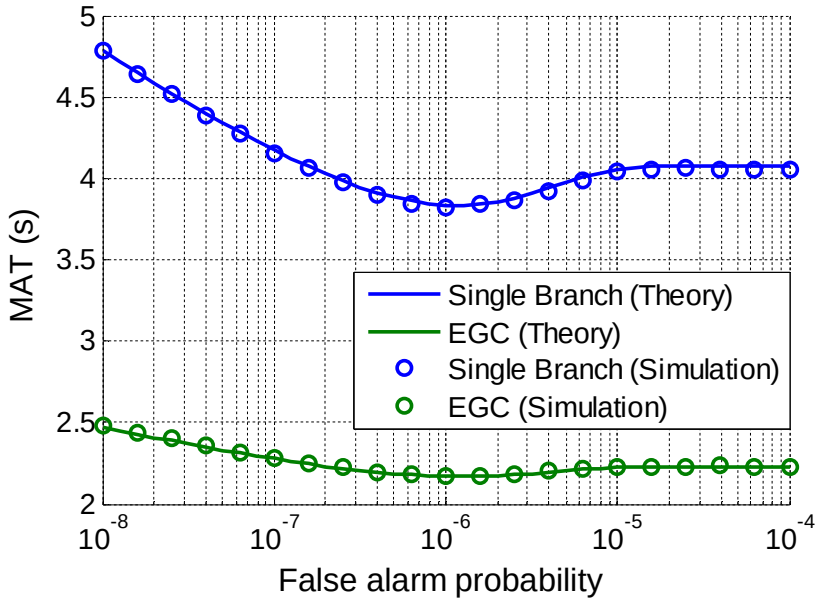

Figure 5-13: Mean acquisition time versus false alarm probability

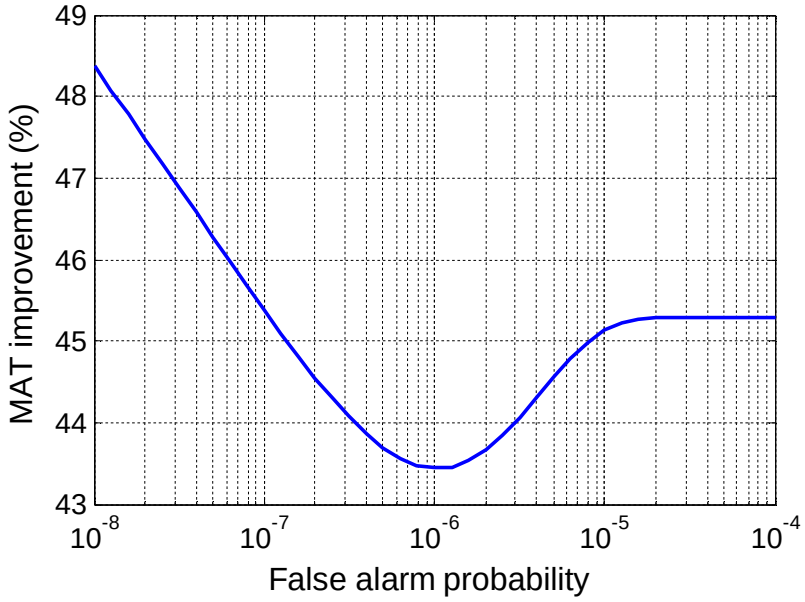

Figure 5-14: Mean acquisition improvement after equal gain combining

While the detection performance of a single channel receiver can be improved by increasing the integration time, the improvement in MAT is not necessarily

possible by doing so. This is due to the fact that increasing the integration time enhances the detection probability which results in faster acquisition; however, due to processing of more samples and searching over a larger search space (in case of longer coherent integration time), acquisition time increases. Therefore, reduction in the acquisition time by using longer integration time is limited.

In addition to MAT, the variance of acquisition time is used to measure how the acquisition time values spread out. As stated earlier, there is no closed form expression for the variance of acquisition time in fading channels and the results presented here are only based on Monte Carlo simulations. In deep fading situations signal power significantly drops and acquisition time dramatically increases. This results in a higher variation in the acquisition time. Since the diversity combining mitigates the fading effect and reduces the moments during which the signal is subject to deep fading, EGC has a lower acquisition time variance than a single branch. According to Figure 5-15, the variance of the acquisition time significantly decreases after applying EGC. This is also obvious from Figure 5-16, which shows this compared to the single branch method; in the EGC case, acquisition time variation (for $P_{fa} = 10^{-6}$) is relatively smooth over time. Because EGC provides a smoother *SNR* compared to a single branch, acquisition time as a function of *SNR* is also smoother and has a lower variance. The spikes in the single branches correspond to fading moments where *SNR* drops and more time should be spent to acquire the signal.

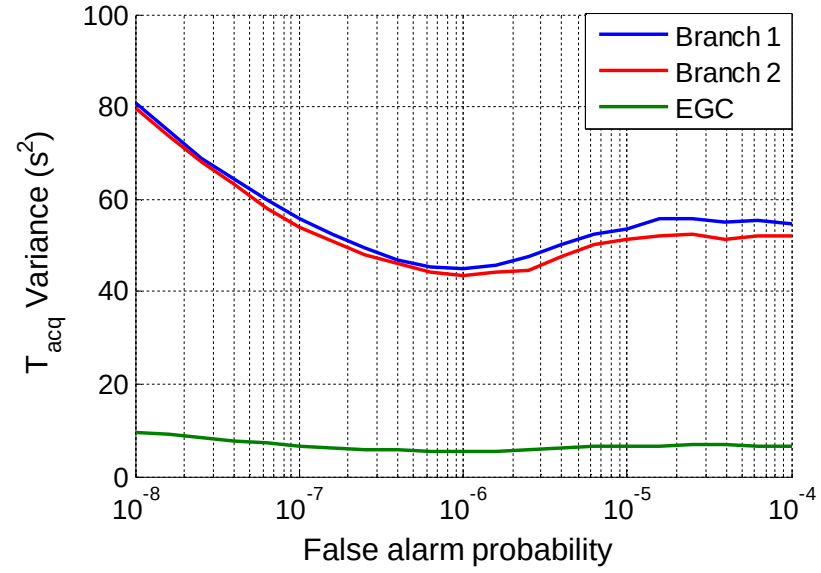

Figure 5-15: Acquisition time variance

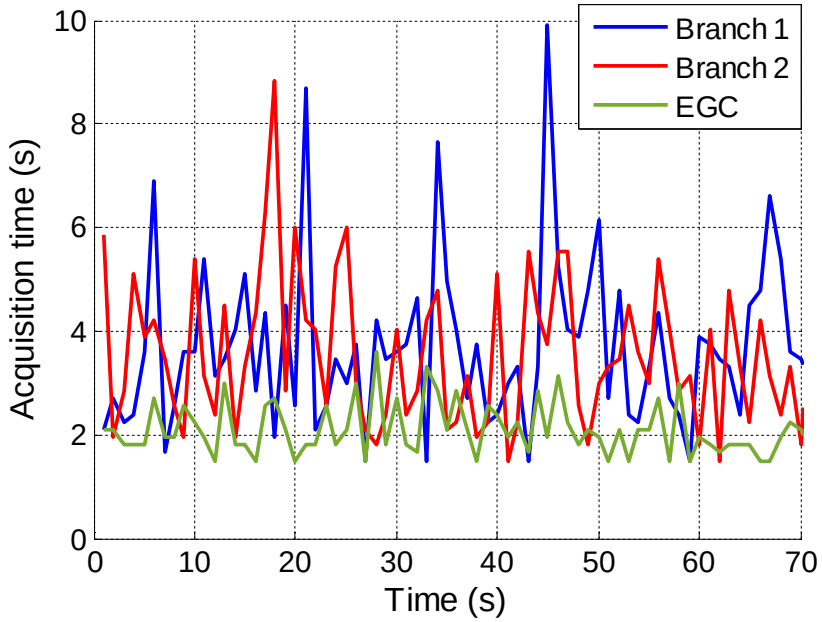

Figure 5-16: Acquisition time over time for $P_{fa}=10^{-6}$

The following figures compare the acquisition time performance of two and four channels equal gain combining using Monte Carlo simulations. Applying EGC to

four channels outperforms the two channels combining in terms of the detection probability as well as mean and variance of acquisition time. Figure 5-18 shows that increasing the number of antennas from two to four provides a 16% improvement in MAT. Further, according to Figure 5-19 by adding more antennas, the acquisition time variance decreases and approaches 0 due to smoother *SNR* values.

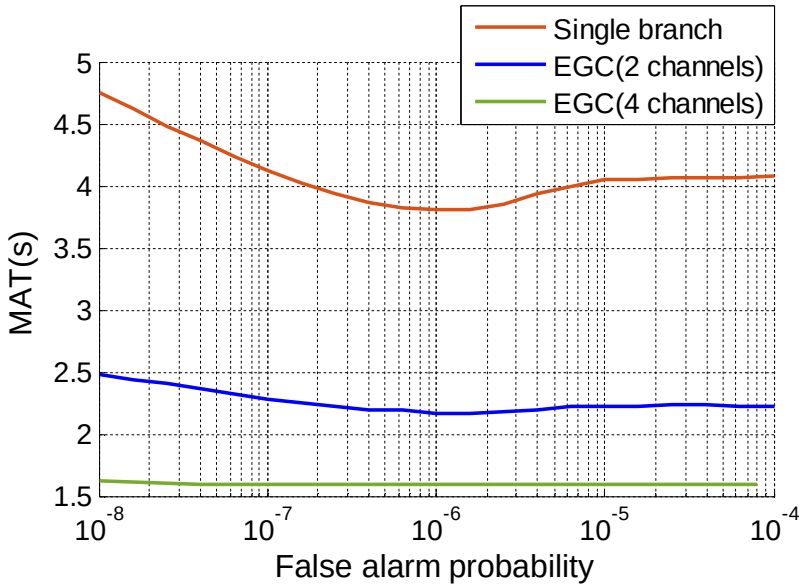

Figure 5-17: Mean acquisition time vs. false alarm probability

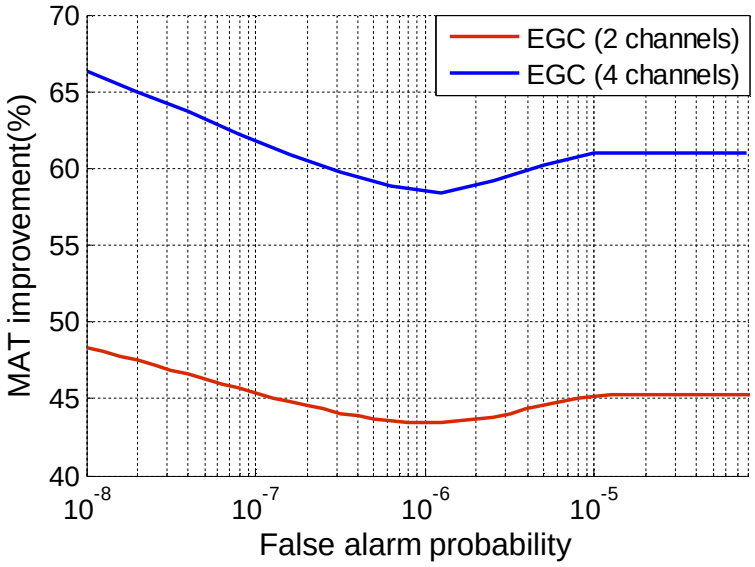

Figure 5-18: MAT improvement after EGC

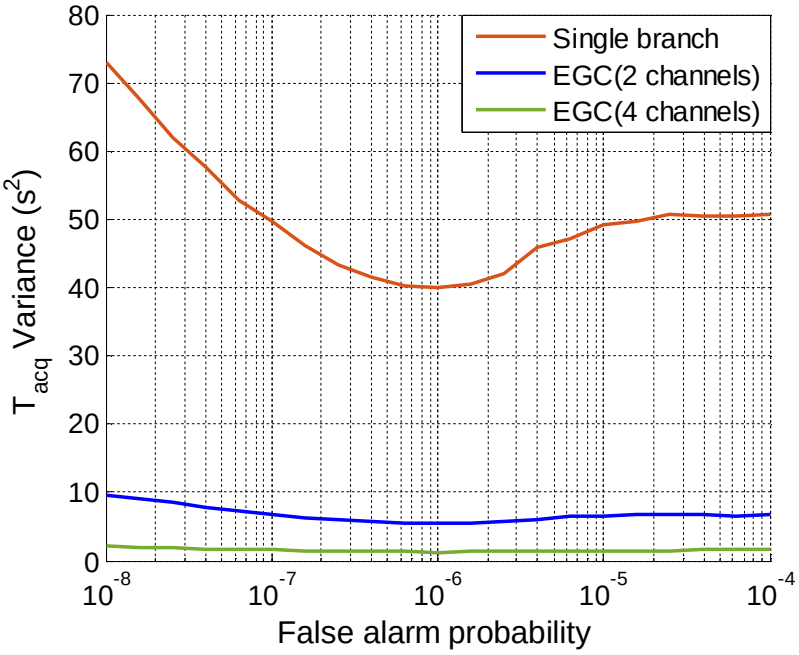

Figure 5-19: Variance of acquisition time vs. false alarm probability

Figure 5-20 shows MAT versus the number of antennas assuming they receive uncorrelated signals. Obviously, by increasing the number of antennas MAT decreases, however, the rate of improvement decreases as the number of antennas increases. The reason is that having a certain number of antennas and utilizing the diversity combining, fading is sufficiently mitigated and the SNR values are relatively smooth. Therefore adding more antennas does not prove to be a considerable improvement in the detection and acquisition time.

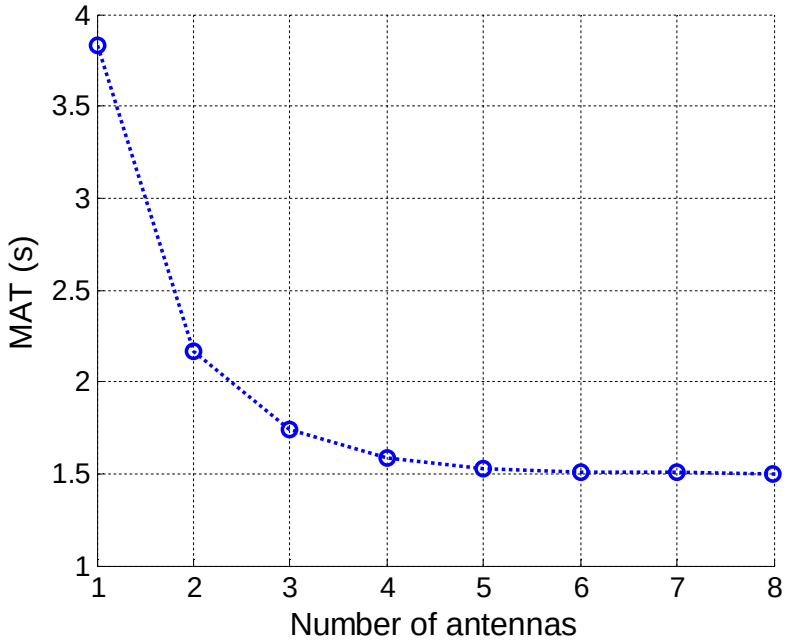

Figure 5-20: MAT versus number of antennas

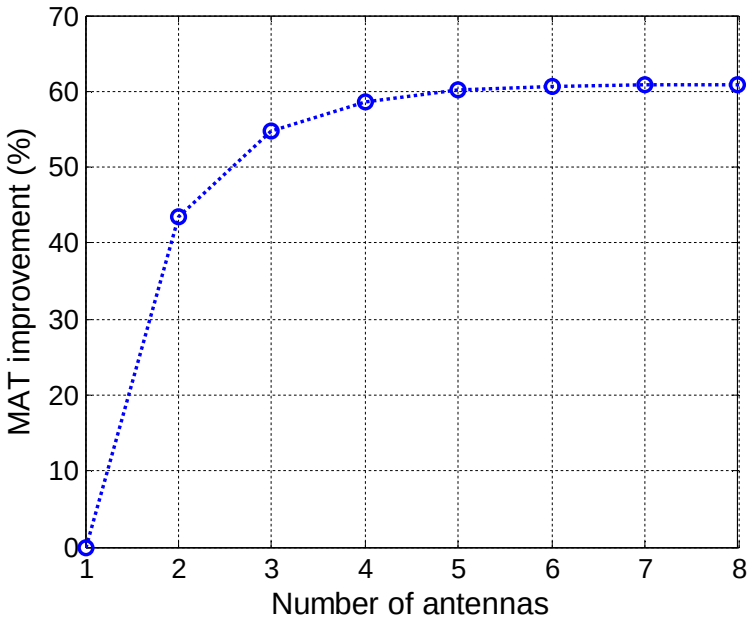

Figure 5-21: MAT improvement by EGC compared to a single antenna

5.2 Real data results

5.2.1 Fading channel characterization

In order to further verify the multipath fading effect, a u-blox GNSS receiver was used to collect data in two different indoor environments. The u-blox receiver is a commercial high sensitivity receiver able to provide a good estimate of C/N_0 values in weak signal situations. In the following, C/N_0 values for different PRNs in the static receiver case are illustrated. Small patch antennas are used and the antennas separation is 20 cm. Herein in order to show the multipath fading effect that causes C/N_0 variations, C/N_0 values are provided using the u-blox GNSS receiver. Further analyses on the detection and false alarm probabilities using IF of GPS L1 signal are discussed in the next section.

The first set of data collection was performed in the Kinesiology-B building on the University of Calgary campus as shown in Figure 5-22 and 5-23. The sky plot of the satellites in view is depicted in Figure 5-24. Multipath fading is observed in Figure 5-25 and 5-26 which illustrate the C/N_0 values at the two branches for two different PRNs. The slow C/N_0 variations are only due to the satellite motion as the receiver was static.

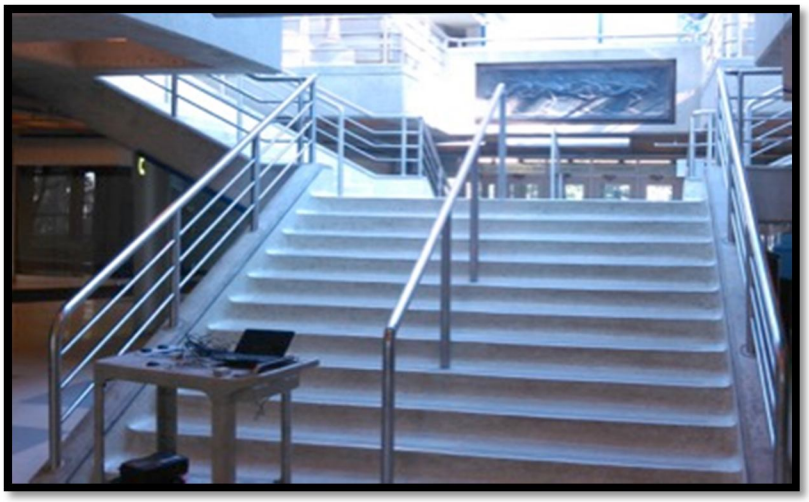

Figure 5-22: Data collection environment

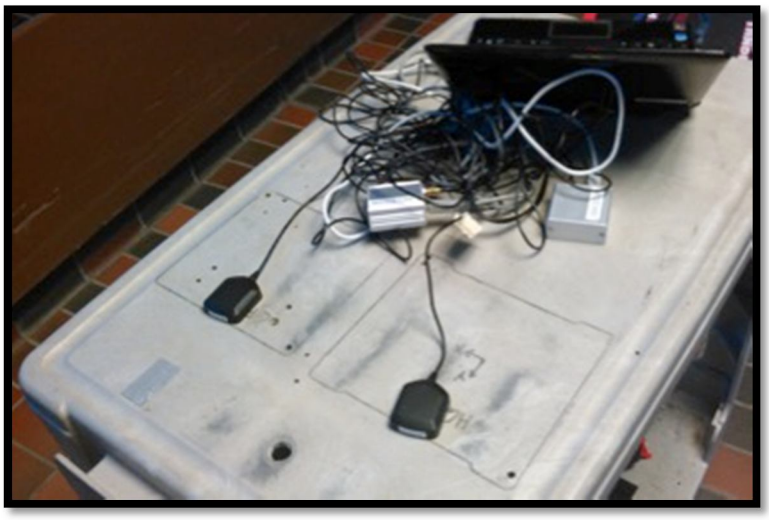

Figure 5-23: Data collection scenario

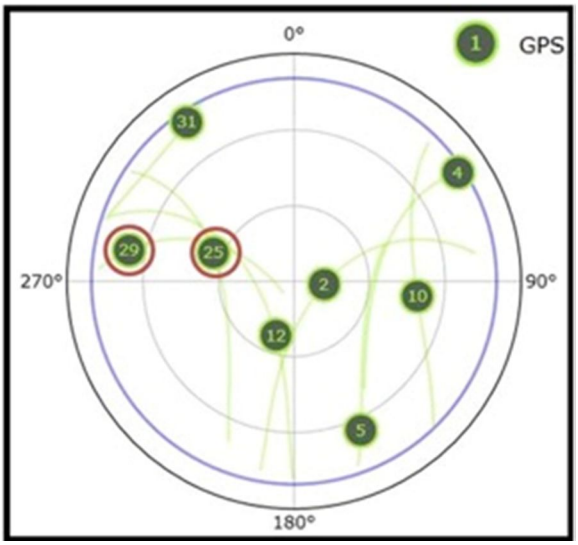

Figure 5- 24: Sky plot of the satellite constellation during data collection, Location: Kinesiology-B building on the University of Calgary campus

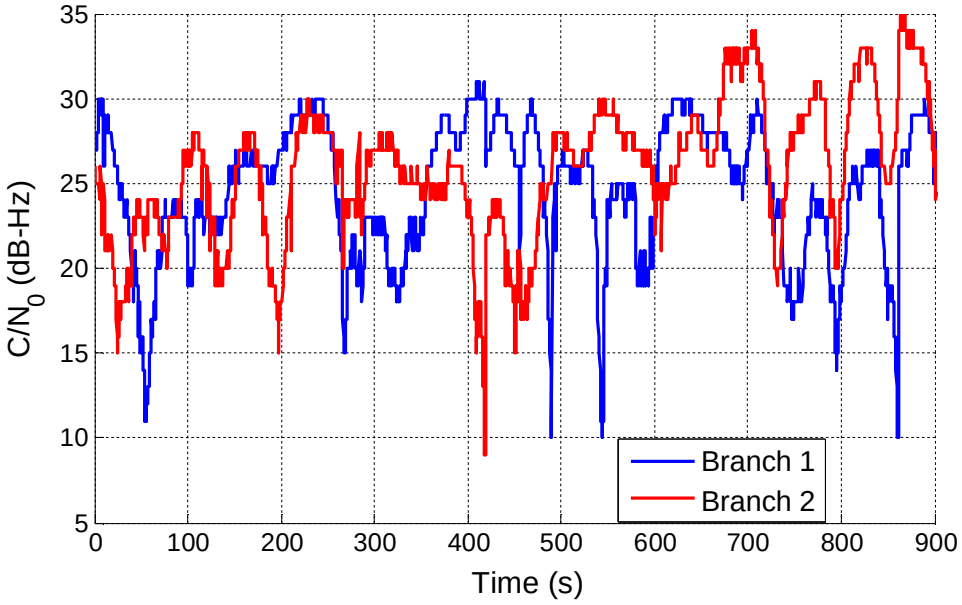

Figure 5-25: *C/N₀* estimation using u-blox receiver, static mode, PRN, Location: Kinesiology-B building on the University of Calgary campus

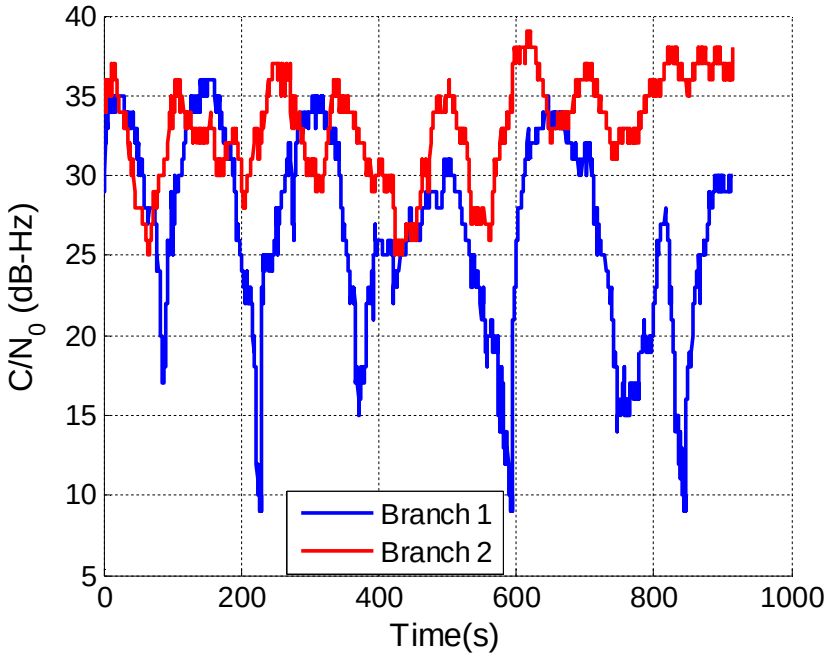

Figure 5-26: *C/N₀* estimation using u-blox receiver, static mode, PRN 25, Location: Kinesiology-B building on the University of Calgary campus

The second set of data collection using the u-blox receiver was performed in the Earth Science building at the University of Calgary as shown in Figure 5-27. The sky plot of the satellites in view is depicted in Figure 5-28. As shown in Figure 5-29 and 5-30, signals fade differently at the two antennas separated by 20 cm.

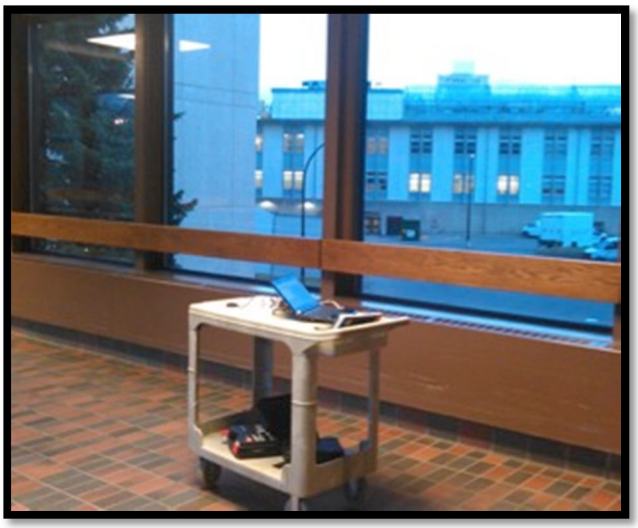

Figure 5-27: Data collection environment

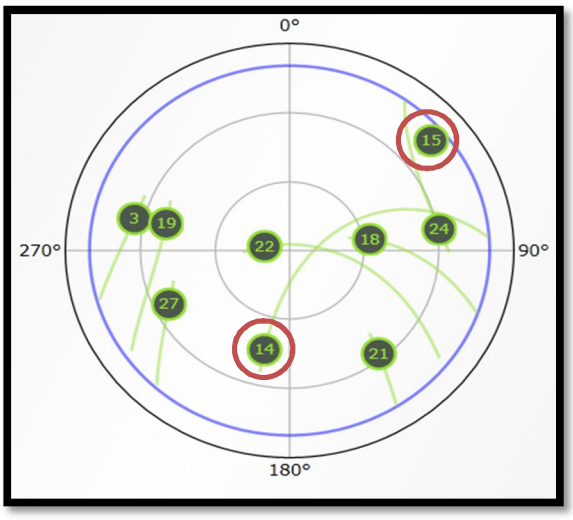

Figure 5-28: Sky plot of the satellite constellation during data collection, Location: Earth Science building at the University of Calgary

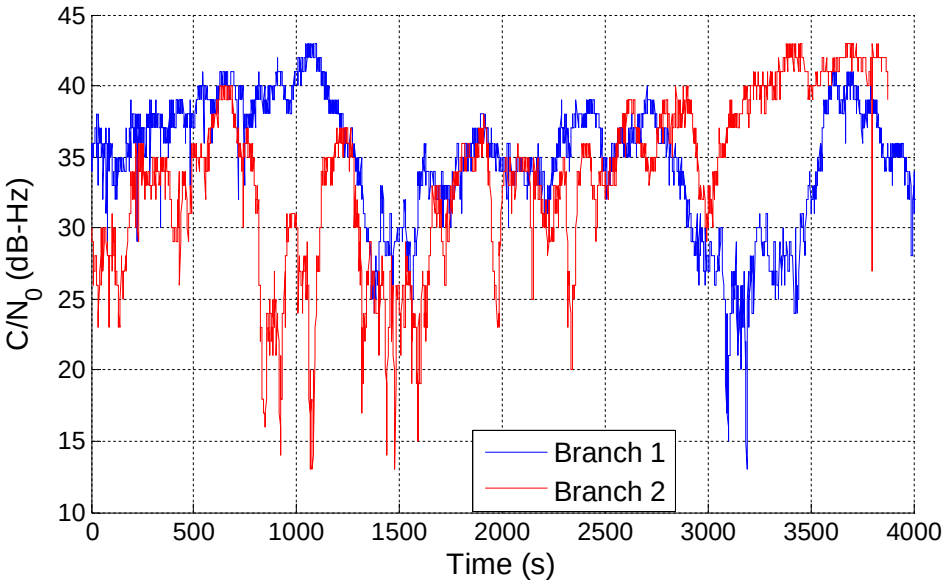

Figure 5-29: C/N_0 estimation using u-blox receiver, static mode, PRN 14, Location: Earth Science building at the University of Calgary

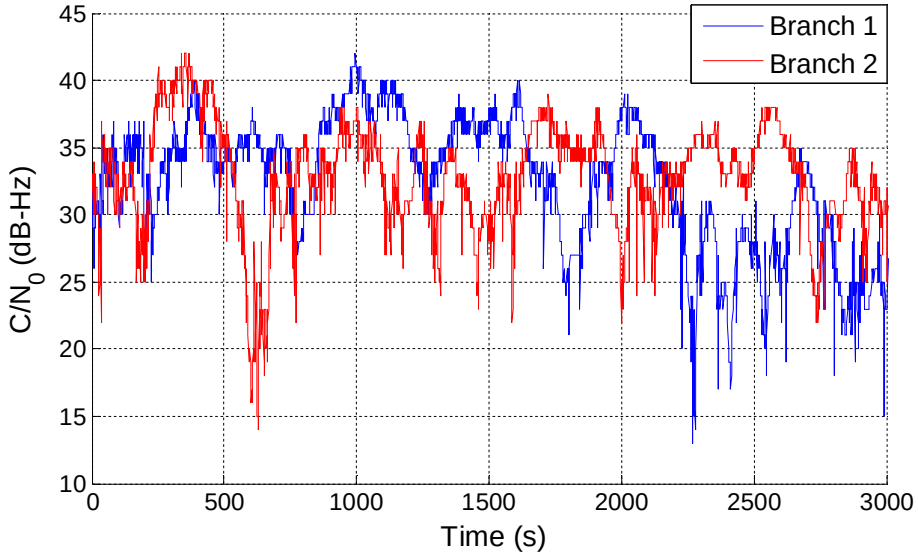

Figure 5-30: C/N_0 estimation using u-blox receiver, static mode, PRN 15, Location: Earth Science building at the University of Calgary

5.2.2 Equal gain combining using IF samples

Data collection was also performed in a concrete and glass building on the University of Calgary campus shown in Figure 5-32. Due to destructive multipath effect significant GNSS signal fading was observed. Using a 3-channel National Instruments (NI) RF front-end, a set of Intermediate Frequency (IF) GPS L1 signal samples was collected in dynamic mode (velocity of 20 m/s). The complex sampling rate was 5 MHz. As shown in Figure 5-31, in addition to two antennas located indoors, one outdoor reference antenna was used to assess the validity of results. The satellite sky plot is shown in Figure 5-33. For PRN 10, PSNR values shown in Figure 5-34 are estimated using the GSNRx-rr software receiver (Petovello et al 2008), which uses data bits extracted from the reference antenna to increase the coherent integration time up to 200 ms in order to acquire the weak indoor signals. This aiding is just used for PSNR estimation to show the signal power variation due to fading and the rest of the analysis is performed based on 10 ms coherent integration. Figure 5-35 shows the instantaneous PSNR improvement achieved by the diversity combining using the real data measurements. According to the experimental results, signal power can drop by up to 30 dB in deep fading situations. This simply means that when only one antenna is available, in order to compensate for 30 dB fading in the acquisition process, about 1000 times additional coherent integration is required. Hence, the necessity of exploiting antenna diversity is evident unless the signals in both antennas are simultaneously deeply faded. However, the diversity performance is affected by the correlation between the signals in different branches. The more

uncorrelated two channels are, the higher the performance attained from the diversity combining. Hence, for uncorrelated fading channels antenna, diversity provides the highest improvement in the acquisition performance. The common metric used to evaluate the similarity between two signals is the correlation coefficient. The complex signal correlation coefficient between S_1 and S_2 signals is expressed as (Colburn et al 1998)

$$\rho_c = \frac{E\left[S_1 \times S_2^*\right]}{\sqrt{E\left[S_1 \times S_1^*\right] \times E\left[S_2 \times S_2^*\right]}} \tag{5-6}$$

The correlation coefficient for the real collected signals is (0.03-0.04j) which shows a very small correlation between the received signals. As a result, the two received signals can be approximately considered as uncorrelated signals.

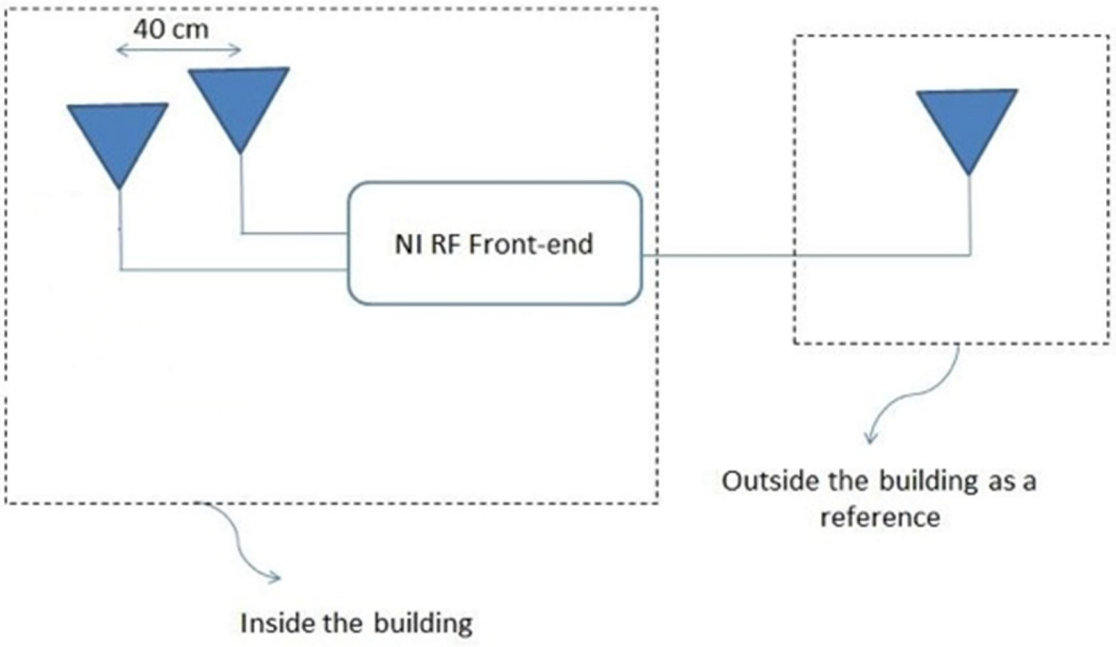

Figure 5-31: Data collection scenario

Table 5- 2: Data collection parameters

Main equipment	RF-front end, Novatel GPS antennas-series 700
Signal	IF samples of GPS L_1 C/A
Sampling rate	5 MHz
Mode	Static and Dynamic
Duration	5 min for dynamic, 25 min for static
Antennas separation	20 cm and 40 cm
Location	Inside the MacHall building at the University of Calgary

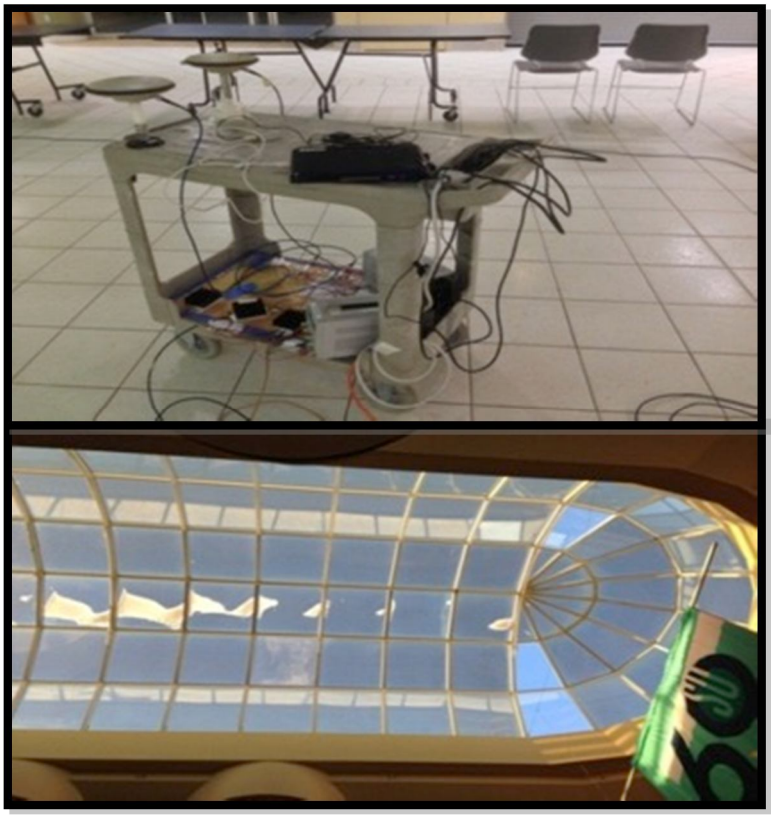

Figure 5-32: Data collection environment

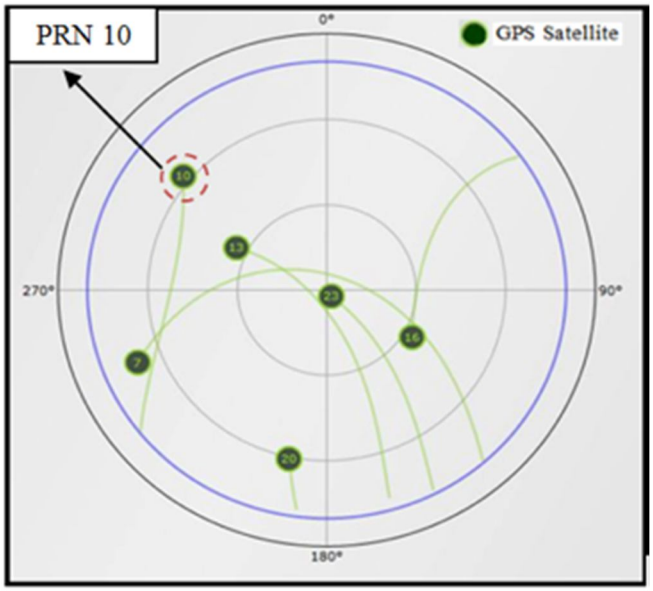

Figure 5-33: Satellite sky plot during data collection, Location: MacHall building on the University of Calgary campus

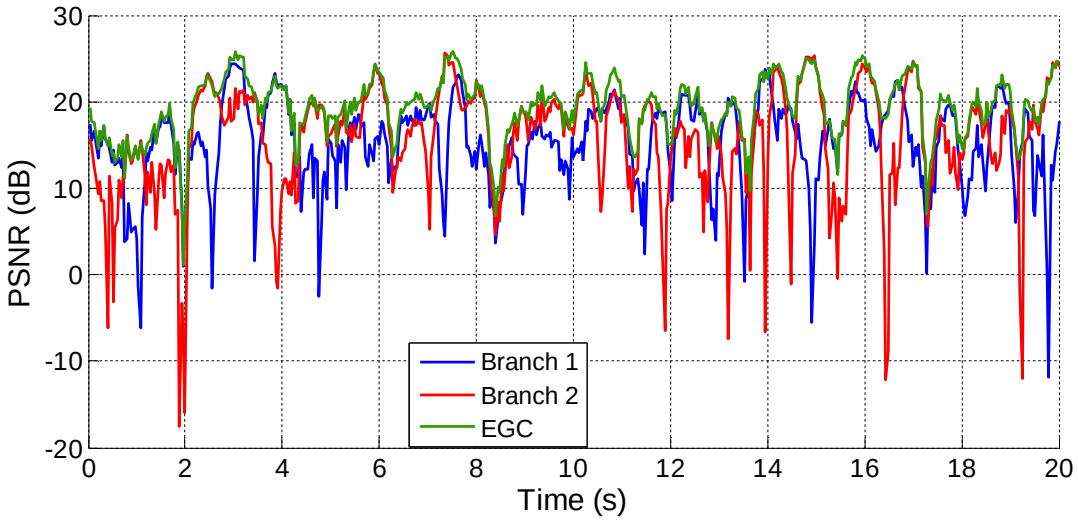

Figure 5-34: Post processing *SNR* – Real data, PRN 10, dynamic, Location: MacHall building on the University of Calgary campus

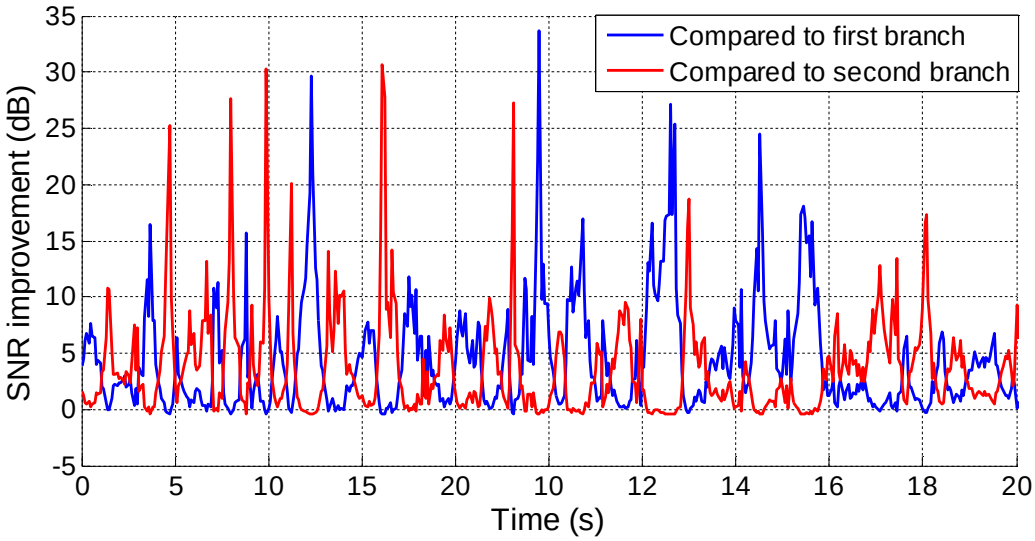

Figure 5-35: *SNR* improvement after equal gain combining versus time - Real data, PRN 10

As discussed earlier, in a Rayleigh fading environment, signal is a random process with the amplitude that follows a Rayleigh distribution and the uniform distributed phase between $[-\pi, \pi]$. The distribution of in-phase and quadrature components of the signal is Gaussian with zero mean value. According to Figure 5-36 and 5-37, which illustrate the histogram of in-phase and quadrature components of the real signal, amplitudes are very close to a zero mean Gaussian distribution. Furthermore, as shown in Figure 5-38, the phase of the signal approximately follows a uniform distribution.

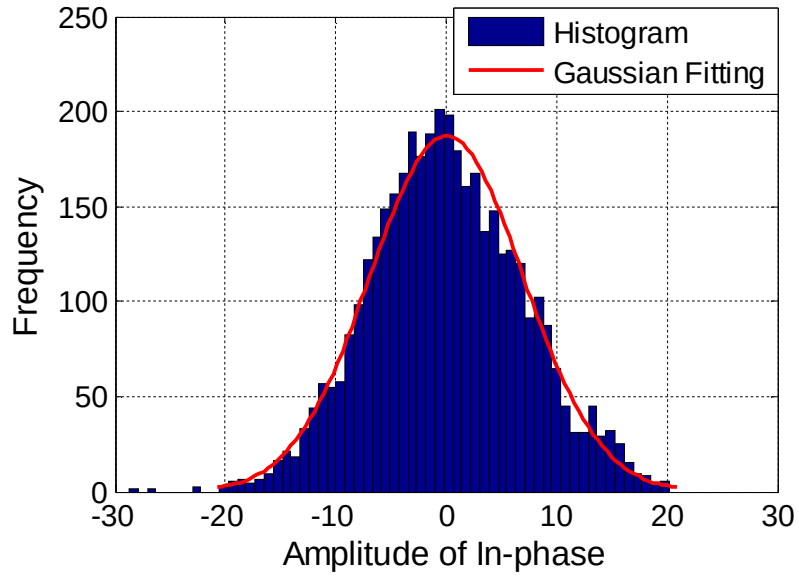

Figure 5-36: Amplitude of In-phase component-Real data

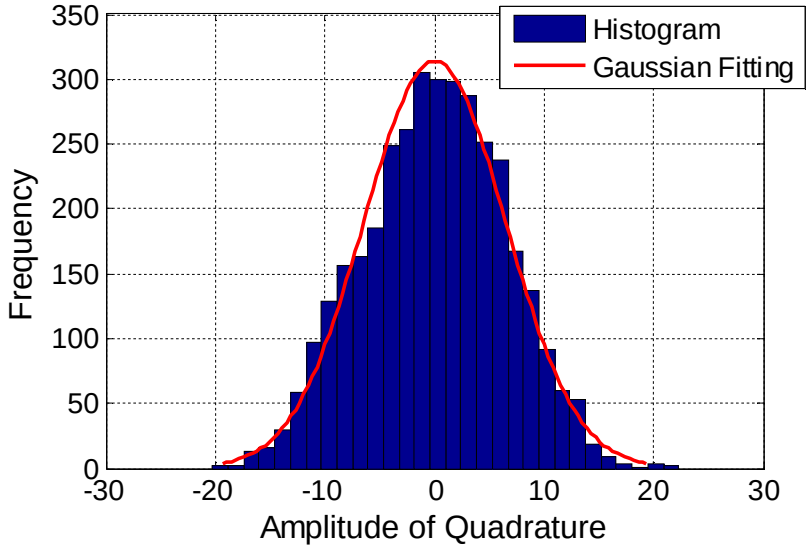

Figure 5-37: Amplitude of quadrature component- Real data

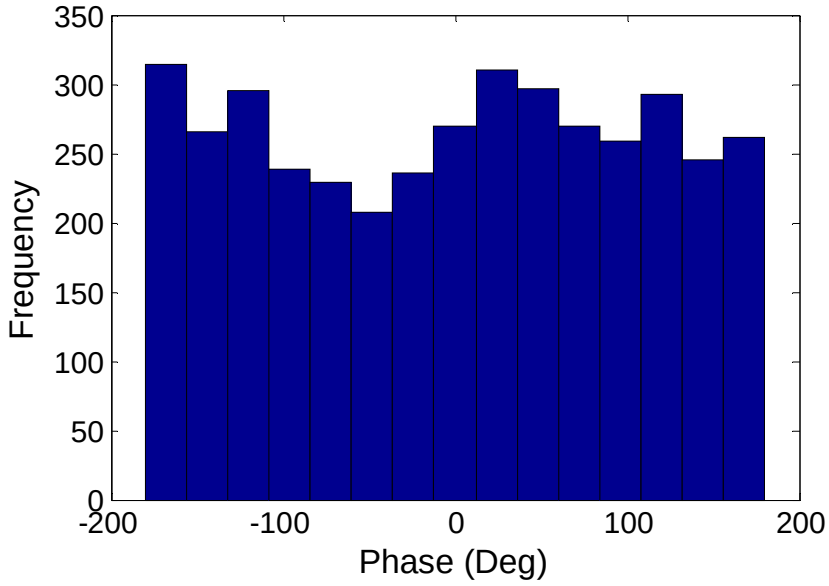

Figure 5-38: Phase of the received signal-Histogram

In order to verify the signal distribution under the H_0 and H_1 conditions provided in the previous chapter, histograms of the real data are shown in the following Figures. Under the H_0 hypothesis, the noise power follows a chi-square distribution with two degrees of freedom, which is equivalent to the exponential distribution. According to Figure 5-40, the signal amplitude has a Rayleigh distribution.

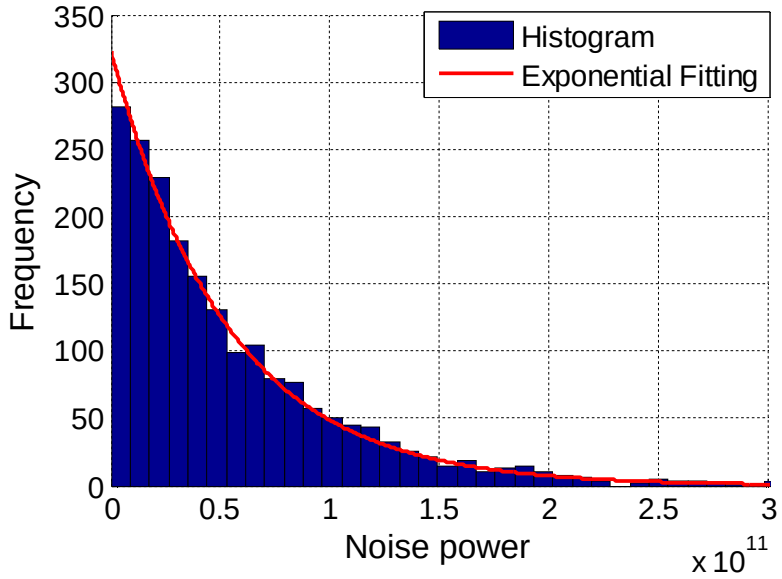

Figure 5-39: Histogram of the data under H_0 condition, PRN 10

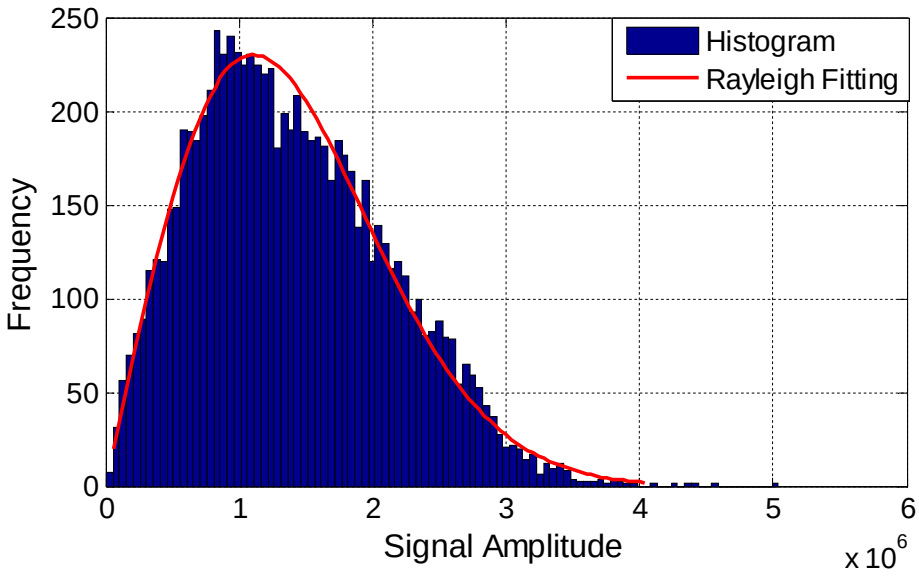

Figure 5-40: Histogram of the data under H_1 condition, PRN 10

According to Figure 5-41 which shows the overall correct detection over time for a specific detection threshold, in the EGC case more successful correct detection is observed compared to the single branches. As shown in the figure, for some

moments the signal is detected only in one of the branches and also in EGC, there are some moments that it is detected only in EGC, and when the both single branches experience deep fading, the signal cannot be acquired. According to Figure 5-42 and Figure 5-43 which show the cell and system level ROC curves using real IF samples, the single branches have similar performance. The ROC curves in cell and system levels from theory, simulation and real data are shown in Figure 5-44 and Figure 5-45. The sample sizes in the Monte Carlo simulations and real data analysis are 10^5 and 4000, respectively. The Monte Carlo simulations and theoretical results match, as expected, and they are similar to the real data results. The main reason for the slight difference between real data and theoretical results is that the real data set sample size is not large enough for a high resolution statistical analysis. In the theoretical analysis it is assumed that the two branches are completely uncorrelated whereas this is not the case for the real data measurements. Moreover, the simulations and theoretical results are based on the assumption of a perfect Rayleigh fading channel. However, having a relatively strong signal component changes the channel characteristics from Rayleigh to Rician. Real data results show that the channel is near Rayleigh since the in-phase and quadrature components of the signal are very close but not exactly zero mean Gaussian.

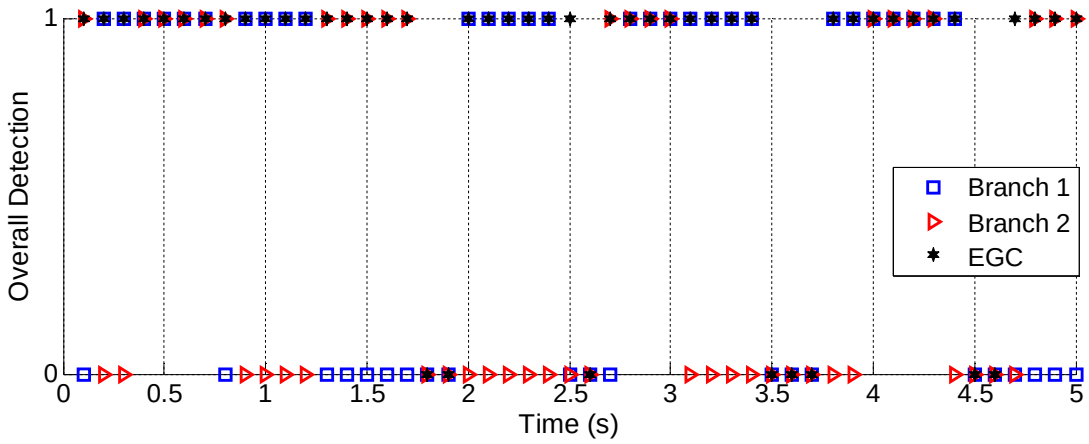

Figure 5-41: Overall detection over time, PRN 10

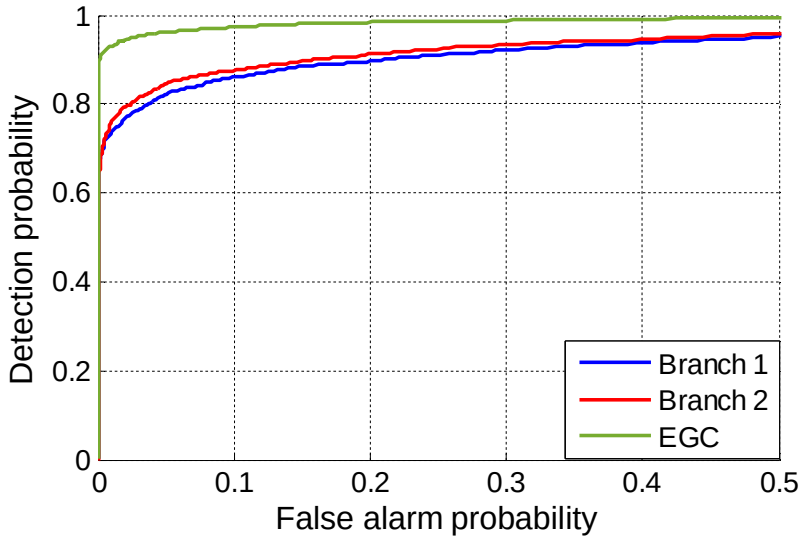

Figure 5-42: Cell level ROC curves-Real data, PRN 10

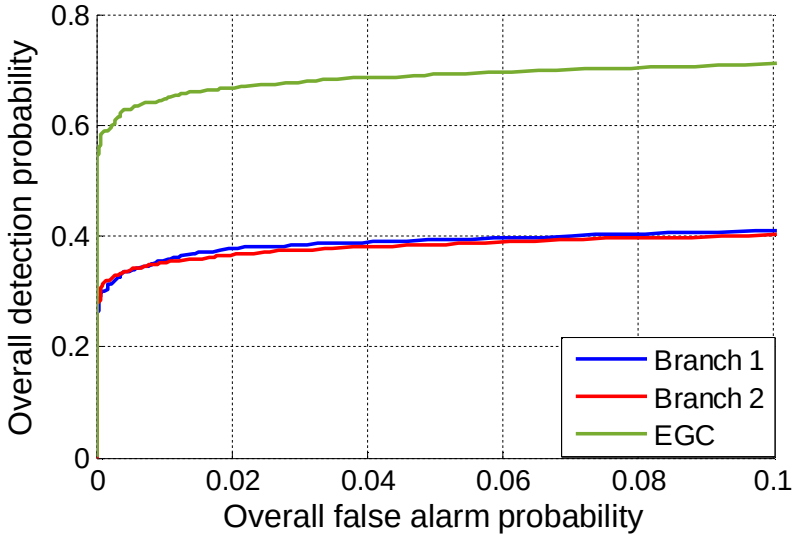

Figure 5- 43: System level ROC curves-Real data, PRN 10

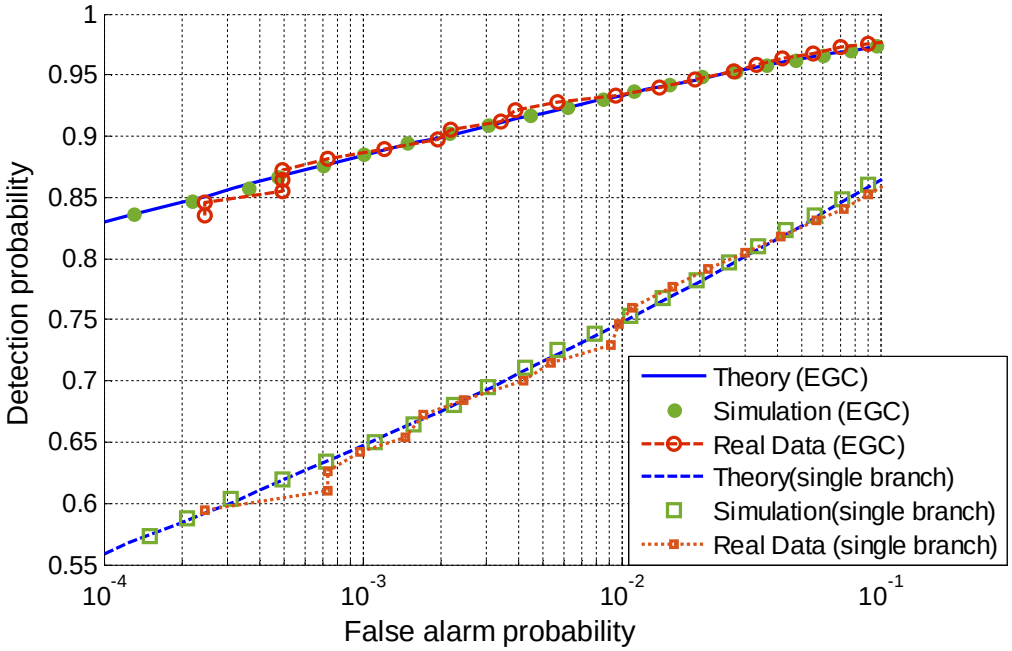

Figure 5-44: Cell level ROC curves for single and combined channels, PRN 10

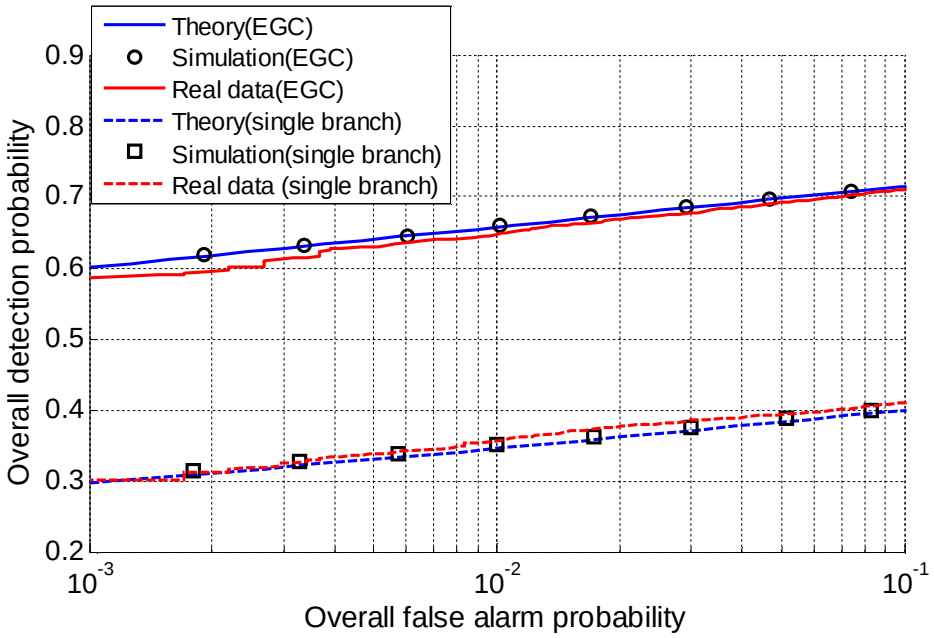

Figure 5- 45: System level ROC curves for single and combined channels, PRN 10

Figure 5-46 shows the *SNR* values for PRN 10 in the static mode receiver. In this data collection scenario, PRN 10 signal is analyzed because it is more affected by multipath fading compared to other PRNs. This is due to the satellite location and also the location of reflectors in the data collection environment. As can be seen, the fading effect exists in both static and dynamic receivers. The main difference between the static and dynamic cases is that the channel variation is remarkably lower in the static mode. Note that the channel variation in the static receiver mode is only due to the satellite motion.

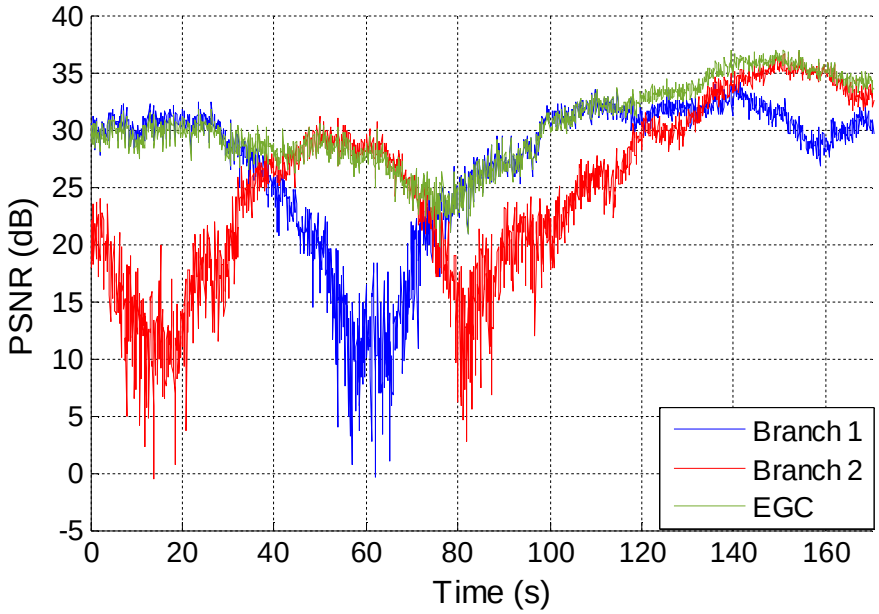

Figure 5-46: Post processing *SNR* – Real data, PRN 10, static, Location: MacHall building on the University of Calgary campus

C/N_0 values for PRN 8 in the static mode are depicted in Figure 5-47. Obviously, the C/N_0 values can easily drop below 20 dB-Hz due to the multipath fading effect.

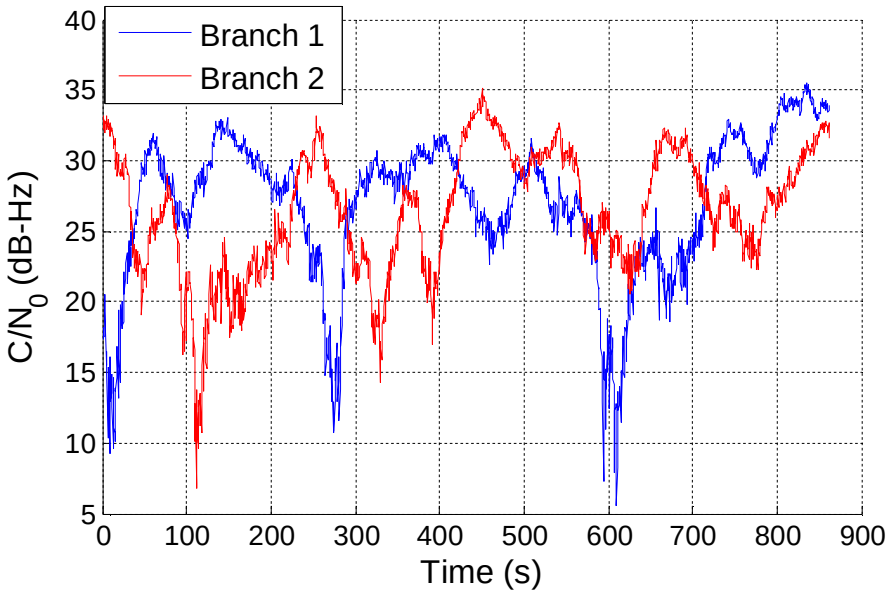

Figure 5-47: C/N_0 values for PRN 8, static mode, Location: MacHall building on the University of Calgary campus

A new set of GPS IF samples was collected using a Fraunhofer multi antenna GTEC RF front-end (Ruegamer et al 2012) in the CCIT building of the University of Calgary. Data collection was performed in a dynamic mode with a very slow motion (around 10 cm/s). The estimated C/N_0 in Figure 5-49 is based on using 200 ms coherent integration time in the GSNRx-rr software receiver. In the test, the antennas separation was 20 cm. To show the improvement achieved by diversity combining the cell level ROC curve is presented in Figure 5-50. Obviously, improvement in this curve leads to enhancement in the system level ROC curve as well as acquisition time.

Figure 5-48: Data collection environment

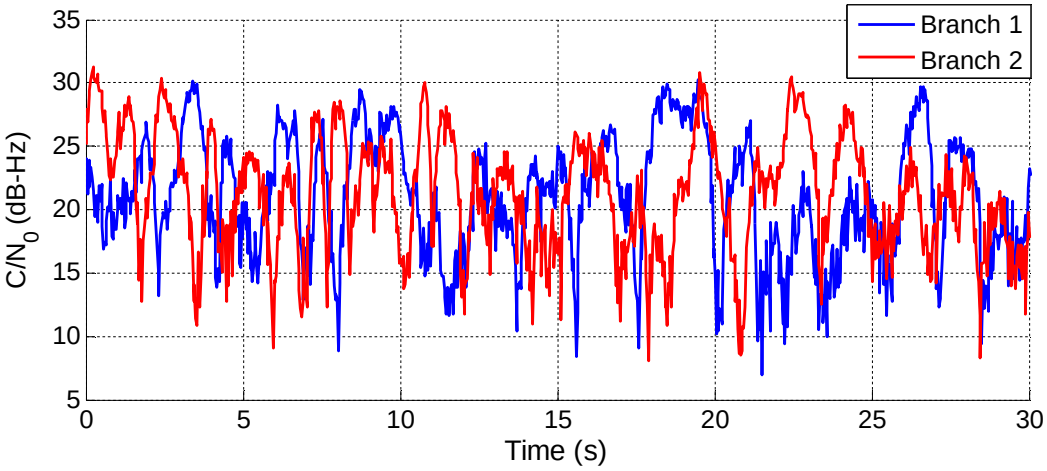

Figure 5-49: *C/N₀* values for PRN 11, dynamic mode, Location: CCIT building of the University of Calgary

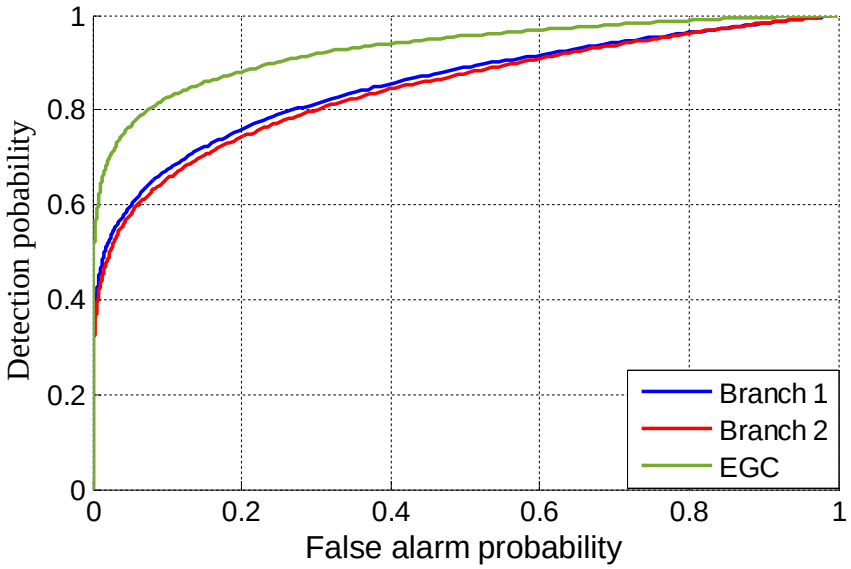

Figure 5-50: Cell level ROC curves

In summary, in this chapter the theoretical results were verified by Monte Carlo simulations and compared with the real data results. The test setup for the real GPS data collection and the antenna diversity system were described. The performances of diversity combining in terms of ROC curves, diversity gain, mean and variance of the acquisition time were compared to those of single branches.

Chapter Six: Conclusions and Recommendations

This chapter provides conclusions and recommendations for future work.

6.1 Conclusions

The GNSS cold start acquisition process, when there is no aiding information available and a search over all possible code and Doppler pairs is required, was investigated. It was also assumed that assisted GPS, where navigation bit transitions are not a problem, is not used. Acquisition performance was evaluated at the cell level, when only a single cell is considered and at the system level, in which the impact of an entire set of cells in the search space is taken into account. Acquisition time, as a critical metric in weak signal situations, was evaluated in terms of mean and variance values. Results show that depending on the C/N_0 value, integration time and the number of coherent and non-coherent integrations, an optimum detection threshold might exist to have the minimum mean acquisition time. Furthermore, considering the effect of detection probability and size of the search space on the acquisition time, there is an optimum combination of coherent and non-coherent integrations for which the mean acquisition time is minimized.

Equal gain combining of the received signals in antennas was performed at the correlator outputs level. Compared to a single antenna, smoother *SNR* values which mitigate the fading effect were observed by applying diversity combining.

Significant improvements were obtained in the cell and system levels detection by equal gain combining utilizing two branches. This leads to a higher successful detection for a given false alarm probability or equivalently fewer false alarms for a specified detection probability. For example, for a *SNR* value of 12 dB obtained using 10 ms coherent integration time, a 30% in the overall detection probability for a given overall false alarm probability of 10^{-3} was realized. The performance of the diversity combining was evaluated in terms of the diversity gain in which more than 4.5 dB gain was achieved. The attained diversity gain significantly reduces the computational load in term of the integration time. Experimental results revealed that due to enhancement in the detection probability and reduced false alarms, the mean acquisition time can be significantly improved using antenna diversity. More than a 43% reduction in the mean acquisition time using two diversity branches was observed. This improvement is even more considerable in weak signal situations where the acquisition is a time demanding process (order of several minutes). A lower acquisition time variance, approximately *1/4* of that of a single branch, was obtained after the equal gain diversity combining. This is due to a reduction of the number of deep fading moments and smoother *SNR* values by utilizing the antenna diversity technique. According to the results, assuming uncorrelated received signals at the antennas, increasing the number of antennas enhances acquisition performance. However, the rate of improvement decreases as the number of antennas increases. The reason is that in a Rayleigh fading channel using a certain number of antennas or more, equal gain diversity combining provides sufficient

processing gain resulting in a successful acquisition within an acceptable time. Hence, after a certain point, adding more antennas does not provide significant acquisition performance improvement.

6.2 Recommendations

Suggestions for future work are as follows:

1. In this work the Rayleigh fading model is considered for the multipath fading channel. In the absence of a dominant component, the amplitude of the received signal can be modeled by a Rayleigh distribution. However, if a dominant component such as a line of sight signal exists, the multipath channel should be modeled by a Rician distribution. The acquisition performance evaluation in terms of the detection probability and acquisition time is of interest.

2. Herein the maximum likelihood search strategy was adopted in the acquisition process. Other search strategies such as serial and hybrid could also be investigated.

3. During the acquisition performance analyzes, it was assumed that there was no verification mode in the acquisition process. However, the effect of verification mode on the detection and false alarm probabilities as well as acquisition time is a relevant question to investigate.

4. In fading environments, *SNR* values can significantly change, resulting in a large variation in the acquisition time. Hence, the variance of acquisition time becomes a more important metric in multipath fading situations. This metric was assessed in this thesis using only Monte Carlo simulations. However, a closed form expression for the acquisition variance needs to be addressed.

5. In the equal gain diversity combining it was assumed that the received signals are uncorrelated. The acquisition performance after the diversity combining can be evaluated considering the correlated received signals.

6. The results presented in this work were based on using standalone receivers. Assisted GPS receivers that have access to aiding information about the navigation data bit and timing information, can also be considered. However, the combined enhancement of both assisted GPS and the proposed method is not fully known.

References

Aissaoui, A. and Z. Hammoudi (2009), “A Rapid Adaptive PN Code Acquisition with Antenna Diversity for DS-CDMA Communication,” In *International Conference on Advances in Computational Tools for Engineering Applications,* pp. 208-213.

Akopian, D. (2001), “A fast satellite acquisition method,” In *Proceedings of the 14th International Technical Meeting of the Satellite Division of The Institute of Navigation (ION GPS 2001)*, pp. 2871-2881.

Alink, O., A. R. Smeenge, A. B. Kokkeler, E. A. Klumperink, G. J. Smit and B. Nauta (2011), “Exploring the use of two antennas for crosscorrelation spectrum sensing,” In *Vehicular Technology Conference (VTC Fall),* pp. 1-5.

Amari, S. V. and R. B. Misra (1997), “Closed-form expressions for distribution of sum of exponential random variables,” *IEEE Transactions on Reliability,* vol. 46, *no.*4, pp. 519-522.

Arfken, G. B. and H. J. Weber (2005), Mathematical Methods for Physicists, International Student Edition, Academic press.

Baum, C. and V. Veeravalli (1994), “Hybrid acquisition schemes for direct sequence CDMA systems,” *IEEE International Conference on Communications*, vol. 3, pp. 1433-143.

Bjornson, E., D. Hammarwall and B. Ottersten (2009), “Exploiting quantized channel norm feedback through conditional statistics in arbitrarily correlated MIMO systems,” *IEEE Transactions on Signal Processing,* vol. 57, no.10, pp. 4027-4041.

Blaunstein, N. and J. B. Andersen (2002), *Multipath phenomena in cellular networks,* Artech House.

Borio, D. (2008), *A Statistical Theory for GNSS Signal Acquisition*, PhD Thesis, Department of Electrical Engineering Politecnico Di Torino, (Available at http://plan.geomatics.ucalgary.ca)

Borio, D., C. O'Driscoll and G. Lachapelle (2010), "Composite GNSS signal acquisition over multiple code periods," *IEEE Transactions on Aerospace and Electronic Systems*, vol. 46, no.1, pp. 193-206.

Borio, D., C. O'Driscoll and G. Lachapelle (2008), "Coherent, Non-Coherent and Differentially Coherent Combining Techniques for the Acquisition of New Composite GNSS Signals," *IEEE Transactions on Aerospace and Electronic Systems,* vol. 45, no. 3, pp. 1227 -1240.

Borio, D., L. Camoriano and L. Lo Presti (2008), "Impact of GPS acquisition strategy on decision probabilities," *IEEE Transactions on Aerospace and Electronic Systems*, vol. 44, no. 3, pp. 996-1011.

Borio, D., C. Gernot, F. Macchi and G. Lachapelle (2008), "The output SNR and its role in quantifying GNSS signal acquisition performance," In *ENC GNSS*, vol. 8, pp. 23-25.

Broumandan, A., J. Nielsen and G. Lachapelle (2011), "Indoor GNSS Signal Acquisition Performance using a Synthetic Antenna Array," *IEEE Transactions on Aerospace and Electronic Systems*, vol. 47, no. 2, pp. 1337-1350.

Broumandan, A., J. Nielsen and G. Lachapelle (2009a), "Performance of Narrowband Signal Detection under Correlated Rayleigh Fading Based on

Synthetic Array," *International Journal of Antennas and Propagation*, Article ID 610109.

Broumandan, A., J. Nielsen and G. Lachapelle (2009b), "Signal detection performance in indoor environments with a synthetic antenna array," In *13th International Symposium on Antenna Technology and Applied Electromagnetics and the Canadian Radio Science Meeting*, *ANTEM/URSI*, pp. 1-4.

Cantrell, P. and A. Ojha (1987), "Comparison of generalized Q-function algorithms (Corresp.)," *IEEE Transactions on Information Theory*, vol. 33, no. 4, pp. 591-596.

Colburn, J. S., Y. Rahmat-Samii, M. A. Jensen and G. J. Pottie (1998), "Evaluation of personal communications dual-antenna handset diversity performance," *IEEE Transactions on Vehicular Technology,* vol. 47, no. 3, pp. 737-746.

Corazza, G. E. (1996), "On the MAX/TC criterion for code acquisition and its application to DS-SSMA systems," *IEEE Transactions on Communications*, vol. 44, no. 9, pp. 1173-1182.

Dietrich Jr, C. B., K. Dietze, J. R. Nealy and W. L. Stutzman (2001), "Spatial, polarization, and pattern diversity for wireless handheld terminals," *IEEE Transactions on Antennas and Propagation*, vol. 49, no. 9, pp. 1271-1281.

Electronic warfare and radar systems engineering handbook (1997), Naval Air Warfare Center.

Fallahin, K., D. Wang and M. Fattouche (2012), “Probability of outlier analysis in weak GPS signal acquisition,” *Journal of the Franklin Institute*, vol. 349, no. 5, pp. 1930-1943.

Geiger, B., M.Soudan and C.Vogel (2010), “On the Detection Probability of Parallel Code Phase Search Algorithms in GPS Receivers*,”* In *Proceedings of the IEEE International Sympsium on Personal, Indoor and Mobile Radio Communications (PIMRC)*, pp. 864-869.

Goldsmith, A. (2005), *Wireless communications*, Cambridge university press.

Holmes, J. and C. Chen (1977), “Acquisition time performance of PN spread-spectrum systems,” *IEEE Transactions on Communications*, vol. 25, no. 8, pp. 778-784.

Kassabian, N. and L. Lo Presti (2012a), “Mean acquisition time of GNSS peer-to-peer networks,” *International Conference on Localization and GNSS (ICL-GNSS)*, pp. 1-6.

Kassabian, N. and L. Presti (2012b), “Technique for MAT Analysis and Performance Assessment of P2P Acquisition Engines,” *In Position Location and Navigation Symposium (PLANS)*, pp. 980-988.

Kay, S. M. (1998), *Fundamentals of Statistical Signal Processing: Detection Theory*, vol. 2, PTR Prentice Hall, New Jersey.

Kim, S. (2004), “Acquisition Performance of CDMA Systems with Multiple Antennas,” *IEEE Transactions on Vehicular Technology*, vol. 53, no. 5, pp. 1341-1353.

Mahmood, F. E. (2012), *Mobile Radio Propagation Prediction for Two Different Districts in Mosul-City*, Edited by Vasilios N. Katsikis.

O'Driscoll, C. (2007), *Performance Analysis of the Parallel Acquisition of Weak GPS Signals*, PhD Thesis, Department of Electrical and Electronic Engineering, National University of Ireland.

O'Driscoll, C. and C. Murphy (2001), "Performance Analysis of an FFT Based Fast Acquisition GPS Receiver," In *Proceedings of the National Technical Meeting of The Institute of Navigation*, pp. 1014-1025.

O'Driscoll, C., M.G. Petovello and G. Lachapelle (2008), "Software Receiver Strategies for the Acquisition and Re-Acquisition of Weak GPS Signals," In *National Technical Meeting of the Institute of Navigation.*

Petovello, M. G., C. O'Driscoll, G. Lachapelle, D. Borio and H. Murtaza (2008), "Architecture and Benefits of an Advanced GNSS Software Receiver," *Journal of Global Positioning Systems*, vol. *7*, no. 2, pp. 156-1681.

Psiaki, M. L. (2001), "Block Acquisition of Weak GPS Signals in a Software Receiver," In *Proceedings of the 14th International Technical Meeting of the Satellite Division of the Institute of Navigation ION GPS*, pp. 2838-2870.

Puska, H. and J. Iinatti (2009), "Serial Search and Maximum Selection Based Code Acquisition Techniques for Single and Multi Antenna Systems," *IEEE Transactions on Wireless Communication*, vol. 8, no. 5, pp. 2317-2327.

Rappaport, T. S. (1996), *Wireless communications: principles and practice*, vol. 2, New Jersey: prentice hall PTR.

Rick, R. and L. Milstein (1997), “Parallel Acquisition of Spread-Spectrum Signals with Antenna Diversity,” *IEEE Transactions on Communication*, vol. 45, no. 8, pp. 903-905.

Rodriguez, J. A., T. Pany and B. Eissfeller (2004), “A theoretical analysis of acquisition algorithms for indoor positioning,” In *Proceedings of the 2nd ESA Workshop on Satellite Navigation User Equipment Technologies NAVITEC.*

Ruegamer, A., F. Foerster, M. Stahl and G. Rohmer (2012) “A flexible and portable multiband GNSS front-end system,” In *Proceedings of the 25th International Technical Meeting of the Satellite Division of the Institute of Navigation (ION GNSS 2012)*, pp. 2378–2389.

Sadrieh, N. (2011), “Spatial Antenna Diversity Performance for Indoor GNSS Applications,” *In Proceedings of GNSS11 (Portland, OR, 20-23 Sep).*

Sadrieh, S. N., A. Broumandan and G. Lachapelle (2012), “A weighted combining method for GPS antenna diversity,” In *Position Location and Navigation Symposium (PLANS)*, IEEE/ION, pp. 961-968.

Sagiraju, P. K., S. Raju and D. Akopian (2008), “Fast acquisition implementation for high sensitivity global positioning systems receivers based on joint and reduced space search,” *In Radar, Sonar & Navigation*, IET, vol. 2, no. 5, pp. 376-387.

Shanmugam, S., J. Nielsen and G. Lachapelle (2007), “Enhanced Differential Detection Scheme for Weak GPS Signal Acquisition,” In *Proceedings of the 20th International Technical Meeting of the Satellite Division of the Institute of Navigation*, Fort Worth, TX, pp. 2499-2509.

Shin, O. S. and K. B. Lee (2003), “Use of multiple antennas for DS/CDMA code acquisition,” *IEEE Transactions on Wireless Communications,* vol. 2, no. 3, pp. 424-430.

Vaughan, R. G. and J. B. Andersen (1987), “Antenna diversity in mobile communications,” *IEEE Transactions on Vehicular Technology*, vol. 36, no. 4, pp. 149-172.

Won, S. and L. Hanzo (2008), “Analysis of Serial-Search-Based Code Acquisition in the Multiple-Transmit/Multiple-Receive-Antenna-Aided DS-CDMA Downlink,” *IEEE Transactions on Vehicular Technology*, vol. 57, no. 2, pp. 1032-1039.

Wu, L., W. Lu and D.Yu (2009), “Research of Weak Signal Acquisition Algorithms for High Sensitivity GPS Receivers,” In *Asia Pacific Conference on Postgraduate Research in Microelectronics & Electronics*, pp. 173-176.

Zaheri, M. (2011a), “Enhanced GNSS signal detection performance utilizing polarization diversity,” In *Masters Abstracts International*, vol. 50, no. 1.

Zaheri, M. (2011b), *Enhanced GNSS Signal Detection Performance Utilizing Polarization Diversity*, MSc Thesis, published as Report No. 20322, Department of Geomatics Engineering, The University of Calgary, Canada.

Zaheri, M., A. Broumandan and G. Lachapelle (2010), “Comparing Detection Performance of Polarization and Spatial Diversity for Indoor GNSS Applications,” In *Position Location and Navigation Symposium (PLANS)*, IEEE/ION, pp. 737-744.

Zaheri, M., A. Broumandan, C. O’Driscoll and G. Lachapelle (2009), “Enhanced GNSS Indoor Signal Detectability Using Polarization Diversity,” In *Proceedings of*

the 22nd International Technical Meeting of The Satellite Division of the Institute of Navigation (ION GNSS'09).